IN-PLANE SHAKE TABLE TESTING OF GRAVITY LOAD DESIGNED REINFORCED CONCRETE FRAMES WITH UNREINFORCED MASONRY INFILL WALLS

by

Jose Centeno

B.E.Sc. Escuela Superior Politécnica del Litoral, 2004

A THESIS SUBMITTED IN PARTIAL FULFILMENT OF
THE REQUIREMENTS FOR THE DEGREE OF

MASTER OF APPLIED SCIENCE

in

The Faculty of Graduate Studies

(Civil Engineering)

THE UNIVERSITY OF BRITISH COLUMBIA
(Vancouver)

April, 2009

Abstract

Common construction practice before modern seismic design codes appeared allowed designing columns lap splices located above the slab in each floor or above the foundation. The lack of lap splices and the shear reinforcement was in the form of stirrups with 90-degree bends and spaced at half the depth of the frame member. As a result, the section at the base of these columns is unconfined and susceptible to shear failure or to a premature failure of the lap splices before yielding of the longitudinal bars.

The masonry infill walls used as partitions were often ignored by design engineers since such walls were considered as nonstructural architectural elements. However, lessons learned from past earthquakes and from several tests performed have shown that those walls tend to interact with the bounding frame when the structural system is subjected to moderate or severe earthquake ground motions.

The first part of an experimental testing program carried out at the University of British Columbia (UBC) in Vancouver, Canada tested the performance of 1/2 scale Gravity Load Designed Reinforced Concrete (GLDRC) frames with unreinforced masonry walls. This testing program consisted of one monotonic loading test on an infilled frame and two series of shake table tests, one on an infilled frame and one on a bare frame with the UBC Earthquake Engineering Research Facility (EERF) unidirectional shake table.

It was concluded from these tests that the interaction with the unreinforced masonry wall stiffens the frame, reduces the deformations, and allows dissipating energy through nonlinear response for several cycles of deformation. It was determined that the governing failure mode for the masonry wall was shear sliding for monotonic and dynamic loading. There was consistent evidence of local lateral deformations at the base of the gravity load designed columns due to construction cold joints and inadequate lap splices that may result in shear failure of the base of the column due to the interaction with the masonry infill during a severe earthquake.

Table of Contents

List of Tables

List of Figures

Acknowledgements

I would first like to express my sincere thanks to my supervisor, Dr. Carlos Ventura, for his encouragement and guidance through out my graduate studies. I was greatly motivated by the vision and enthusiasm he had for this thesis project and all of my work at UBC.

Secondly, I would like to acknowledge Dr. Sveltana Bzerv, of the British Columbia Institute of Technology. Her contributions to the development of this thesis are greatly appreciated. Thank you.

Andy Vizer, of Cement Association of Canada and Bill McEwen, from the Masonry Institute of British Columbia; were instrumental in providing the materials and technical support during the construction of the test specimens. This research was conducted with the financial support of Public Works and Government Services of Canada, the Canadian Cement Association, and the Masonry Institute of British Columbia.

The technicians at UBC were most helpful in all the stages of test setup. The skill and efforts put in by Max Nazar, Doug Hudniuk, Doug Smith and Scott Jackson were very valuable to this research project.

To my colleagues and friends at the University of British Columbia, Freddy Piña, Katherine Thibert, Devin Sauer, Ali Reza Ahmadnia, Ottón Lara who put their time and effort in making this testing program a success. In particular, Hugón Juarez and Juan Carlos Carvajal, for their guidance and feedback during the course of the work.

And to my loving parents, Pepe and Cuty who have supported me throughout my years of education.

Chapter 1 – Introduction

1.1 General

A large number of existing buildings, particularly those constructed prior to the enforcement of ductile seismic design provisions introduced in 1970's, were primarily designed and detailed to resist gravity loads. Structures of this type do not have the current reinforcement detailing required by modern codes in high and medium seismic zones, and hence they are considered potential life–safety hazards.

Unreinforced Masonry (URM) wall infill panels can be frequently found as interior and exterior partitions in Reinforced Concrete (RC) and steel structures. URM infills fulfill architectural and other functional requirements, such as forming a significant portion of building envelope, enclosing space, providing protection from external temperature and acting as sound barrier, while also providing adequate protection from fire. Masonry is a locally available building technology that has a long history of successful use in the construction industry. Since these panels are normally considered as architectural elements, their presence usually is ignored in structural design.

Lessons learned from past earthquakes have shown that there is an interaction between the masonry infill with the bounding frame when subjected to moderate to strong earthquake loads. Such interaction may or may not be beneficial to the structural performance, and has been a subject of many debates because of the brittle behavior of masonry and possible undesirable effects characteristic for seismic response of this system.

1.2 Seismic Performance of Gravity Load Designed Reinforced Concrete Frames

The design of most reinforced concrete frame structures built in the late 1950s or 1960s [ACI-318, 1963] was governed by gravity loads, mainly due to the fact that the design lateral forces the structure was designed for according to the older design codes were

much lower than those required by current code provisions. In addition, current knowledge and understanding of the behavior of RC members was not available at the time of design and construction of such buildings. A typical reinforcement detailing of the past design practice is shown in Figure 1.1. The implications of this detailing on the expected behavior of the structure are described below:

Figure 1.1 Typical reinforcing details of moment frames designed in late 1950s and 1960s. (reproduced from Pincheira & Jirsa, 1995)

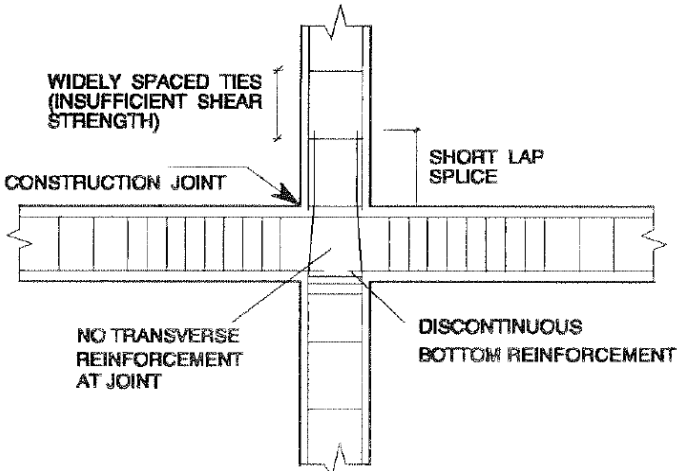

a) Inadequate shear reinforcement of frame members

The transverse reinforcement in column and beam members was typically detailed in the form of closed hoops with 90-degree bends and widely spaced ties along the member length. The seismic performance of such reinforcement detailing results in shear failure of the column, which occurs by opening up the 90-degree hooks and losing the limited strength and confinement provided by the transverse reinforcement (see Figure 1.2).

b) Inadequate lap splices in columns

Common construction practice before seismic design codes considered columns as compression members and their lap splices were designed only to transmit compression. These lap splices were located above the floor slab at the region of higher moment. The length of lap splices specified in older codes was 20 or 24 bar diameters [ACI-1963]. The resulting structural behavior has shown slip of the rebar along the splice, and

occasional failure before reaching yielding of the bars in tension as shown in Figure 1.3 [Cho and Pincheira, 2006].

Figure 1.2. Observed behavior of RC columns with inadequate transverse reinforcement during earthquakes

Northridge, 1994
(reproduced from EERI Photo Collection)

Kocaeli, 1999
(reproduced from Sezen, Whittaker, Elwood, Mosalam, 2003)

Bhuj, 2001
(reproduced from Jaiswal, K., Sinha, R., Goyal, A. 2003)

Past studies of anchored bars have identified two main types of bond failure mechanisms. If the surrounding concrete area is large and the concrete is well confined, bond failure occurs by pullout. On the other hand, if the concrete cover is small and the concrete is poorly confined, bond failure occurs by splitting of the surrounding concrete [Eligehausen, Popov; and Bertero, 1983].

Figure 1.3. Observed lap splice failure in RC columns during earthquakes

Northridge, 1994
(reproduced from
Melek, Wallace, Conte 2003)

Kocaeli, 1999
(reproduced from
Sezen, Whittaker, Elwood, Mosalam, 2003)

c) Inadequate shear resistance of beam-column joints

The role of the beam-column joint is to transfer the forces developed in the columns and beams, therefore adequate strength of the joint is essential for the development of the full capacity of the framing members. Joint provisions for seismic loading in which transverse reinforcement is required throughout the connection were first introduced in the 1971 edition of the ACI code [ACI 318-1963]. As a result, most structures built prior to this time are likely to have beam-column joints without any transverse reinforcement. Damage to beam-column joints is shown in Figure. 1.4.

Figure 1.4. Building collapse due to failure of beam-column joints. (reproduced from Sezen, Whittaker, Elwood, Mosalam, 2003)

d) Strong beam- weak column

In many cases, frames in buildings were constructed with deep beams and flexible column elements. During the earthquake response, because the moment capacity is higher for the deep beams than for the columns, plastic hinging forms only in the columns and results in a soft story mechanism. The earthquake displacement demands have to be met by the soft story with unachievable rotational ductility demands for its columns, which result in total collapse of the building.

Figure 1.5. Weak-Column Strong Beam failure observed for Chi Chi Earthquake 1999. (reproduced from Nan, Su 2002)

1.3 Seismic Performance of Masonry Infills

The interaction mechanism between an infill wall and the surrounding structural frame depends on the contact area at the interfaces of these two components. Thus, the extent of composite action will depend on the level of lateral load, extent of bond in anchorage at the interfaces, and geometric and stiffness characteristics of the two components [Drysdale, Hamid, and Baker , 1999]. In addition, the failure mode of an URM infill wall depends on its geometric and material properties [Öztürk, 2005].

Based on the knowledge gained from both analytical and experimental studies during the last five decades, different failure modes of masonry-infilled frames have been categorized into the following five distinct modes [El-Dakhakhni, Elgaaly, Hamid, 2003]: corner crushing, diagonal compression, sliding shear, diagonal cracking, and frame failure.

1. Corner crushing (CC) denotes crushing of the infill in at least one of its loaded corners. This mode is usually associated with infill of weak masonry blocks surrounded by a frame with weak joints and strong members.

2. Diagonal compression (DC) is associated with crushing of the infill within its central region. This mode is associated with a relatively slender infill, where failure results from out-of-plane buckling instability of the infill due to in-plane loads.

3. The diagonal cracking (DK) is seen in the form of a crack connecting the two loaded corners, as shown in Figure 1.5. Experimental investigators [Polyakov 1960, Holmes 1963, Stafford Smith 1966] have concluded that the masonry wall acts as an equivalent diagonal compression strut within the frame, as shown in Figure 1.6a which converts the structural system to a type of truss. This mode is associated with a weak frame or a frame with weak joints and strong members infilled with a rather strong infill.

Figure 1.5. Diagonal Sliding Shear Failure of Masonry Infill
(reproduced from Axley and Bertero 1979)

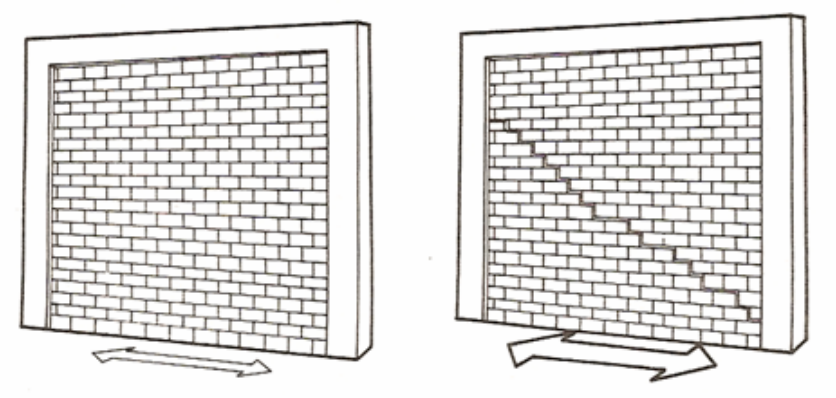

4. Sliding shear (SS) represents horizontal sliding shear failure through bed joints of a masonry infill, as shown in Figure 1.6(b). The formation of the shear crack separates the panel into two parts so that the effective column height can be reduced. In this post-cracked condition, the system will behave as a knee-braced system [Fiorato et al, 1970]. This mode is associated with infill of weak mortar joints and a strong frame.

5. Frame failure (FF) mode is seen in the form of plastic hinges in the columns or the beam–column connection. This mode is also associated with a weak frame or a frame with weak joints and strong members infilled with a rather strong infill.

Figure 1.6. Failure Modes of Masonry Infilled Frames
(reproduced from Paulay & Priestley 1992)

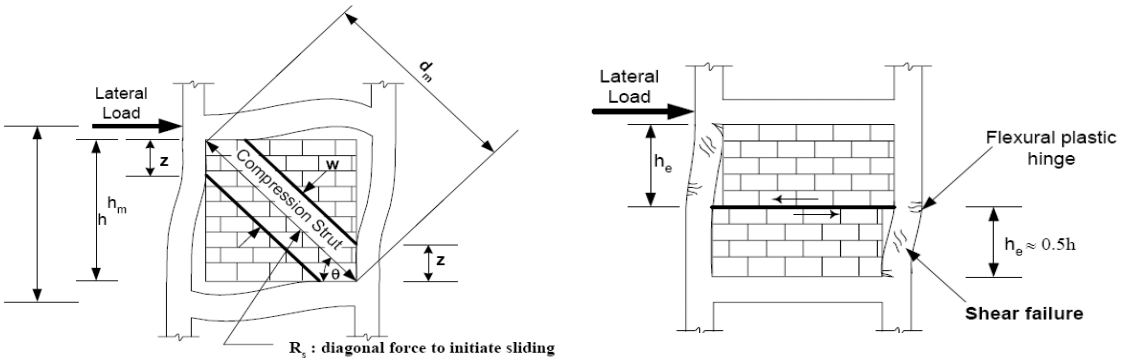

a) Diagonal Compression Strut b) Horizontal Shear Sliding

1.4 Research Objectives

The primary goal of this research program was to evaluate the seismic performance of GLDRC frames with unreinforced masonry infill walls. This study provides an understanding of the in-plane interaction between the frame and the infill wall and its effect on the lateral stiffness, strength and deformation capacity of the overall structure. The tasks in this research program consist of performing and documenting the results of in-plane shake table testing of half-scale GLDRC frames with and without unreinforced concrete block infill walls.

1.5 Research Scope

This research is focused to the in-plane testing of two half-scale GLDRC frames infilled with an unreinforced masonry wall, and one bare frame. The half scale masonry infill walls are nonloadbearing concrete block masonry walls. Each of the frames and masonry walls had identical dimensions. This study did not include simulation of any effects of out-of-plane motion of unreinforced masonry walls.

Chapter 2 – Literature Review

2.1 General

The uncertainties of the interaction and failure mechanisms of Gravity Load Designed Reinforced Concrete (GLDRC) frames with unreinforced masonry infill walls lead to conservative seismic retrofits or demolishing these walls altogether. Experimental research evidence related to the dynamic response of these structures is limited. This section presents the results of experimental research performed on GLDRC frames with different masonry infill panels and their observed failure mechanisms. There is a significant amount of research done on the seismic performance of reinforced concrete frames with masonry infills, however only the studies most relevant to the scope of this study are summarized here.

2.2 Monotonic and Cyclic Testing of Non Ductile Reinforced Concrete Frames with Masonry Infill Walls

Brokken and Bertero [1981] performed a series of quasi-static cyclic and monotonic load tests on a 1/3-scale specimen designed based on the lower 3-1/2 stories of an 11 story-three bay reinforced concrete frame infilled in the outer two bays. The reinforced concrete moment frame was designed for high rotational ductility, and tested with various infill walls built using different materials and reinforcing combinations. In particular, one fully grouted concrete block infill wall with ρ=0.60% reinforcement was tested.

The authors showed that for monotonic in-plane loading the failure mode was different than that for cyclic lateral loading, but both tests involved only the first story of the building. For the case of monotonic loading (Test#3), the failure mode was triggered by crushing of the infill acting as a diagonal compression strut, with frame finally forming a sidesway mechanism with hinges at the top and bottom of the first story in both columns. For the case of cyclic loading (Test#8), the failure mode was triggered by sliding shear and then crushing of the infill. The spiral steel on the left column fractured in the first

story of the test model, and shear deformations were concentrated in the column at this level, see Figure 2.1.

Their results showed that after the addition of an infill of concrete block infill there was an observed singificant increase in stiffness of 506% and in load capacity of 273%, relative to the completely bare frame.

The authors inferred that non-ductile moment resisting frames infilled with unreinforced masonry walls should not be used in seismic regions, except for the cases where a building can resist elastically the effect of the most severe earthquake ground motion.

Mehrabi A. and Shing P. Benson, 1996 studied two types of half-scaled RC frames, one of which was a "weak" frame designed for a lateral wind load corresponding to a basic wind speed of 100mph (44.5 m/s), and the other was a "strong" frame which was designed following the UBC 1991 seismic provisions for a Seismic Zone 4 of U.S. The testing program consisted of several weak and strong frames with hollow and solid concrete block masonry infill walls subjected to monotonic and cyclic loading.

This study observed that the weak bare frame (only bare frame tested) exhibited a fairly ductile behavior. In the case of the infilled frames, nonlinear behavior was usually initiated by the cracking of the infill under approximately 45^{o} angle with regards to horizontal. These cracks were later joined by horizontal sliding cracks developed along the bed joints near the midheight panels. This cracking pattern was referred as a diagonal / sliding crack. Out of all the pushover tests, the weak infill resulted in the least increase in stiffness with respect to the bare frame's initial stiffness, as shown in Figure 2.1.

The authors showed that the failure mechanism of an infilled frame depends very much on the relative strengths of the frame and the infill. In general, lateral resistance for a frame with a weak (hollow) panel was governed by the sliding of the panel along its bed joints. In the case of a strong (solid) infill and a weak frame, the ultimate resistance and failure were dominated by the diagonal sliding crack and the shear failure of the columns. Figure 2.2 shows of the tested specimen after the failure and the force vs displacement

hysteresis curves for the cyclic tests. It can be observed that the specimen with the weak infill shows less energy dissipation capacity than that with the strong infill.

Figure 2.1. Load Displacement Curves for Monotonically Loaded Specimens (reproduced from Mehrabi A. and Shing P. Benson, 1996)

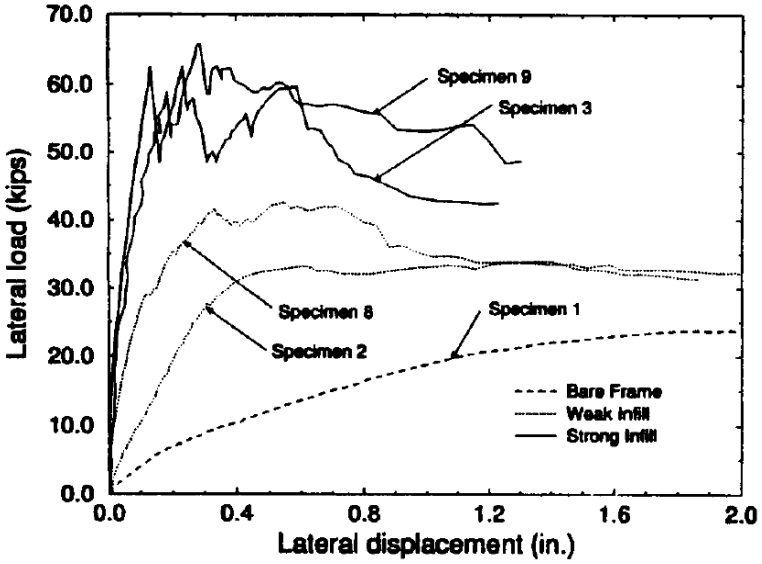

The authors concluded that for an existing nonductile frame, infill panels can be potentially used to improve their performance if the shear resistance of nonductile columns is enhanced to avoid irreparable damage and brittle failure.

Murty and Jain [2000] tested twelve single bay single storey ductile reinforced concrete frames of 1:2:7 reduced scale under reverse cyclic displacement. Ten specimens were infilled with full scale and half scale burnt clay brick masonry in cement mortar.

The authors found that the size of the bricks influenced the mode of failure of the infill. For the specimen with half scale bricks, crushing of the bricks was observed at the frame corners; implying a diagonal strut mechanism. In the case of the full scale bricks infill, no diagonal strut formed, instead the mode of failure was sliding along the mortar bed joints. The findings showed that masonry infill wall panels increase stiffness, strength, ductility and energy dissipation of a building.

Al-Chaar, Issa and Sweeny [2002] performed in-plane monotonic loading, pushover tests on half-scale single story non-ductile reinforced concrete frames infilled with unreinforced concrete masonry units and brick units. Each model was 1524 mm high and all infill specimens had an aspect ratio of 0.75.

Figure 2.2. Specimens with weak frames and h/L ratio of 0.67 (reproduced Mehrabi, A. and Shing, P. Benson, 1996)

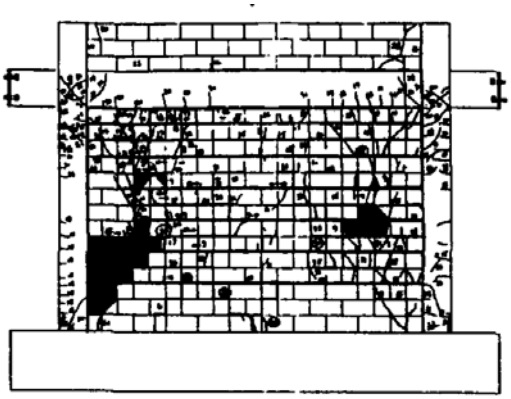

a) Weak infill weak frame
failure mode
(Sliding of Bed Joints)

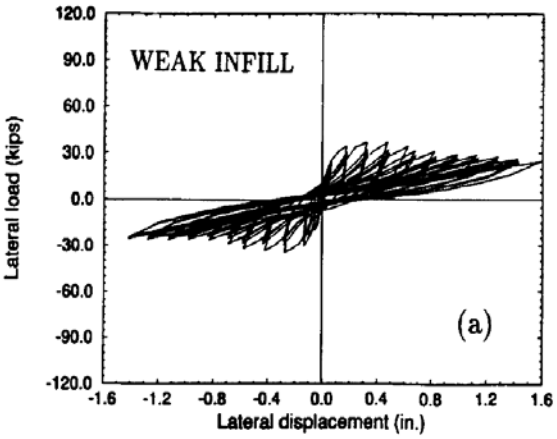

b) Weak infill weak frame
Force vs Displacement Plot

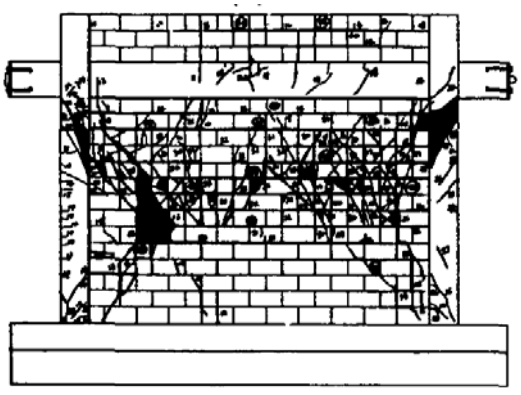

c) Strong infill weak frame
failure mode
(Shear Failure of Columns)

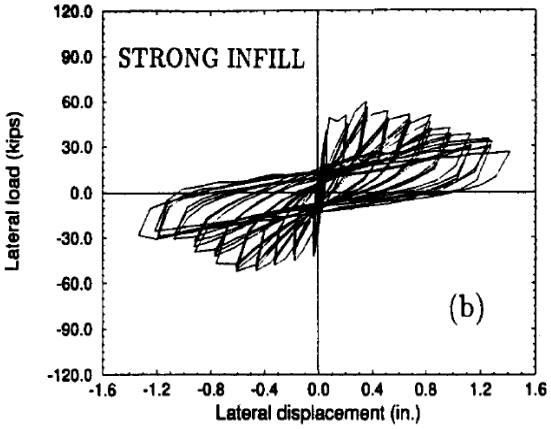

d) Strong infill weak frame
Force vs Displacement Plot

The mode of failure for the concrete masonry units infill specimen was shear-based, diagonal stair stepping without strut development. This mode of failure is a function of

the infill's high compression strength-to-shear capacity ratio (approx 30:1). In addition, the observations of this study also showed that unreinforced masonry infills can significantly increase the lateral stiffness, and strength with respect to the corresponding bare frame, while exhibiting ductile performance characteristics.

Saatcioglu M., Serrato F., and Foo S. [2004] studied the response of two half-scale GLDRC frames with hollow concrete block infill walls involving one benchmark specimen and a retrofitted specimen with CFRP sheets, under quasi static cyclic loading. Vertical loads were applied, 400 kN for each column and 120 kN distributed on the top beam, to simulate gravity loading. This was done by means of externally post-tensioned cables anchored to steel loading assemblies. For the unretrofitted specimen, the initial resistance was provided mostly by the walls, and was gradually transferred to the frames through progressive cracking and softening of the masonry.

The mode of failure of the unretrofitted specimen was due to bond slip of the lap splice. This bond slip was initiated at 1.5% drift, where vertical cracks were observed indicating bond slip due to splitting of concrete. In addition, spalling at the base of concrete was observed for the same drift value, see Figure 2.3a. When the specimen reached 2% lateral drift the column ties opened up and lap splice is debonded from the concrete, see Figure 2.3b. A significant portion of the cracked infill wall remained intact, until the maximum lateral drift has been reached.

Figure 2.3 Failure mode of GLDRC with URM infill (reproduced from Saatcioglu M., Serrato F., Foo S. 2004)

a) Vertical cracking and spalling of concrete at the column base 1.5% Drift

b) Ties with 90° hooks and lap splice exposed at 2% Drift

2.3 Dynamic and Pseudo Dynamic Testing of Non Ductile Reinforced Concrete Frames with Masonry Infill Walls

Hashemi and Mosalam [2007], performed a comprehensive study to evaluate the seismic performance of RC buildings with URM infill walls. A reduced scale, one storey high test structure was constructed to represent a substructure of the prototype building, as shown in Figure 2.4a, and subjected to shake table testing simulating a sequence of ground motions. The test structure was based on a hypothetical five story three bay by two bay RC building containing URM infill wall. The masonry walls were made of clay bricks and mortar type N. In this study the test structure is only subjected to the ground motion in the longitudinal direction (parallel to the URM infill wall).

Figure 2.4 Dynamic test of reduced scale one storey high test structure (reproduced from Hashemi and Mosalam, 2007)

a) Reduced scale one storey high test structure

b) Failed URM infill after dynamic testing

Failure mode of the URM infill wall is characterized by 45^o cracks at the bottom corners of each of the wall diagonals and 60^o cracks at the top corners. Early signs of corner crushing were observed at the top corners, as shown in Figure 2.4b. The authors concluded that the URM infills have a significant role in the strength and ductility of RC frame structures and increasing global stiffness and damping level.

Pinto and Tauser [2006], performed pseudo-dynamic tests on two full scale frames which were 4 storeys high and have 3 bays in plan. The frames were representative of existing

older gravity load designed reinforced concrete structures. The longitudinal reinforcement in the columns had lap splices at the base of the 1st and 3rd storey. The testing program included tests on one bare frame amd one masonry infilled frame. These models were subjected to input motions with increasing intensities and the testing was discontiued prior to imminent collapse. Both frames were repaired and subsequently retrofitted to test the efficiency of the strengthening solution.

Observations from the response of the non-ductile bare frame indicated a strong concentration of inelastic demands at the member ends and the development of premature shear cracks at the lap splice termination zone. In the case of the infilled frame significant damage was observed in the masonry infill at the ground storey level, where with some minor damage to the beam-column joints and several columns was observed.

2.4 Summary

Several experimental monotonic static and dynamic tests have been performed on gravity load designed reinforced concrete frames with masonry infill walls. The results and observations made for these tests show that the mechanical and geometrical characteristics of the concrete block masonry infill influence the behavior mode of the combined structure from diagonal compression to sliding shear. Both behavior modes result in a system with higher stiffness and deformation capacity than that of the bare GLDRC frame. Shear failure in GLDRC columns was observed in the several tests. The occurrence ov this mechanism was found to vary significantly depending on the mechanical properties of the infill and the applied loading time history.

Chapter 3 Experimental Program

3.1 Introduction

This section describes the construction of the test specimens, the testing protocol and the instrumentation selected to meet the objective of this study. Ten half scale GLDRC frames with URM infill walls were constructed with identical material and reinforcement characteristics. Only one of these URM walls was built not to have any mortar interface around the perimeter of the frame resulting in one bare frame with an unattached URM infill and nine infilled frames, as shown in Figure 3.1. This section describes the design and construction of the test specimens as well as the results of the material tests. The description of the setup for the static and shakes table tests in this testing program are also included. This thesis presents the first part of the experimental testing program, consisting of one monotonic loading test on an infilled frame (Specimen #1), one series of shake table tests on one infilled frame (Specimen #2) and one series of shake table tests on a bare frame (Specimen #3).

Figure 3.1. Image of test specimens during the construction of concrete block infills.

3.2 GLDRC frame and URM Infill Wall Specimen Design and Construction

3.2.1 Design Details

a) Foundation Beam

A reinforced concrete foundation was constructed for every specimen. The beam was designed to provide a base for each specimen, to allow lifting up the specimen without loading the frame and ensure that the specimen is rigidly connected to the shake table. The beam can be considered equivalent to a fixed support condition for the frame. The foundation consisted of one longitudinal beam 3270mm long by 480mm wide by 350mm depth with 10-25M deformed reinforcement bars and two transverse beams 1320mm long by 480mm wide by 350mm depth with 12-25M deformed reinforcement bars. The transverse beams were designed to have 100mm diameter holes at each end to allow to be mounted on the shake table.

b) Gravity Load Designed Reinforced Concrete Frame

The original frame design was prepared at the University of Ottawa, and follows the design requirements of ACI 318-1963, to represent older buildings before modern seismic design requirements [Saatcioglu M., Serrato F. and Foo S. 2004]. The columns had a 250 mm square section and 8-5M deformed bars. The longitudinal column reinforcement was lap spliced just above the foundation, with 26 bar-diameter lap lengths. Column ties consisted of 6.35 mm diameter smooth wire with 90-degree bends and 6 bar diameter extensions. The ties were spaced at 125 mm on centre (1/2 the column dimension). The beams were 300 mm wide and 350 mm deep, with longitudinal reinforcement consisting of 3-15M top bars and 2-15M bottom bars. The beam stirrups were in the form of closed hoops with 90-degree bends with 125 mm spacing. Figure 3.2 illustrates the reinforcement details of the frame members.

Figure 3.2. Gravity load designed reinforced concrete frame dimensions and reinforcement details

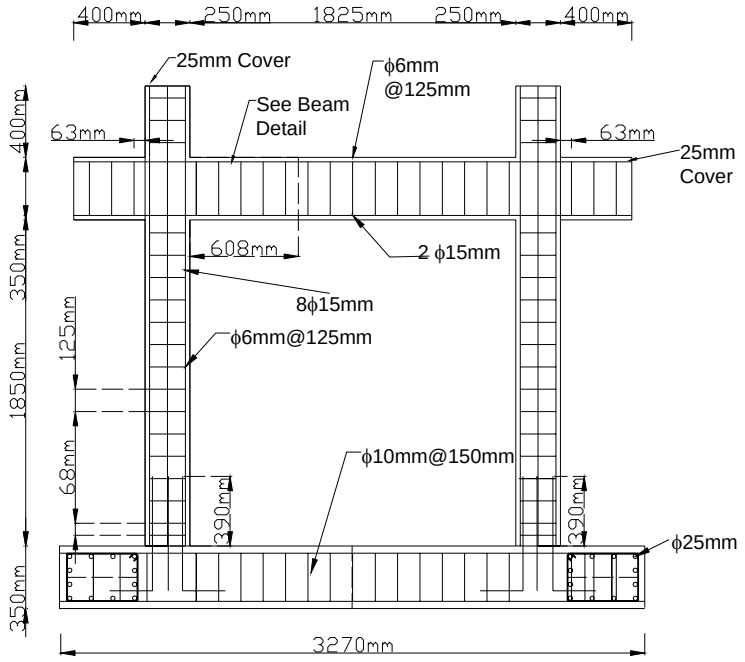

a) Front View

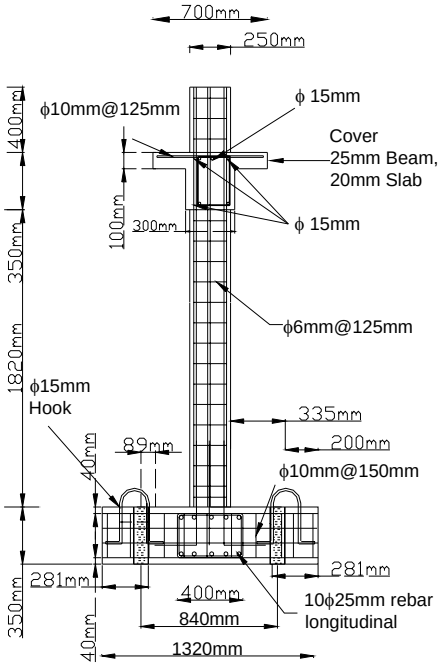

b) Side View

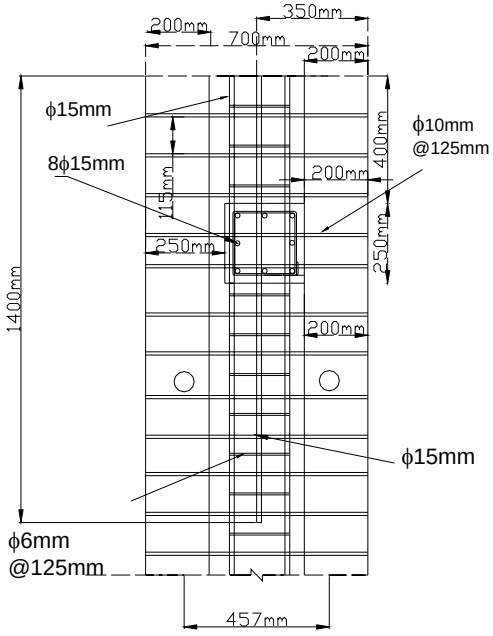

c) Beam and Slab View

3.2.2 Construction

Ten identical reinforced concrete frame specimens were constructed at the UBC Earthquake Engineering Research Facility (EERF). The shake table frame originally designed for a full-scale two story house test [Kharrazi, 2001], was tilted up and fixed firmly to two adjacent steel frames. The free space left by the shake table allowed for the construction of the RC frames within the facilities (see Figure 3.3a).

A professional contractor was retained for the construction of the test specimens. Concrete was supplied by the local ready-mix company Ocean Cement for all stages of construction. The ready mix concrete was specified for a compression strength of 28 MPa with a maximum size of coarse aggregate of 14 mm with 4% air content.

Foundation beams of the ten reinforced concrete test specimens were cast first (see Figure 3.3b). The foundation beam formwork had four 4½" diameter PVC pipes that after casting concrete would form the holes needed for later fastening each of these bases to the shake table platform for testing. Vertical rebar was put for the column longitudinal reinforcement and cut to the design lap length of 26 d_b (bar-diameters). The moment frames were constructed following the requirements specified in the design drawings. Figure 3.3 c and d illustrate the reinforcement details.

After completion of the frames, a professional mason was recommended by the Masonry Institute of B.C. to implement the actual industry practice for building of masonry partition walls. The infill walls were constructed to meet the testing specifications using Mortar Type N and half-scale hollow concrete blocks, which were provided by the Masonry Institute of B.C. Type N mortar is composed of 1 part cement, 1¼ parts lime, and 6¾ parts sand. Type N mortar does not have the strength of Type S mortar but was used frequently in construction for its excellent workability due to its high lime content.

Figure 3.3. Construction process of the reinforced concrete frames.

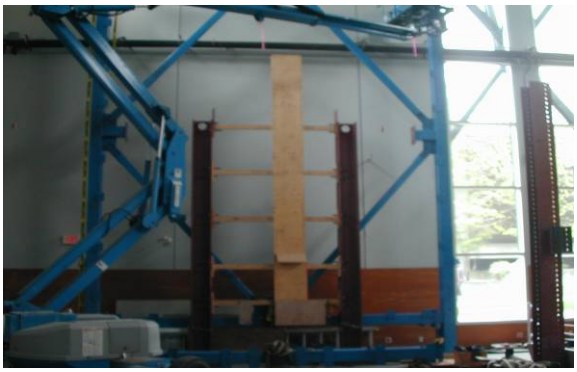

a) The shake table frame was secured to two adjacent steel frames.

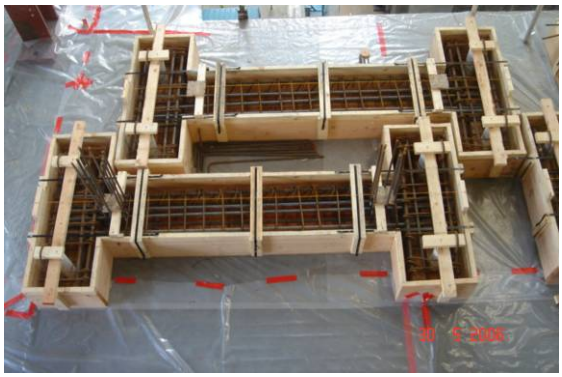

b) Formwork and rebar for foundation

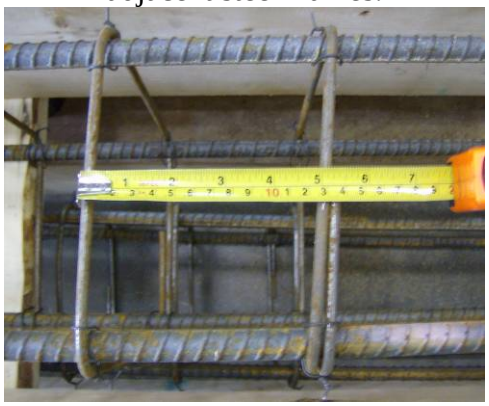

c) Beam stirrups ϕ_s=6.35 mm using smooth wire with 90-degree hooks

d) Column lap splice 26 d_b length column using smooth wire

e) Formwork and rebar for frame

f) Finished RC frame and foundation

No anchors were used to connect the infill walls to the frame. Nine infill walls were built to have a mortar joint thickness of 19mm (3/4") around the perimeter of the GLDRC frame, and only one infill wall was built with an air gap around the perimeter. The mortar head and bed joints had an average thickness of 9mm (3/8").

Figure 3.4. Construction of URM infill walls

a) Wall Construction

b) Mortar joints

c) Mortar applied only on face shells

3.3 Material Tests

3.3.1 Concrete Cylinder Tests

The ready mix concrete was designed to achieve a 28 MPa compression strength with a maximum size of coarse aggregate of 14mm with 4% air content. Six test cylinders were taken from one delivered concrete batch used in the foundation construction, and 5 test cylinders for each of the three supplied for the construction of the moment frames. Compression tests were performed on these test cylinders and the results provide an indication of the quality of the concrete tested.

The dimensions of test cylinders dimensions were 100 mm diameter and 200mm length. The testing equipment used was the Forney Concrete Testing Machine FX500, at the UBC Civil Engineering Materials Lab (see Figure 3.5a). The loading rate was 0.24 MPa/sec. Test cylinders were tested at 7 days and 28 days after construction. The compression strengths and average values are summarized in Table 3.1.

Figure 3.5 Concrete Cylinder Compression Tests

a) Compression testing machine

b) A concrete cylinder prior to compression test

Table 3.1 Concrete Compression Strength Tests

Concrete - Foundation				**Concrete - Frame**			
June 08 2006		**June 29 2006**		**July 24 2006**		**July 25 2006**	
7 days	f'c (MPa)	28 days	f'c (MPa)	7 days	f'c (MPa)	28 days	f'c (MPa)
A1	22.62	A4	29.52	A1	19.10	A3	30.23
A2	22.10	A5	33.97	A2	27.94	A4	9.93
A3	22.92	A6	33.77	B1	18.00	A5	21.53
				B2	22.23	B3	24.14
				C1	20.64	B4	19.57
				C2	21.22	C3	24.14
						C4	22.02
						C5	33.60
Average	22.55	Average	32.42	Average	21.52	Average	23.15

3.3.2 Masonry Material Tests

An investigation on the mechanical properties of the masonry was performed as a student project at the British Columbia Institute of Technology, BCIT [Avendaño,2007]. Samples were made during the construction of the masonry infill walls by the mason and tested at the BCIT Department of Civil Engineering Materials Lab. These tests were performed to provide an indication of the quality of masonry tested and to obtain material properties, such as masonry compressive strength, f'm, as shown in Figure 3.6.

Figure 3.6. Experimental study on mechanical properties of masonry (reproduced from Avendano, 2007)

a) Compression test on concrete block unit

b) Mortar cubes made during construction

c) Bond strength test on prism sample

The masonry properties assessed through testing were the compressive strength, the modulus of elasticity, and bond strength of mortar to masonry units. The resulting values are presented in Table 3.2. The material tests were performed approximately 5 months after the walls were constructed, and 4 months before the first set of tests of the GLDRC infilled frames took place.

Table 3.2 Masonry Material Properties

	Compression Strength (MPa)	Modulus of Elasticity (MPa)	Bond Strength (MPa)
Concrete Block Units	55.0	---	---
Type N Mortat Cubes	1.0	---	---
Two Block High Prism	16.0	5060	---
Three Block High Prism	10.6	---	---
Four Block High Prism	16.3	---	---
Bond Test Prism Sample	---	---	0.21

This study showed that the resulting averaged elastic modulus, E_m=5060 MPa, and the masonry compression strength, f'm=16 MPa, based on 2-prism samples, were significantly lower than the CSA S304.1-04 code value, E_m=850f'm = 13562 MPa [CSA S304.1-04, 2004]. In addition, for the compression tests done on two high prisms the observed failure mode was affected by the type of capping used. When using MDF capping, the prism failure mode was "Face Shell Separation", as shown in figures 3.7.a and b, and when using hydro-stone capping, the prism failed in the "Tension Break" mode as shown in figure3.7c.

Figure 3.7. Failure mode of masonry prism samples under compression load (Avendano, 2007)

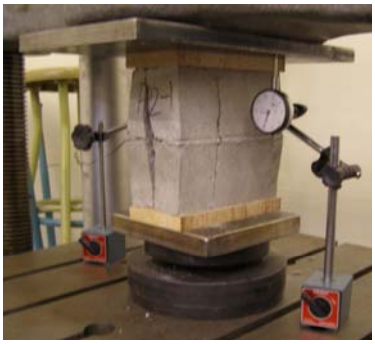

a) Compression test failure mode: Face Shell Separation

b) Compression test failure mode: Face Shell Separation

c) Compression test failure mode: Tension Break Mode

3.3.3 Dynamic Characteristics of Specimens

The equipment used included three Pinocchio WL 380 geophone sensors (Figure 3.8a). The sensors are tri-axial and each contains six geophone sensor elements used in a dual coordinate configuration. Wl 380 sensors have two modes of data collection: sensitive mode and dynamic range mode. The sensitive mode is used at a site where the vibration noise level is low. The dynamic range mode is used when the noise level is higher and the full dynamic range of the instrument is needed. The SC sensors also use GPS technology for time synchronization (Brincker, R., Ventura, C.E., and Larsen, J.A., 2007; Brincker, R., and Larsen, J.A., 2007).

Figure 3.8 Ambient vibration measurements

a) Pinocchio WL 380 geophone sensor

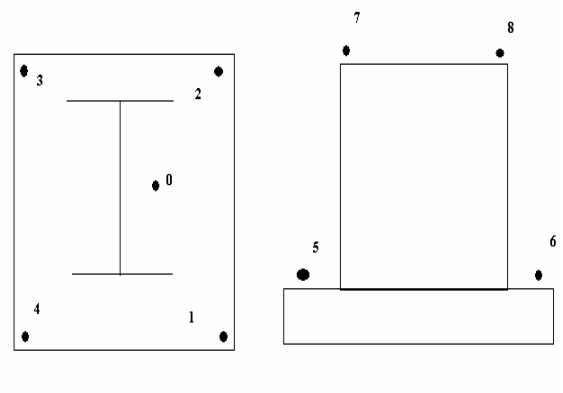

b) Diagram of location of sensors for Ambient Vibrations Tests

c) Setup for ambient vibration measurements test# 2

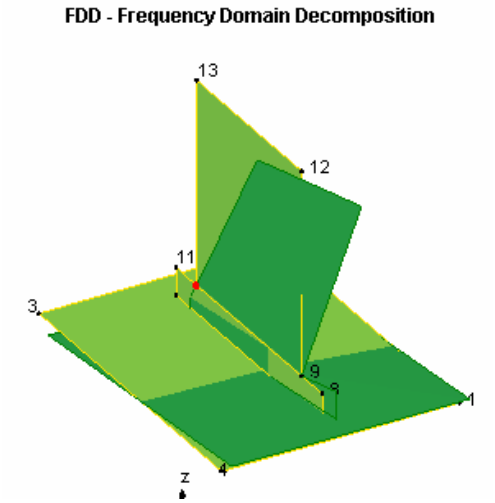

d) First mode, with f_1=7.32 Hz frequency of vibration

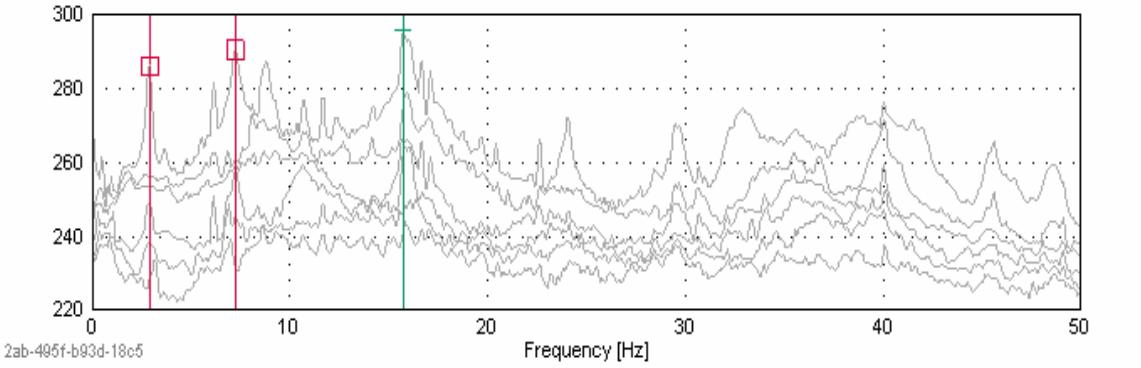

e) Frequency Domain Decomposition – Peak Picking Singular Values of Spectral Density Matrices of Test Setup 1

Two ambient vibration tests were performed. Test#1 was performed to measure the vibrations of the test specimen itself, and test#2 recorded the vibrations of the test specimen and the unidirectional shake table. Figure 3.8b presents a diagram of sensor location for tests #1 and #2. For test #1, the sensors were placed on the foundation (Figure 3.8b point 5) and at the top of the test specimen (Figure 3.8b point 7 & point 8). For test 2, sensors were placed on the four corners and center of the unidirectional shake table as well as the top of the specimen and the foundation, Figures 3.8c and 3.8d show a diagram and an illustration of the location of the sensor. Measurements were taken for 10 minutes at sampling rate of 100Hz.

The analysis was performed using the ARTeMIS Extractor software (Structural Vibration Solutions, 2003). The Frequency Domain Decomposition (FDD) method was used to estimate frequencies and mode shapes of the test specimen. The FDD technique consists of performing an approximate decomposition of the system response into a set of independent single degree of freedom (SDOF) systems for each mode. The singular values are estimates of the spectral density of the SDOF systems, and the singular vectors are estimates of the mode shapes (Brincker, R., Zhang, L., Andersen, P., 2000).

Using singular value decomposition lines the measured vibrations for test #1 determined the first in-plane mode for specimen #2, the infilled frame, to be at a frequency of 7.32 Hz and for specimen #3, the bare frame, at a frequency of 6.86 Hz.

3.5 Monotonic Tests

One test specimen was tested under monotonic static loading at the Civil Engineering Structures Laboratory. To make a distinction between this test and the dynamic tests performed later, the specimen is referred to as Specimen #1. The objective of this testing was to determine the force vs. displacement relation and failure mode for the infilled frame under static loading.

No simulation of gravity loading was provided. Lateral loading was applied by an actuator in deformation control mode, as the increments of lateral drift ratios were increased. The test was set to stop when the lateral strength of specimen was reduced by more than 20% of its ultimate resistance or when the maximum stroke of the actuator was reached.

3.5.1 Support Conditions

The test specimen's connection holes located in the foundation did not coincide with the ones existing in the strong floor of the Structures Laboratory. The support conditions required for this testing were obtained by using two structures to restrain the foundation movement. Figures 3.9 a and b illustrate the sliding restraint and vertical supports, respectively.

The specimen was restrained from sliding by placing the transverse foundation beam, expected to be in compression during loading, in contact with a rigid steel angle with stiffeners fixed to the strong floor by high strength steel rods. A gap between the specimen foundation and the anti-sliding support was filled by a hollow steel section HSS 150x150x9.5 mm.

The transverse foundation beam, to be in tension due to the resulting overturning moment during testing, was restrained from vertical movement by 2 pairs of high strength steel rods fixed to the strong floor. Each pair of high strength steel rods was joined by an HSS 350x150x9.5mm which was in contact with the transverse foundation beam by means of two 50 mm steel plates.

3.5.2 Actuator

An MTS hydraulic actuator with a force capacity of 500 kN and a stroke capacity of 150 mm was used to apply in-plane monotonic lateral loading. The actuator was rigidly joined to a steel reaction column at one end and supported with a sweible connection to a

loading plate to the top beam of the infilled frame to apply the horizontal load. The connection to the loading plate allowed for free rotations. Figure 3.10b shows the connection of the actuator to specimen 1.

Figure 3.9. Supports to restrain foundation motion for monotonic test

a) Sliding Restraint

b) Vertical support

Figure 3.10. Instrumentation for monotonic test

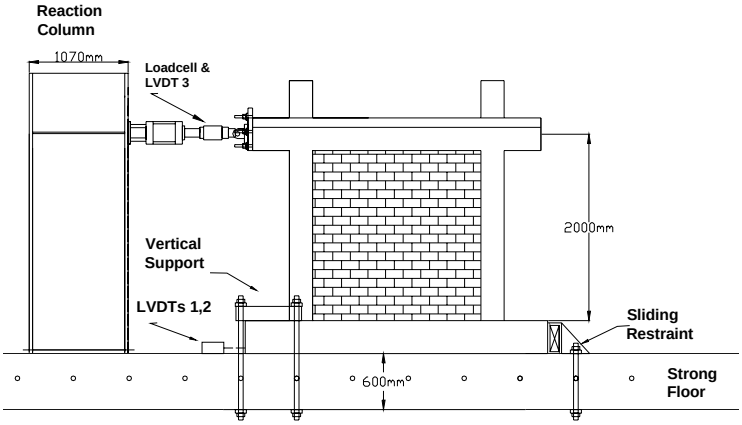

a) Instrumentation layout front view

b) Actuator and load cell

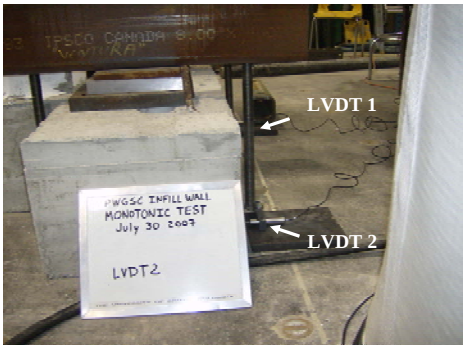

c) LVDTs measuring sliding

3.5.3 Instrumentation

The instrumentation setup monitored the applied displacements by the actuator control and the applied load by the attached load cell. In addition, lateral displacements at the base of the foundation were measured using two linear variable differential transducers (LVDT), to confirm the restraint set by the supports. Figure 3.10c illustrates the location of the instrumentation for this test.

3.6 Shake Table Tests

The primary focus of the research program was to document experimental data on the dynamic interaction of an unreinforced hollow concrete block masonry infill wall and the bounding GLDRC frame. For this objective, two GLDRC frames were tested, one bounded by an infill URM wall (specimen #2), as shown in Figure 3.11a, and one with a gap between the frame and the infill wall (specimen #3), shown in Figure 3.11b. Both specimens were tested under the same dynamic loading protocol described below.

Figure 3.11. Specimens tested on the EERF shake table

a) Specimen #2 prior to shake table test #01

b) Specimen #3 prior to shake table test #07

3.6.1 UBC EERF Shake Table

The UBC EERF shake table allows simulation of ground motions in one direction. The dimensions of the shake table are 3 m by 4 m. It has a pump with a maximum capacity of 0.53 m^3/min (140gal/min) at 20MPa pressure. This pump is driven by a 200 HP electric motor that can produce a rotational velocity of 1800 rpm.

The shake table is displacement controlled. The table is pushed and pulled by a hydraulic actuator and rides on four frictionless rollers located at the four corners. The stroke of the actuator allows the shake table to displace +/- 450mm, with a maximum applied force of 260 kN. The hydraulic pressure controls the displacement position of the table and allows up to a maximum velocity of 75 cm/s.

The earthquake ground motion is entered as a displacement command signal. The displacement signal is then normalized into a voltage value by the control computer. The command signal is sent to the MTS servo-controller, and this controller determines the level of voltage that is output to the actuator [Turek, 2002]. The input signal and measured shake table motion are monitored and stored in the control computer.

3.6.2 Selection of Ground Motions

Prior to testing, different types of ground motions that would subject the test specimens to different levels of seismic demand, varying from low to severe, were selected. The selection conditions also included that the ground motion should generate a dynamic amplification of displacements for low period structures, such as infilled frames.

The extreme-level acceleration records, called VERTEQII, were found to meet the test program conditions and were selected for this study. These records were synthetically generated ground motions for testing of telecommunications equipment [Telcordia Technologies, 1995] and designed to have a broadband frequency spectrum. The VERTEQII Z2 and the VERTEQII Z4 were selected for this study. VERTEQII Z2 had a uniform period content indicating similar acceleration demands for short and long period

systems, while VERTEQII Z4 presented a period content with high demand for short period and low demand for long period systems. In addition, an artificial record, the Extended VERTEQII Z4, was developed to simulate an extreme level long duration event. It was developed using 3 repetitions of the acceleration time history of VERTEQII Z4, resulting in a longer duration record of 80 seconds.

Also, from the 1985 Michoacan, Mexico earthquake the acceleration record from station SCT1-1985 was chosen for this study. This record presented a high dynamic amplification of 5.8 in the response spectra for a period T=2.0 seconds. Two acceleration records were developed by modifying the time step in SCT1-1985 so as to obtain high dynamic amplification factors for the period of vibration of the test specimen (obtained from the dynamic characteristic study performed prior to shake table testing). As a result, two acceleration records were obtained, that is SCT1-1 Modified #1 and Modified #2 with predominant periods of T_p=0.20 sec and T_p=0.50 sec respectively.

All acceleration records were normalized to have maximum acceleration of 0.50g at the 100% amplitude. Figures 3.12 and 3.13 show the acceleration and displacement time histories of each selected ground motion record. The response spectra of each selected ground motion at 100% amplitude was compared to the Canadian national building 2005 code design spectrum for Vancouver, B.C., soil class “C” [NRC, 2005] as shown in Figure 3.14.

3.6.3 Series of Shake Table Tests

As illustrated in Figure 3.15, initially the surcharge load was set at 62 kN and used for testing for the VERTEQII Z2 ground motion record. To increase the quality of the motion output, the surcharge load was reduced to 33 kN for all subsequent ground motion records. Tests #11 to #14 were performed with no surcharge load, to monitor its effect on the measured displacements of the shake table relative to the control signal displacements for VERTEQII Z4.

Figure 3.12. Acceleration time history of selected ground motions at 100% amplitude

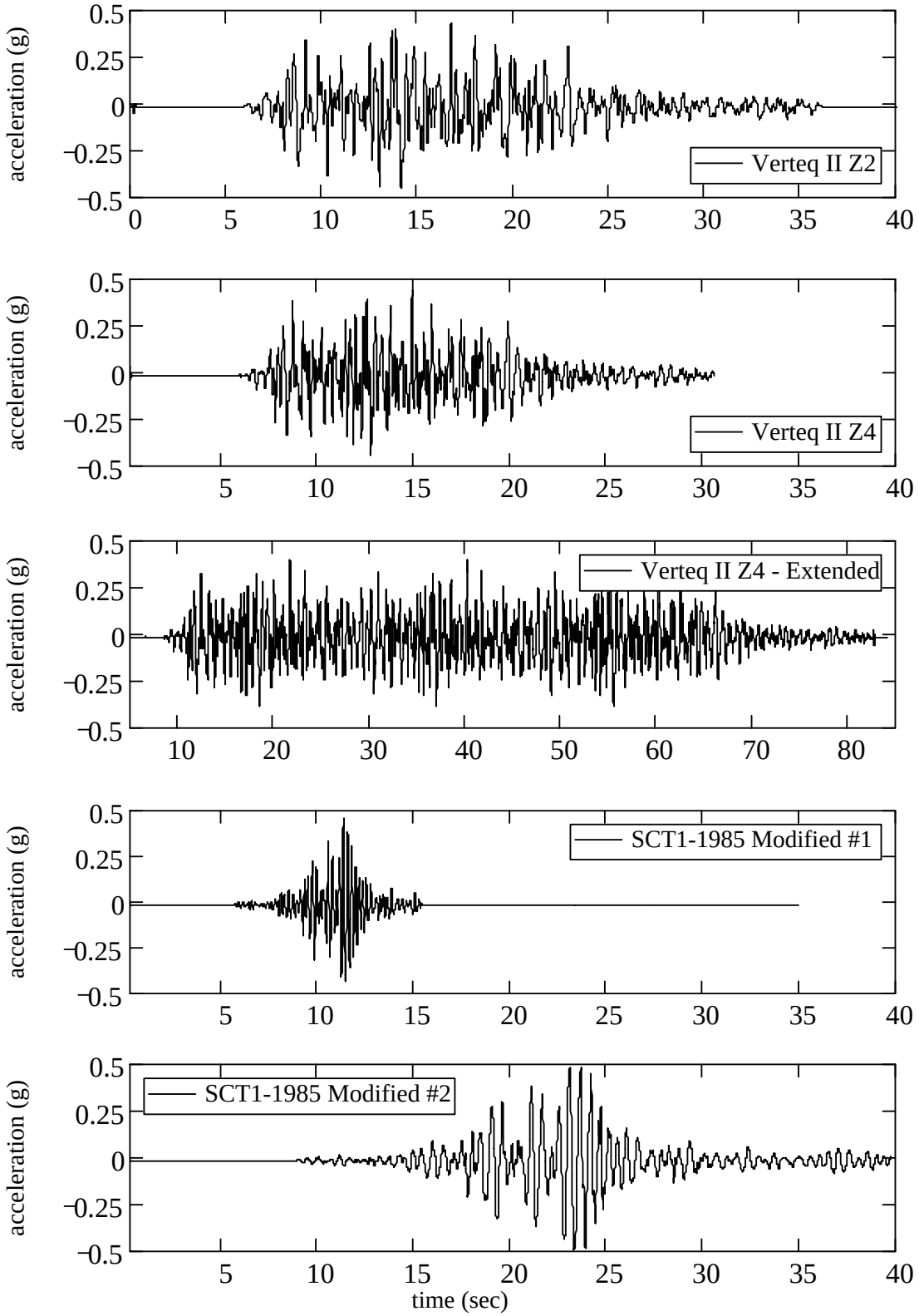

Figure 3.13. Displacement time history of selected ground motions at 100% amplitude

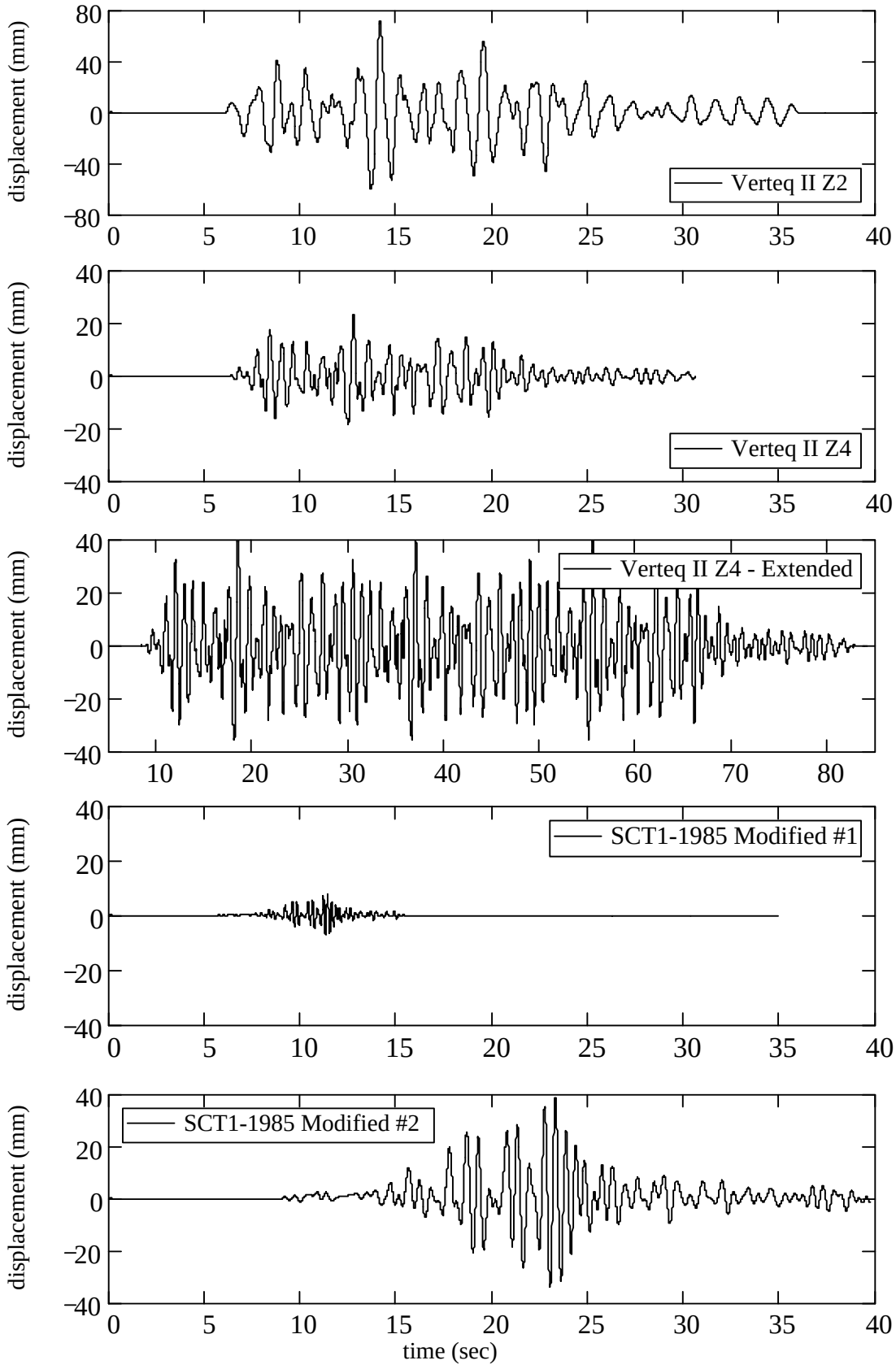

Figure 3.14. Comparison of acceleration response spectrum of selected ground motions at 100% amplitude vs NBCC 2005 design spectrum for Vancouver, B.C.

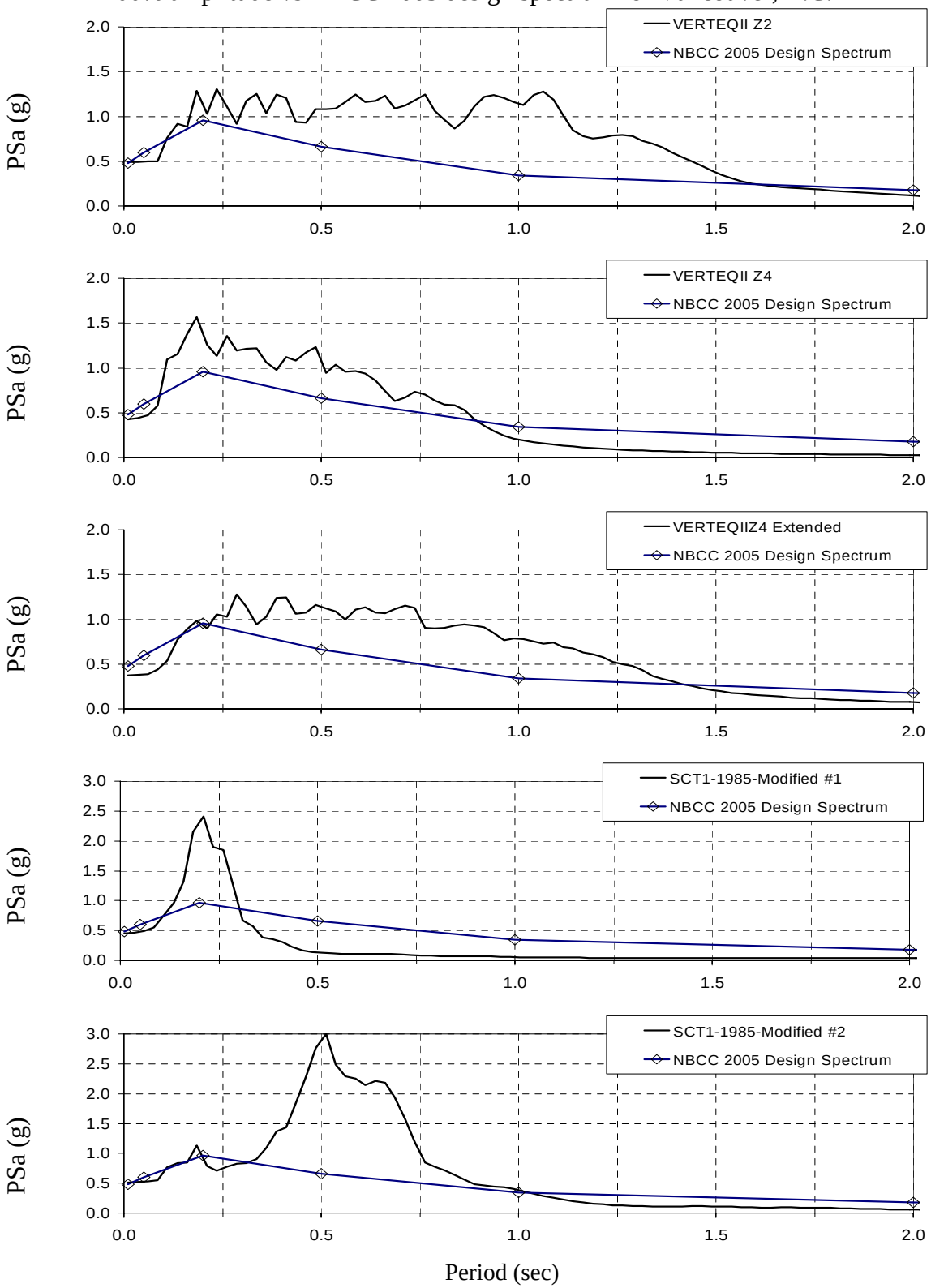

Figure 3.15 Surcharge loads used during shake table tests

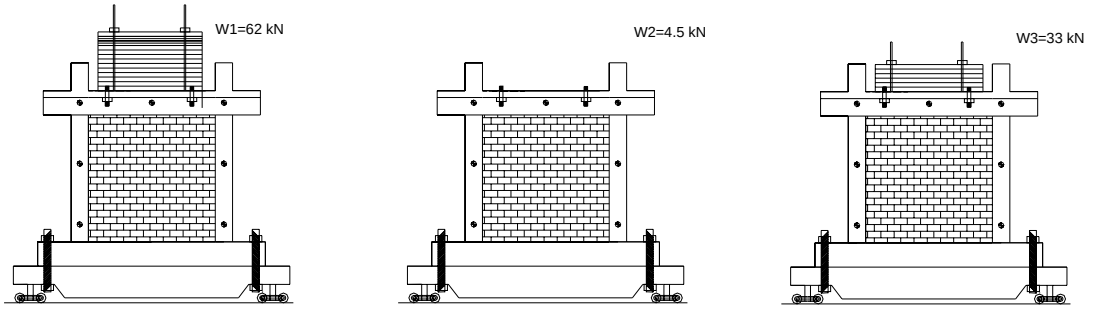

a) Tests 1 - 10 b) Tests 11 - 14 c) Tests 15 - 31

The shake table test program was organized into 5 series of tests, presented in Table 3.3. The surcharge load was changed at different stages of the testing program. Specimen #2 was subjected to all 33 shake table tests and specimen #3 was subjected only to the first 8 tests in test series A.

3.6.4 Test Setup

Each specimen was lifted by four lifting hooks located at four corners of the foundation, as shown in Figure 3.16a. The lifting hooks were 15M rebar deformed and embedded into the concrete foundation during construction. The location of each hook is illustrated in Figure 3.16b.

The test specimen was lifted by the EERF crane and located on top of the shake table. Between the specimen foundation and the shake table, a 3.4" (19mm) thick plywood sheet was set to ensure improved surface contact. The specimen was then fixed to the shake table by use of high strength threaded steel fasteners. Four connection points were set in the shake table and the foundation for the threaded fasteners to go through, as shown in Figure 3.16b. This sliding friction connection ensured there are no relative displacements between the specimens foundation and the shake table.

Table 3.3: Shake Table Testing Protocol

Test Series	test #	Earthquake Record	Amplitude	Max Accel (g)	NOTE
A	01	VERTEQII Z2	50%	0.25	Surcharge Weight = 62 kN
	02		100%	0.50	
	03		150%	0.75	
	04		200%	1.00	
	05		250%	1.25	
	06		300%	1.50	
	07		320%	1.60	
	08		340%	1.70	
	09		400%	2.00	
	10	VERTEQII Z2 Sequence of 3	400%	2.00	3 sequential records are run with 30 secs waiting time
B	11	VERTEQII Z4	100%	0.50	Steel Plates Removed
	12		150%	0.75	
	13		200%	1.00	
	14		250%	1.25	
C	15		100%	0.50	6 Steel Plates Added Surcharge Weight = 31 kN
	16		150%	0.75	
	17		200%	1.00	
	18		250%	1.25	
	19	VERTEQII Z4 Sequence of 3	225%	1.13	3 sequential records are run with 30 secs waiting time
D	20	Extended VERTEQII Z4	300%	1.50	
	21	Modified SCT1 1985 1	300%	1.50	
	22		300%	1.50	
	23		300%	1.50	
	24	Extended VERTEQII Z4	200%	1.00	
	25		225%	1.13	
	26		250%	1.25	
	27		275%	1.38	
	28		300%	1.50	
	29		300%	1.50	
	30		300%	1.50	
E	31	Modified SCT1 1985 2	400%	2.00	
	32	Extended VERTEQII Z4	200%	1.00	
	33		200%	1.00	

Figure 3.16. Test Setup- Specimen Foundation Details

a) Specimen #2 lifted by crane by foundation

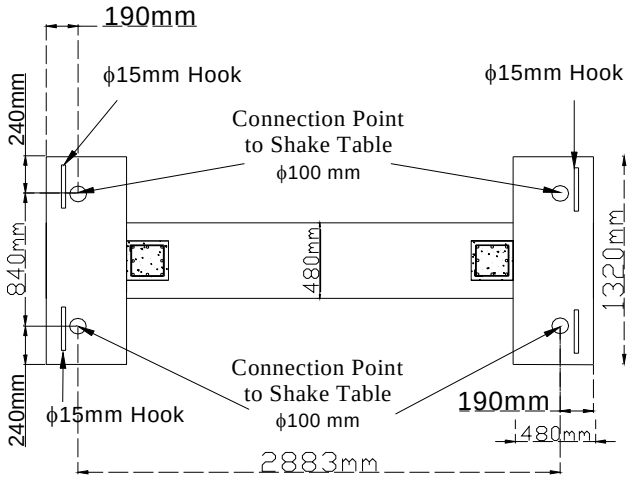

b) Connection Points Foudnation. Plan View

A surcharge load was added to the top of the specimen. The surcharge load was selected to generate inertial forces in the specimen during the simulated earthquakes. The surcharge load was achieved by the use of a set of steel plates. Plate dimensions were 1500mm x 700 mm x 65mm, weighing approximately 4.45 kN.

Threaded fasteners, ϕ22mm, were used to assemble the surcharge mass by passing through predrilled holes in the steel plates. Different surcharge assemblies were used in accordance to the testing protocol. The surcharge assembly was connected to the specimen slab by four threaded fasteners, ϕ38mm. Figure 3.17a shows an illustration of the connection points of the steel plates in one assembled surcharge load.

To restrain the out-of-plane motion of the surcharge load assembly, a steel angle was welded at each side of the top plate. These angles allowed for the attachment of two cables to be connected to two respective turnbuckles, as illustrated in Figure 3.17b. Each turnbuckle was connected firmly to the shake table.

A safety mechanism was provided to catch the surcharge load in case of specimen collapse. Steel nuts were threaded onto the top plate where two eyebolts would be connected to the overhead crane by a set of straps.

Figure 3.17. Test Setup- Surcharge Load Details

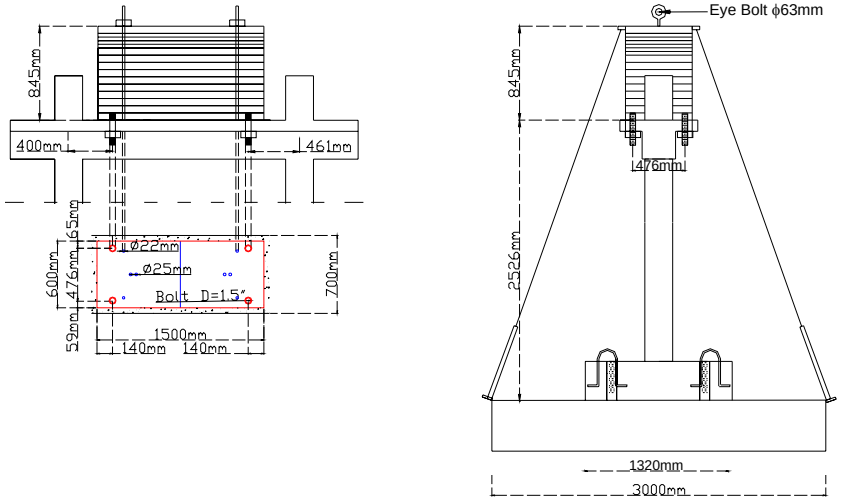

a) Surcharge Load Assembly Front and Plan View

b) Surcharge Load Assembled Side View

3.6.4 Instrumentation

The instrumentation for this experimental program consisted of piezo resistive accelerometers, position transducers and LVDTs to measure the lateral motion of the specimen and shake table. The following section describes the instrumentation scheme used for each specimen.

All signals captured by the instrumentation were stored in one data acquisition system. All signals were recorded with a low pass filter of 50 Hz. The motion was also tracked by the use of a high speed camera. A total of seven target points were located on each specimen.

Specimen #2

Figure 3.18 shows the layout of the location of the instrumentation for specimen #2, with each instrument represented by a letter. Table 3.4 shows the instrumentation information associated with each letter, which are the instrument, type, the channel ID used for the data acquisition and the measurable amplitude range of the signal.

Figure 3.18 Instrumentation layout for specimen #2.

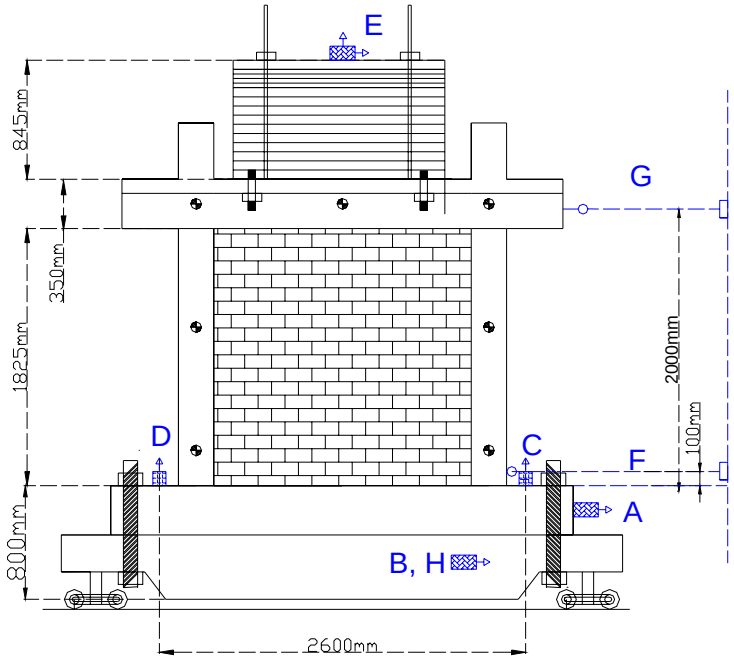

Table 3.4: Instrumentation specifications for specimen #2

Instrument		Channel ID	Type	Range
Uniaxial Piezo Resistive Accelerometer	A	A1D-8	ICSensors Model 3110	+/- 10 g
	B	TAccel		+/- 10 g
	C	A1D-5		+/- 10 g
	D	A1D-6		+/- 10 g
Triaxial Piezo Resistive Accelerometer	EX	A3D-X	ICSensors Model 3026	+/- 5 g
	EY	A3D-Y		+/- 5 g
	EZ	A3D-Z		+/- 5 g
Position Transducer	F	SP13	Celesco Cable-Extension Model PT101-0150-111-1110	3000 mm
	G	SP19		3000 mm
LVDT	H	TDisp	MTS Model LPRCVU03601	920 mm

Accelerometer A was used to monitor if sliding of the foundation had occurred during testing. Accelerometer B measured the base excitation generated by the shake table. Accelerometers C&D were used to measure absolute vertical motion of the specimen above the foundation level, to later calculate the rotations due to foundation flexibility or uplift during testing. Accelerometer E measured the inertial acceleration of the surcharge mass at the top of the specimen.

To later calculate relative displacements, position transducer F was connected at the base of the RC column and position transducer G connected at the level of the slab, while the shake table displacements were measured by the LVDT H connected to the actuator.

Specimen #3

The instrumentation for specimen #3 follows the same layout described for specimen #2 with the addition of some new instrumentation to monitor in more detail the response of the GLDRC frame response. Similar to specimen #2, Figure 3.19 and Table 3.5 show the instrumentation location and information. Additional position transducers, K and J, were located along the length of one of the specimen's columns to obtain its deformation shape. High precision position transducers were located at the base of the opposite column to measure absolute vertical deformations to later calculate total and relative column rotations.

Figure 3.19 Instrumentation layout for specimen #3.

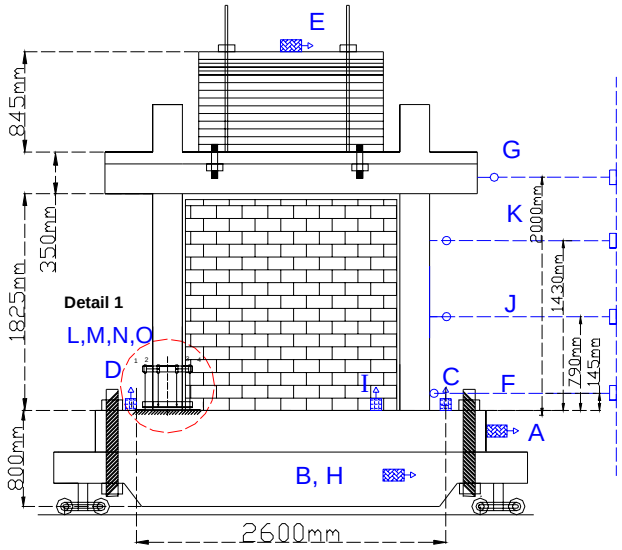

a) Instrumentation layout front view.

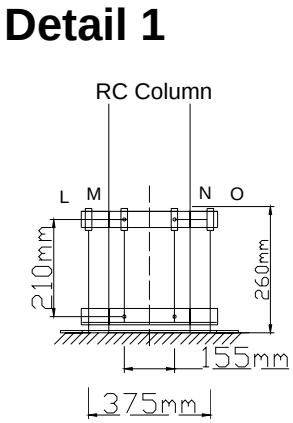

b) Instrumentation Column Base

Table 3.5: Instrumentation Specifications for Specimen #3

Instrument		Channel ID	Type	Range
Uniaxial Piezo Resistive Accelerometer	A	A1D-1	ICSensors Model 3110	+/- 10 g
	B	TAccel		+/- 10 g
	C	A1D-5		+/- 10 g
	D	A1D-3		+/- 10 g
	E	A1D-2		+/- 10 g
	I	A1D-4		+/- 10 g
Position Transducer	F	SP-14	Celesco Cable-Extension Model PT101-0150-111-1110	3000 mm
	G	SP-19		3000 mm
	J	SP-17		3000 mm
	K	SP-18		3000 mm
	L	LP-07	Novotechnik Type TR100	105 mm
	M	LP-08		105 mm
	N	LP-09		105 mm
	O	LP-10		105 mm
LVDT	H	TDisp	MTS Model LPRCVU03601	920 mm

Chapter 4 – Results and Observations

4.1 General

This chapter presents the results of the test programs described in Chapter 3 performed on the selected test specimens. Section 4.2 summarizes the results of the monotonic test, which determined the maximum attained in-plane attained lateral strength and deformation capacity under monotonic loading, as well as the structural weakness at the location of the connection of the columns to the foundation. Sections 4.3 and 4.4 summarize the observations of the dynamic response for the series of shake table tests performed on specimen #2 and specimen #3, respectively.

4.2 Specimen #1 Monotonic Loading

A GLDRC frame bounded by an URM infill wall was tested under monotonic loading until reaching the maximum drift of 3.80%. The objective of this test was to determine the force vs. displacement curve and the failure mechanism for this structure under in-plane static loading.

Instrumentation data captured the sliding displacement history at the foundation level, which only reached a total value of 2.2 mm. This indicated that the foundation could be treated as a fixed support condition. The top lateral deformations presented in this section have been corrected and do not include the sliding displacement component.

At different displacement values, the test was interrupted to mark cracking in the specimen components. During this pause the actuator maintained the applied load and displacement. Incremental loading continued to increase after each pause and it was observed that the load readings would drop slightly from the previous value. This effect is influenced significantly by the unreinforced masonry infill strength, because these drops in the readings increased in value once the infill was significantly cracked.

4.2.1 Force vs Displacement Curve

The force vs displacement relation is shown in Figure 4.1. The linear elastic stiffness was determined to be 11.5 kN/mm. Yielding was observed at 1.00% drift, reaching a lateral load of 205 kN. After yielding, there was a slight strain hardening effect reaching a maximum value of 220 kN. No strength degradation occurred before the maximum displacement was reached.

Figure 4.1 Force vs drift curve for monotonic loading

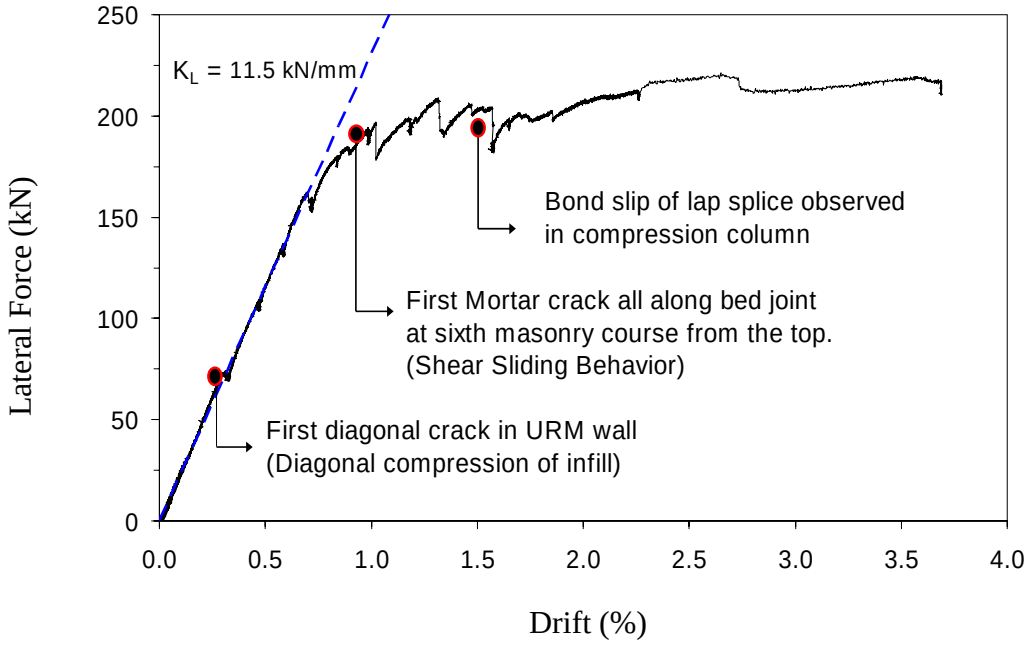

The constant slope in the force vs. displacement curve, prior to yielding, indicates that the infill contributes to the overall stiffness at low load levels. This may suggest that the mortar interface transmits compression stresses to the masonry infill even at small displacement amplitudes.

4.2.2 Load Resisting Behavior and Failure Mechanism

The cracking pattern of the specimen was monitored to observe the behavior of the specimen at the different loading stages. The mechamism of lateral load resistance specimen lateral load resisting behavior changed from a diagonal compression mode to

shear sliding mode and culminated with a full plastic mechanism governed by bond slip of the rebar at the column base.

Diagonal Compression Behavior

Initiation of cracking developed at the masonry infill wall first, at 0.30% drift, in the form of a set of two diagonal cracks, with a 45 degree inclination, as shown in Figure 4.2a. As loading continued, no additional diagonals were formed, and the existing diagonal patterns only increased in length. At the drift level of 0.625% diagonal crack pattern extended on both sides of the bounding frame, as shown in Figures 4.2b and c. At 0.77% drift, a new diagonal crack was observed formed close to the compression column, as shown in Figure 4.2d. In addition, two horizontal cracks were observed along the bed joints.

Figure 4.2 Diagonal Compression Mode of URM Infill Wall

a) Drift 0.30%

b) Drift 0.50%

c) Drift 0.625%

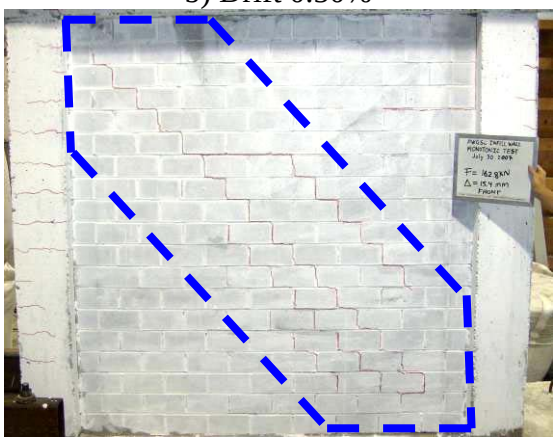

d) Drift 0.77%

The diagonal cracks were located in close vicinity to one another tracing the region of highest compression stress in the masonry infill, see Figure 4.2d. As described in the literature, [Paulay and Priestley, 1992], this behavior is often compared to a diagonal compression strut. The width of this compression strut was approximately one quarter the diagonal length.

At 0.625% drift, at the tension column, hairline flexural cracks developed along the entire length, and a hairline flexural crack developed at the end of the connecting beam, see Figure 4.3a. At the compression column, hairline flexural cracks were observed along the top third of its length, see Figure 4.3b. These flexural cracks were formed at the location of the column transverse reinforcement.

Figure 4.3 Hairline cracks in GLDRC frame

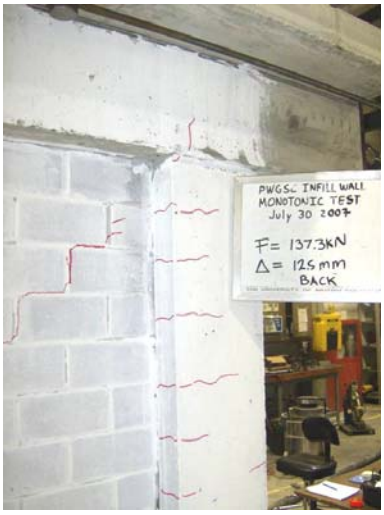

a) Drift 0.625%
Tension Column

b) Drift 0.77%
Compression Column

Shear Sliding Behavior

At 1.00% drift, the sliding mode was observed confirmed by relative displacement of the blocks with respect to the cracked header joints, as shown in Figure 4.4a. In addition, the end of the beam connected to the tension column showed an increase in length top of the previously observed hairline flexural crack. This flexural crack ran all across the top of

the beam; this indicates that the positive cracking moment was exceeded for this location, and represents a loss in rotational stiffness of the beam.

Figure 4.4 Shear sliding behavior of infill

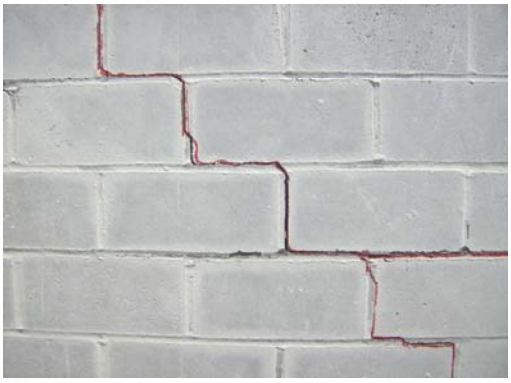

a) Opening of head joints

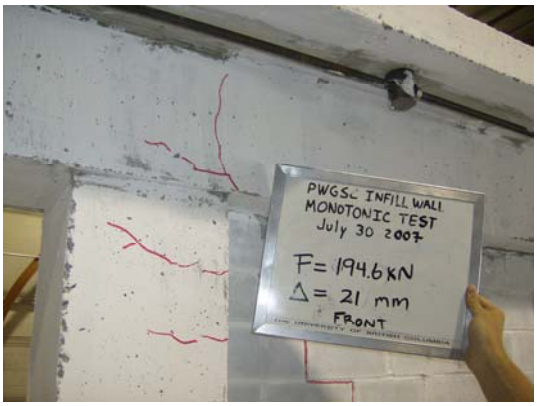

b) Flexural crack at the end of the beam connected to tension column

At 1.00% drift, several horizontal cracks formed along the bed joints of the URM wall due to bed-joint sliding mechanism. One horizontal crack extended along the full length of the wall was formed at the sixth course from the top of the URM wall as shown in Figure 4.5a. Additional smaller horizontal cracks were formed at higher drift levels, located at the bottom two courses. Also, new diagonal cracks were observed located closest to the compression column and ending at the intersection with the longer horizontal crack.

Figure 4.5 Shear Sliding Mode of URM Infill Wall Drift 1.00% - 1.25%

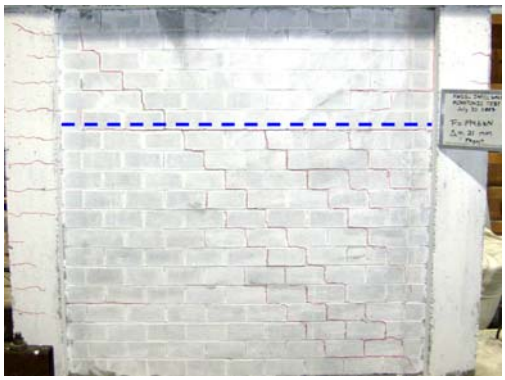

a) Drift 1.00%

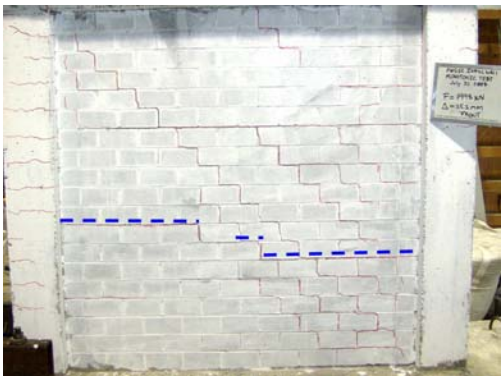

b) Drift 1.25%

During this lateral load resisting behavior, the variations of the force deformation curve (Figure 4.1) is attributed to load based cracking and subsequent load redistribution in the infill panels. As the deformation increased to 1.25% drift, three new horizontal cracks formed, spreading along the full length of the specimen, as shown in Figure 4.5b. At a drift of 1.65%, several new horizontal cracks formed, as shown in Figure 4.6a. At a drift of 3.55%, no additional horizontal cracks were found, as shown in Figure 4.6b. The sliding mechanism was not observed beyond the 1.65% drift level.

Figure 4.6 Shear sliding mode of URM infill wall and bond slip of lap splice
Drift 1.65% - 1.25%

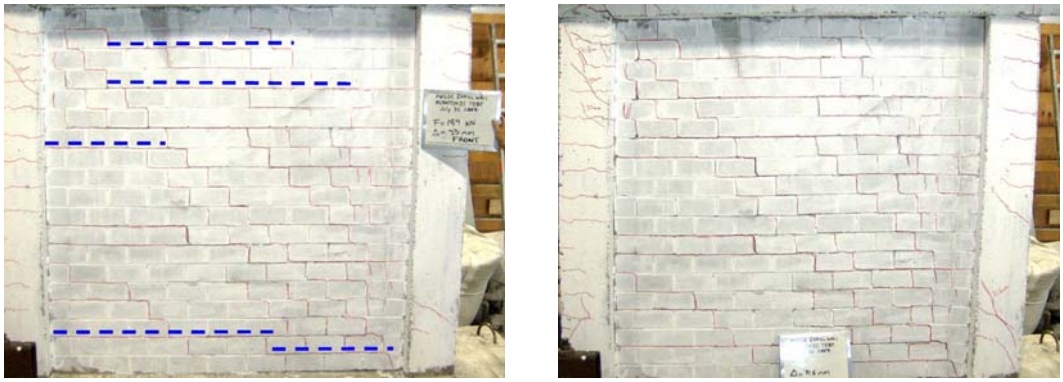

a) Drift 1.65% b) Drift 3.55%

Bond Slip of Lap Splice Behavior

At a drift of 1.65%, the base of the compression column in contact with the foundation beam showed splitting of the concrete that continued onto the foundation in the form of a vertical crack, see Figure 4.7a. As the deformation increased to 3.55% drift, the cracked concrete at the base of the compression column opened up and allowed free rotation, see Figure 4.7b.

At 1.65% drift, vertical cracks were observed at the base of the tension column, coinciding with the location of the lap splice of the longitudinal rebar, see Figure 4.8a. At 3.55% drift, vertical cracks observed as split cracking of concrete were found that extended in length until the end of the lap splice of the longitudinal rebar. In addition,

the 90 degree hooks of the column ties opened up losing confinement and allowing the rebar to bend outwards, see Figure 4.8b.

There was no physical indication of the formation of plastic hinges at the column base despite having reached a perfectly plastic behavior and a drift of 3.55%. Both columns, along the length of their lap splices, showed no clear development of flexural cracks. This suggests that the free rotation and splitting of concrete are evidence of problems due to cold construction joints and inadequate lap splices, thus preventing rebar yielding, as confirmed in the literature [Cho and Pincheira, 2006].

At this stage, shear cracks developed at the top of the tension column and the corresponding joint, as shown in Figure 4.9a. Flexural cracks were observed at the concrete slab for 1.65% drift of, as shown in Figure 4.9b.

Figure 4.7 Rotations at the base of the compression column

a) Drift 1.65%

b) Drift 3.55%

Figure 4.8 Concrete splitting at the lap splice of the tension column

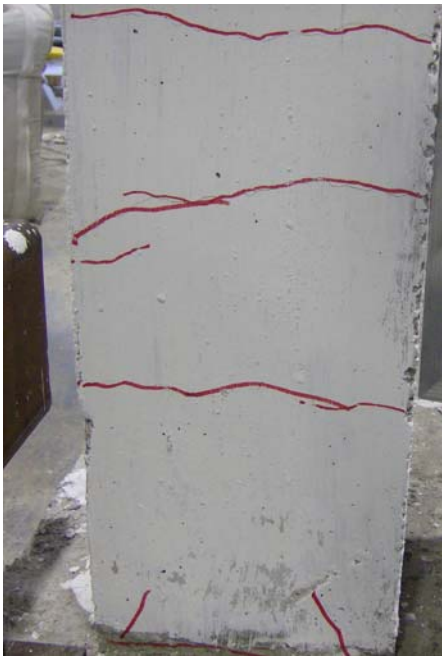

a) Drift 1.65%

b) Drift 3.55%

Figure 4.9 Additional damage in GLDRC frame

a) Drift 1.65 - 3.55%
shear cracks developed
top the tension column and the
beam-column joint

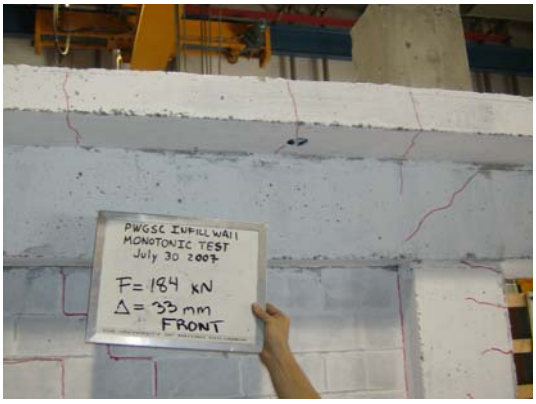

b) Drift 1.65%
flexural cracks formed
at GLDRC slab

4.3 Specimen #2 Dynamic Loading of Infilled Frame

This section describes the results of the shake table tests that were performed on the Specimen #2, a GLDRC frame bounded by an URM infill wall. A total of 33 separate earthquake runs were performed on Specimen #2, divided into five series, following the testing protocol presented in Table 3.5. The excitation acceleration, top absolute acceleration and top displacement time histories, as well as the hysteretic response and instantaneous displacement for all the performed shake table tests, are presented in Appendix B.

4.3.1 Observations

This section presents a description of the significant behavior of specimen #2 during the different earthquake runs. The descriptions are obtained based on the study of the test videos as well as inspections made on the specimen after each test.

Test Series A

For this initial testing series the surcharge weight used was 62 kN. This series of tests consisted on 10 shake table tests using the VerteqIIZ2 acceleration record. The testing program initiated at 50% amplitude to reach a maximum peak ground acceleration of 0.25g, as described in Table 3.4. All 10 shake table tests were performed on June 08 2007.

The observed effects of the dynamic response of the specimen were mainly concentrated on the URM wall. The cables of the accelerometers measuring vertical motions showed large amplitude motion in the lateral direction at all times during testing.

The response for tests #01 through #03 showed vibrations with small amplitudes, demonstrating a highly rigid body motion. After these first three tests there was a noticeable loss of bond at the interface between the URM wall and the GLDRC frame.

This was observed as a cracked mortar joint that left a 2 mm gap between the infill wall and frame, as shown in Figure 4.10a. This gap allowed for out-of-plane flexibility; however it did not allow for sufficient rotation of the top masonry blocks under the GLDRC beam to result in out–of-plane collapse of the URM wall.

Figure 4.10 Observed damage of specimen 2 during tests #01-#03

a) After test #03
Mortar interface cracked

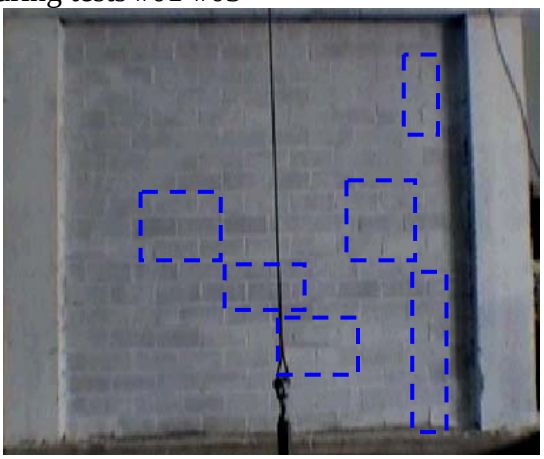

b) During test #02
Header joints opening in tension
(URM wall back view)

During the response for test #02, the test video shows some head joints of the URM wall opening in tension with the location of these head joints shown in Figure 4.10b. This same behavior was seen in tests #03 though #06. After the end of each of these shake table tests, no cracks were noticed in the masonry joints.

During test #07, there was spalling of the mortar joint at the right side of the URM wall located at the eighth masonry course from the top. After the test, two diagonal patterns of mortar cracking were found in the URM wall, each spanning to opposite ends of the wall. One diagonal crack pattern spans from the left of the fourth masonry course from the top, to the bottom right corner of the wall. The other diagonal crack pattern spans from the right of the seventh masonry course from the top, to the bottom left corner of the wall. Both cracks intersected in the middle of the twelfth masonry course from the top. In addition, the initiation of shear sliding cracks began developing at the bed joints of the

seventh masonry course from the top, at both the left and the right of the URM wall. Figure 4.11 shows the front and back view of the cracked URM wall after test#07.

Figure 4.11 Observed damage of specimen 2 after test#07

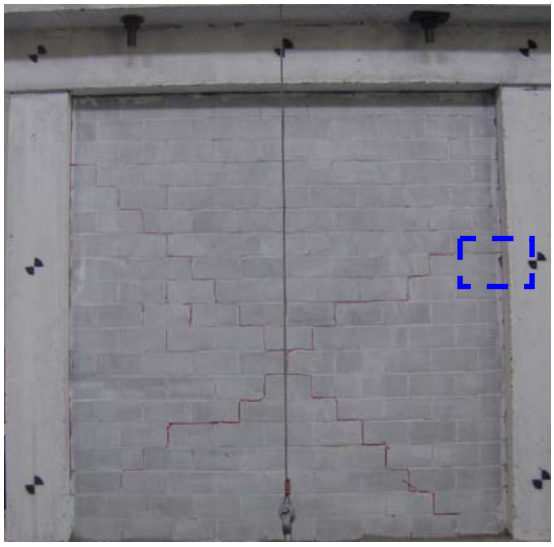

a) After test #07
Diagonal crack patterns initiated
Spalling of mortar joint
(URM wall front view)

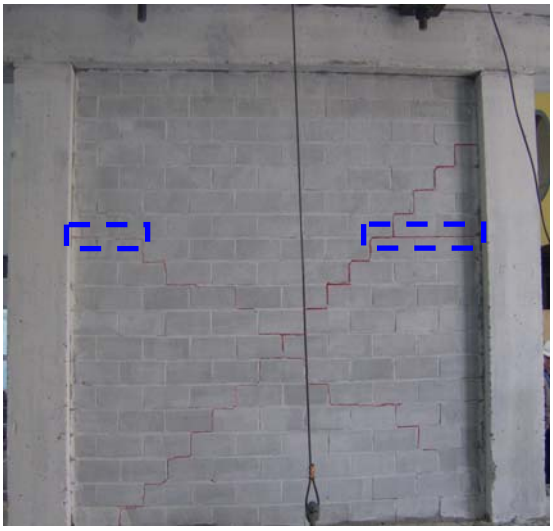

b) After test #07
Mortar cracks due to sliding at eight
masonry course from the top
(URM wall back view)

During test #08, the shake table tests began to show sporadic vertical displacements resulting in the rocking motion at the foundation level of the specimen. At this stage of testing the steel plates showed significant sliding between plates.

The dynamic response of the specimen during test #08 showed significant sliding of the URM wall along the longer diagonal crack pattern. During this rocking motion, the sliding displacement of the wall showed some deformation in the direction perpendicular to the diagonal crack pattern.

After test #08, more mortar cracks were observed in the lower courses of the masonry wall, as shown in Figure 4.12a. For this test, there was the first observation of flexural cracks in the GLDRC frame. This crack was found in the left end of the beam and within the beam column joint, as shown in Figure 4.12b.

Mortar cracks formed across all the bed joints of courses seven, nine and fourteen from the top of the URM wall, after test #09, indicating the shear sliding failure of the masonry wall. Also observed after this test, was the first crack developed in one of the concrete blocks in the masonry wall. The concrete block, located at the lower right corner of the wall, presented a diagonal crack across half of its face shell which were consistent with observed damage for the prism compression tests shown in section 3.3.2. The GLDRC beam developed more flexural cracks in the flange, near the ends of the beam. Also a flexural crack at the right corner indicated that beam reached its negative cracking moment at this location. Mortar spalling was observed in the center of the wall, mostly at the bed joints at the intersection between the two diagonal crack patterns.

Figure 4.12 Observed damage of specimen 2 after test#08

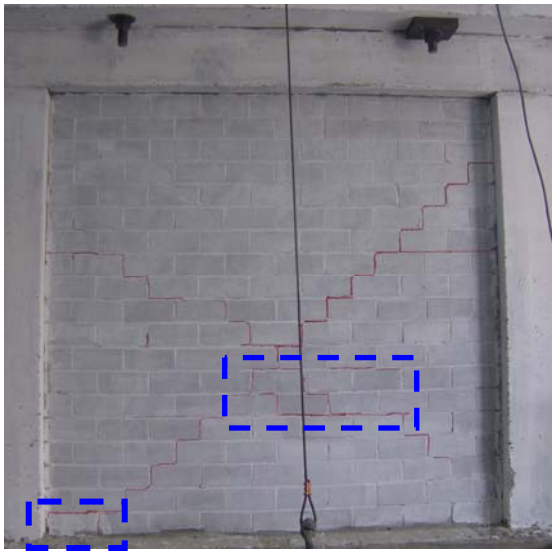

a) After test #08
More mortar cracks due to sliding
(URM wall back view)

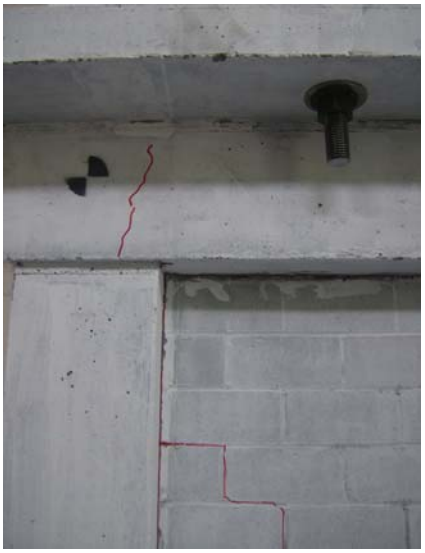

b) First flexural crack formed at
left end of GLDRC beam

Test Series B

For this testing series the assembled steel plate surcharge weight was removed. This series of tests consisted of 4 shake table tests using the VerteqIIZ4 acceleration record. The testing program initiated at 100% amplitude to reach a maximum peak ground

acceleration of 0.50g, as described in Table 3.4. These 4 shake table tests were performed on June 13, 2007.

Figure 4.13 Observed damage of specimen 2 for tests #09 and #14

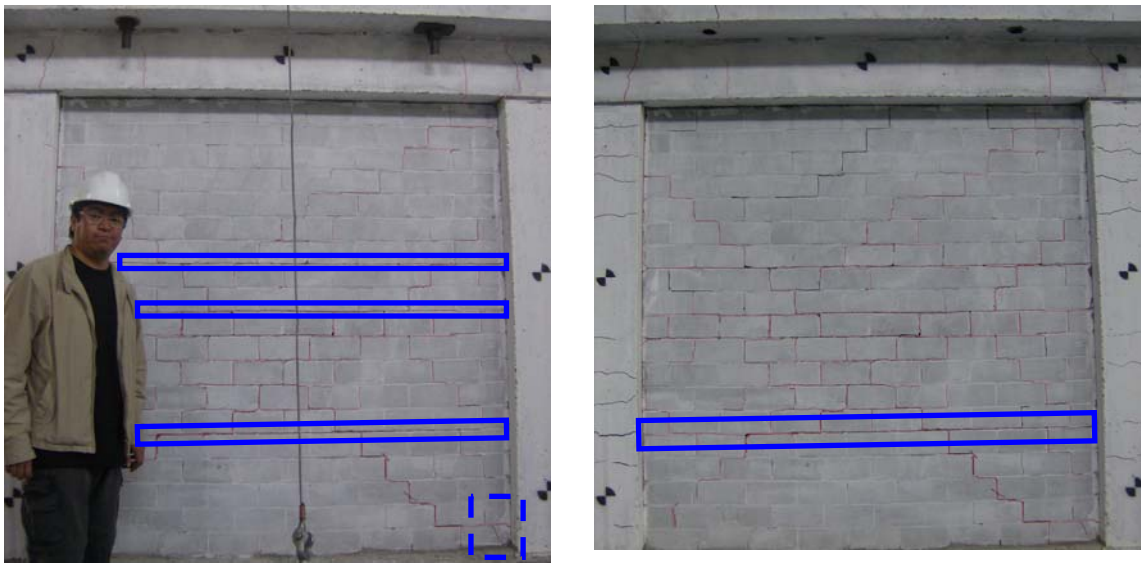

a) After test #09
Initiation of Shear Sliding
(URM wall front view)

b) After test #14
Flexural cracks in columns
(URM wall front view)

The removal of the surcharge weight for this test was to improve the shake table fidelity in reproducing the input ground motion. This also provided the opportunity to observe the response of the infilled frame specimen without the contribution of loading on the GLDRC beam.

By following the response of the specimen for tests #13 and #14, as the amplitude of motion was significantly larger, it was clearly observed that a great portion of the masonry wall slid along the lowest existing shear sliding crack formed during test #09, located on the fourteenth masonry course from the top. During this motion, the existing mortar cracks opened and closed in the portion of the wall above this sliding plane. During the sliding phase, the GLDRC frame confines the URM wall as well as restrains its motion. During these tests the opening and closing of existing cracks, in particular the flexural crack located on the left end of the beam, was observed in the GLDRC beam.

After test #14, several hairline flexural cracks were found all along the length of the GLDRC columns. These cracks were found on all four faces of the columns and coincide with the location of the column transverse reinforcement, as shown in Figure 4.13b. For both columns, four flexural cracks were found below the beam column joint and four above the end of the reinforcement lap splice. Only one flexural crack was formed in the location of the reinforcement lap splice for the left column, approximately 100 mm above the foundation level.

Test Series C

For this testing series a surcharge weight was added of 31 kN. This series of tests consisted of 5 shake table tests using the VerteqIIZ4 acceleration record. The testing program initiated at 100% amplitude to reach a maximum peak ground acceleration of 0.50g, as described in Table 3.4. These 5 shake table tests were performed on June 15, 2007.

The shake table tests performed during this series of tests showed no rocking motion for tests #15 through #17. The shake table presented significant rocking motion for tests #18 and #19.

During the response of the specimen for tests #15 through #19, the URM wall maintained the sliding behavior along the bed joints of the fourteenth masonry course. The video records, facing the back view of the specimen, show the GLDRC columns having significant rotations at 500 mm above the foundation level, observed as the flexural cracks opening and closing. These local deformations coincide with the location of the sliding plane of the cracked URM wall, as shown in Figure 4.14a.

As the specimen became more flexible, the response also showed important local deformations at the lower ends of the GLDRC columns and URM wall. The video recordings do not allow determining if there are cracks opening and closing at the location of the column-foundation interface.

Figure 4.14 Observed damage of specimen 2 for tests #19 and #27

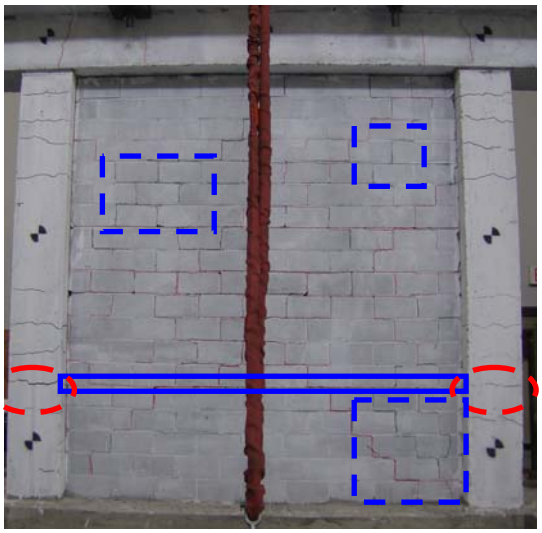

a) After test #19
Significant local deformations of the GLDRC columns at the location of the sliding plane of the URM wall
(URM wall front view)

b) After test #27
Sliding of URM blocks out of plane
(URM wall front view)

After these tests, new mortar joint cracks were observed mainly in the upper corners of the URM wall. During test #19, significant mortar spalling occurred at the bed joints of the wall along the sliding plane of the URM wall.

Test Series D

For this testing series the surcharge weight used in the previous test series was maintained. This series of tests consisted on 10 shake table tests using the Extended VerteqIIZ4 and the Modified SCT1-1985-#1 acceleration records. The testing program initiated at 100% amplitude to reach a maximum peak ground acceleration of 0.50g, as described in Table 3.4. The 10 shake table tests were performed on two days (June 15 and 19, 2007).

The shake table tests #21 through #23 were performed using the Modified SCT1-1985-#1 acceleration record, at amplitude of 300%, and resulted in high rocking motions. The shake table resulting displacement time history was not close to the selected input record. The shake table tests #24 through #30 were performed using the Extended VerteqIIZ4

acceleration record. The shake table tests #27 through #30 resulted in high amplitude rocking motion.

During tests #20 through #26 the specimen responded in a shear sliding behavior and additional cracks developed in the GLDRC beam. On test #27, the specimen's URM wall presented mortar spalling and sliding out-of-plane of several concrete blocks in the upper courses, as shown in Figure 4.14b. Tests #28 and #29 showed more concrete blocks in the URM wall sliding out-of-plane. During test #30, the upper right corner of the URM wall collapsed out of plane as shown in Figure 4.15. The video of the response shows the concrete blocks sliding along empty space left by the spalled masonry in the head joints of the top first masonry course and at the interface with the GLDRC frame.

Figure 4.15 Observed damage of specimen #2 for test #30

a) top corner concrete block sliding out of plane (back view of URM wall)

b) URM wall out of plane collapse (back view of URM wall)

Test Series E

This series consisted of a total of 3 shake table tests using the Extended VerteqIIZ4 and the Modified SCT1-1985-#2 acceleration records. All shake table tests were performed on June 20, 2007. The testing program was stopped after test#33 due to observed buckling of the shake table vertical supports, which had resulted from the high amplitude

rocking motion of previous tests and the consequent impact loading of the vertical supports.

For this test series, the GLDRC frame was tested with the masonry wall that had remained after the out of plane failure in test #30. The objective was to observe how this failed infill wall that resulted in a captive column, as observed in Figure 4.16, could cause shear failure in the GLDRC frame during the dynamic response. The tested masonry wall consisted of the first 10 lower masonry courses and the concrete blocks above that remained bonded.

Figure 4.16 Observed damage of specimen 2 for tests #30 and #33

a) After test #30
(URM wall front view)

b) After test #33
(URM wall front view)

During test #31 the specimen showed higher amplitude deformations. For this test, high amplitude rocking motion was observed. For tests #32 and #33, the shake table showed problems with representing the selected input motion. The testing program was stopped after test #33. No shear cracks developed despite the effect of the captive column.

After test #33, along a 400mm length above the foundation level, both columns presented longitudinal cracks. These cracks indicated the debonding of the lap splice due to

splitting of the concrete. Also found were cracks at the base of the concrete columns extending to the foundation as shown in Figure 4.17c. After test #33, as shown in Figure 4.16, the right GLDRC column developed a shear crack at 400 mm above the foundation level.

Figure 4.17 Observed damage of specimen #2 for test #33

a) Longitudinal cracks formed in left column (side view)

b) Longitudinal cracks formed in right column (side view)

c) Crack at base of right column extending to foundation level (back view)

4.4 Specimen #3 Dynamic Loading of Bare Frame

This section describes the results of the shake table tests that were performed on Specimen #3, a GLDRC bare frame with an unattached URM infill wall. A total of 8 separate earthquake runs were performed on Specimen #3, following testing series A, presented in Table 3.5. The excitation acceleration, top absolute acceleration and top displacement time histories, as well as the hysteretic response and instantaneous displacement for all the performed shake table tests, are presented in Appendix C.

4.4.1 Observations

Test Series A

For this initial testing series the surcharge weight used was 62 kN. This series of tests consisted on 10 shake table tests using the VerteqIIZ2 acceleration record. The testing

program initiated at 50% amplitude to reach a maximum peak ground acceleration of 0.25g, as described in Table 3.4. All 9 shake table tests were performed on December 13, 2007.

Test # F was intended to be the first shake table test of Series A for the testing protocol using VERTEQII.Z2 at amplitude of 50%. Due to a saturation of the displacement control instrument of the shake table, after it was turned on, the shake table moved suddenly for a full stroke of 450 mm. The control of the shake table was regained by rebooting all electrical equipment simultaneously and this resulted in a sudden recentering of the shake table, equivalent to an additional impulse motion of 450 mm amplitude.

The response of the specimen to the two sets of impulse motions resulted in cracks in the GLDRC beam and in the URM wall. Since the instrumentation had not been set to measure motion at the time of the first shake table impulse, only the response to the second impulse was recorded.

The video recording on camera 04 for test F, shows that for the first impulse motion the applied force on the specimen is applied at the instant when the shake table reached its maximum stroke. As the force is applied on the specimen it results in a visible relative deformation with uplift of the URM wall and shake table pivoting on the right support.

Figure 4.18 presents the observed cracks developed after the two impulse motions. Mortar cracking was observed on two head joints at the lower right corner of the URM wall, as shown in Figure 4.18b, and was a result of the wall pivoting on that corner during the response to the impulse motion.

At each end of the GLDRC beam a flexural crack developed, corresponding to a positive moment, observed in figures 4.18c and 4.18d. No flexural cracks were found along the length of the GLDRC columns.

Figure 4.18 Observed damage of specimen 3 after test# F

a) After test F
Flexural cracks in beam ends
(URM wall front view)

b) After test F
Mortar cracks at lower right corner
of URM wall
(URM wall front view)

c) After test F
Flexural crack left end of beam
(URM wall front view)

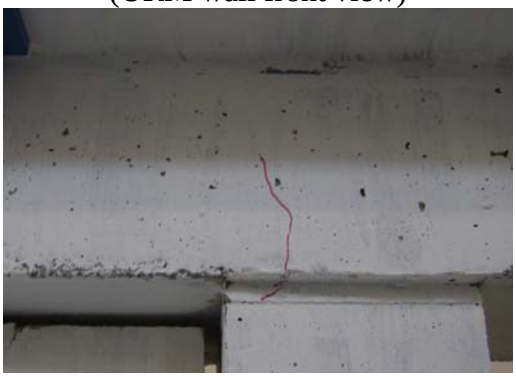

d) After test F
Flexural crack right end of beam
(URM wall front view)

Test #01 in the testing protocol resulted in a response of the test specimen with visible relative displacements with respect to the shake table. Following the high speed camera recording for this test it was determined that during the response the bare frame did not come in contact with the URM wall.

After test #01 several cracks were observed distributed along the length of the columns of the bare frame, as shown in Figure 4.19. From the base of the left column up to midheight, flexural cracks were found starting from the extreme fiber to the left of the cross section with an average length of 100mm, as presented in Figure 4.19a. For the

right column, from midheight up to the top, flexural cracks were found starting from extreme fiber to the right of the cross section with an average length of 80mm. This indicates that the cracking moment was reached while the frame displaced in the right (positive) direction during the response.

In test# 01 additional cracks were formed in the URM wall. A crack pattern was found at the lower left corner similar to the crack pattern observed in the opposite corner of the URM wall formed in the impulse motion.

New flexural cracks were formed along the length of the beam, as shown in Figure 4.19c and 4.19d. At each end of the beam, there was found one flexural crack starting from the top fiber of the cross section, and one flexural crack starting from bottom fiber. These two sets of cracks indicate that during the response of the structure the applied moments at the ends of the beam resulted in the negative and positive cracking moment of the beams cross section, respectively. The previously formed cracks in the beam did not vary in length or thickness.

Also observed was a flexural crack at the foundation beam near the location of the right column. The flexural crack started from the top fiber to the center of the cross section of the foundation beam, as shown in Figure 4.19b.

After test#02, it was observed that no new cracks developed in the bare frame or the URM wall, as presented in Figure 4.20a. A new flexural crack, shown in Figure 4.20b, was observed at midspan of the foundation beam, starting at the top fiber of the cross section and extending 100 mm in length.

Figure 4.19 Observed damage of specimen 3 after test#01

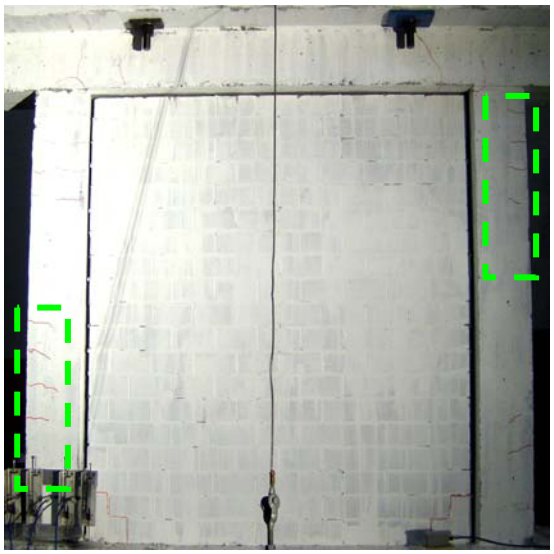

a) After test #01
Flexural cracks formed in
GLDRC columns
(URM wall front view)

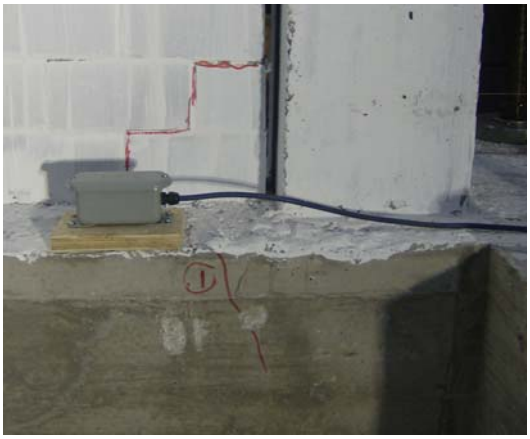

b) After test #01
Flexural cracks formed at top fibers of
foundation beam
(URM wall front view)

c) After test #01
Flexural crack left end of beam
(URM wall front view)

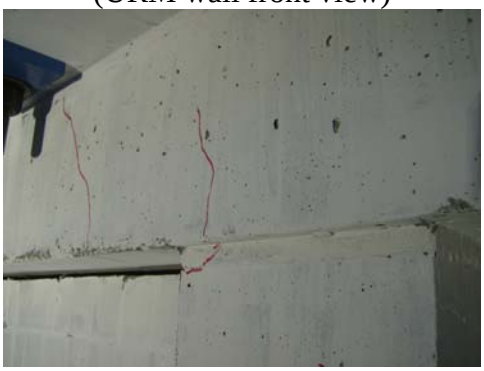

d) After test #01
Flexural crack right end of beam
(URM wall front view)

For test #03, the high speed camera video file for specimen#3 shows that during the response of the bare frame, it came in contact with the URM wall causing it to pivot on one of its corners. One instance is observed at t=14hr 52min and 50.112 sec, where the top portion of the columns came in contact with the top left corner of the URM wall. This contact generated an impulse on the masonry wall that resulted in a rigid body uplift motion with a duration of 0.15 sec, where the wall pivoted on the lower right corner and returned back down. It can also be seen in this video that one oscillation in the response of the bare frame had a duration of 0.230 sec.

Figure 4.20 Observed damage of specimen 3 after test#02

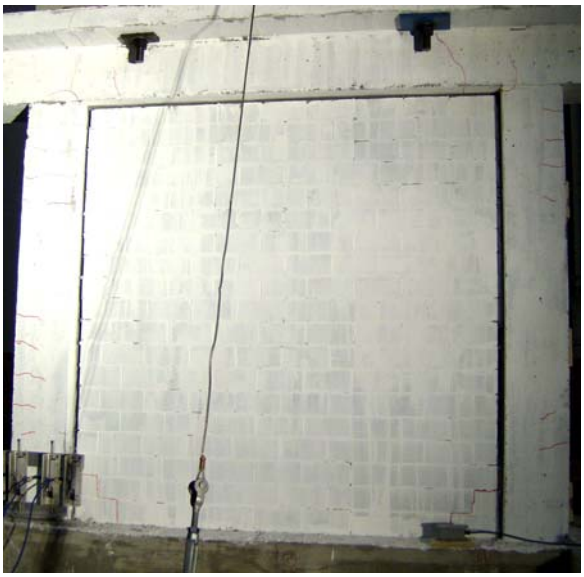

a) Test specimen after test #02
No additional cracks found in frame
(URM wall front view)

b) After test #02
Flexural crack at foundation beam
at midspan
(URM wall front view)

After test #3, a mortar crack was observed at the bed joint of the bottom course of the URM wall, presented in Figure 4.21a. This crack pattern in the masonry course lead to recognize that the wall was pivoting on the two previously cracked lower corners.

After test#04, no additional cracks had been found along the length of the columns or the beam of the bare frame. One crack was found at the interface between the foundation beam and the base of the right column and extended from the right extreme fiber until the center of the column cross section, as shown in Figure 4.21b. No observed additional damage developed on the URM wall, or the foundation beam.

The video recordings show that during test #05, due to the inertial forces being generated by the response of the test specimen, the shake table test presented several instances of uplift motion. During one of the uplifts, it is observed that the URM wall moves in a vertical motion.

Figure 4.21 Observed damage of specimen 3 after test#03 and test#04

a) After test #03
Mortar cracking at bed joint
of bottom course of URM wall
(URM wall front view)

b) After test #04
Concrete cracking at interface of right
column and foundation beam
(Specimen side view)

After test #05, one additional flexural crack had been formed at each end of the GLDRC beam, as observed in Figures 4.22a and 4.22b. Each crack initiated at the bottom fiber of the beams cross section with a length of 200 mm.

After test #05, an additional flexural crack was found on the right end of the foundation beam. This flexural crack was located under the right column of the bare frame, as can be seen in Figure 4.22c. In addition, some concrete spalling was observed at midspan of the foundation beam, as shown in Figure 4.22d.

For test #06, it is shown in video file test6.cin for specimen#3 that after the bare frame came in contact with the top left corner of the URM wall, it produced a rigid body sliding and uplift motion. One instance is observed at t=15hr 57min and 28.240 sec, where the top portion of the bare frame pushed the masonry wall and resulted in a sliding motion with a duration of 0.04 sec and then, an uplift motion of 0.11 secs, where the wall pivoted on the lower right corner and returned back down.

For test #06, the video records show how the pounding of the bare frame with the URM wall deformed the wall in bending and resulted in mortar cracks in the bed joints of the

fourth and fifth course from the bottom of the wall, as shown in Figure 4.23. This bending failure of the URM wall occurred at t=32.46 sec after the initiation of the test and corresponds to the instant in the response where the wall reached a maximum negative deformation of -18.8 mm and a maximum inertial force of 95 kN.

Figure 4.22 Observed damage of specimen 3 after test#05

a) After test #05
Flexural cracks left end of beam
(URM wall front view)

b) After test #05
Flexural cracks right end of beam
(URM wall front view)

c) After test #05
Flexural crack in foundation beam
under base of right column

d) After test #05
Concrete spalling of foundation beam
at misdspan

Figure 4.23 Observed damage of specimen 3 after test#06

a) After test #06
Additional crack patterns
in the URM wall
(URM wall front view)

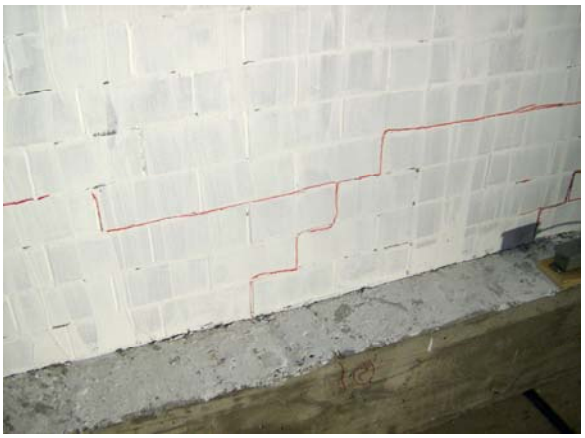

b) After test #06
Mortar crack pattern
bending failure of URM wall
(URM wall front view)

c) After test #06
Mortar crack pattern at the left side
of URM wall (URM wall front view)

d) After test #06
Mortar crack pattern right side
of URM wall (URM wall back view)

4.5 Summary of Test Results

4.5.1 Infilled Frame Specimen Response to Monotonic Loading

For the monotonic testing of specimen #1, as the top lateral drift demand was increased 3 distinct behavior modes were observed: diagonal compression, shear sliding and bond slip. Diagonal compression was observed as the behavior mode for the linear response of the system, with a constant stiffness of K_L=11.5 kN/mm. Horizontal shear sliding behavior was initiated as the lateral load vs. drift curve indicated yielding at 1.0% drift and 195 kN lateral resistance was not observed beyond 1.65% drift. This mechanism results in several horizontal mortar cracks on the bed joints extending all along the length of the URM wall. Bond Slip of the longitudinal rebar at the lap splice was observed as longitudinal splitting cracks in concrete at the base of the GLDRC columns. The bond slip behavior resulted in large rotations at the base of the columns without the formation of plastic hinges. The tested structure reached a maximum drift of 3.55% without loss in lateral strength.

4.5.2 Infilled Frame Specimen Response to Shake Table Testing

A total of 33 shake table tests were performed on the infilled frame, specimen #2. The levels of shaking followed the established testing program. The response of the specimen showed three behavior modes: diagonal compression, horizontal shear sliding and bond slip. Diagonal compression was observed for the first set of tests. The shear sliding behavior was observed during test #09, with the formation of a mortar cracking along the bed joints extending along the full length of the URM wall. For tests #15 through #19, the shear sliding behavior resulted in the knee braced effect on the GLDRC columns which generated plastic rotations above the expected location for plastic hinges in columns. The URM wall failed at test #30 due to loss of mortar bond of the concrete blocks in the center and the corners of the wall. After test #33, longitudinal splitting cracks in the concrete were found at the base of the GLDRC columns. At the end of the

shake table tests, no plastic hinges or flexural cracks were found along the location of the lap splice of the longitudinal rebar for the GLDRC columns.

4.5.3 Bare frame Specimen Response to Shake Table Testing

A total of 8 shake table tests were performed on the bare frame, specimen #3, following the same testing program as for specimen #2. Due to an unexpected response of the shake table system, prior to starting the test protocol two large pulse motions were applied to the specimen which resulted in flexural cracks at the ends of the GLDRC beam. The response to test #01 showed cracking in the GLDRC columns and beam. The behavior was observed to have larger amplitudes of vibration.

Chapter 5 – Analysis and Interpretation of Results

5.1 General

The previous chapter presented a detailed description of the developing of cracks at the different levels of dynamic excitation applied on tested specimens #2 and #3. In this chapter the measured displacements and accelerations, obtained through the selected instrumentation, are used to objectively evaluate the deformations and lateral forces that occurred during each level of testing. The excitation acceleration, top absolute acceleration and top displacement time histories, as well as, the hysteretic response and instantaneous displacement for all the performed shake table tests are presented in Appendix B.

Section 5.2 presents a discussion of the rocking motion of the specimen's foundation and the resulting rigid body lateral displacement component that needs to be considered in order to calculate the top relative displacement of the specimen. Section 5.3 shows the degradation of effective lateral stiffness and section 5.4, the hysteretic and instantaneous displacement response of specimens #2 and #3. Section 5.5 presents the measured values of the rotation at the base of one column for specimen #3. Section 5.6 presents a comparison of the response of specimen #2 and #3, for each test performed in test Series A, using the maximum measured dynamic response parameters. Finally, section 5.7 is a discussion of the behavior of GLDRC frames with concrete block walls based on the observations made from this testing program.

Instrumentation was also used to monitor sliding between the foundation of the specimen and the shake table, although this behavior was negligibe. The top lateral deformations presented here in have been corrected and do not include the displacement components produced by rocking or sliding.

5.2 Subtracting Lateral Displacement Component due to Foundation Rocking

During the shake table testing program performed on specimen #2 and specimen #3, several instances of rocking motion were observed at the level of the shake table. This motion is a result of the dynamic interaction during testing between the shake table and the specimen. This section presents the rocking motion measured with respect to the foundation level and how this affected the dynamic response of the tested specimen.

Figure 5.1 Illustration of motion during Shake table testing

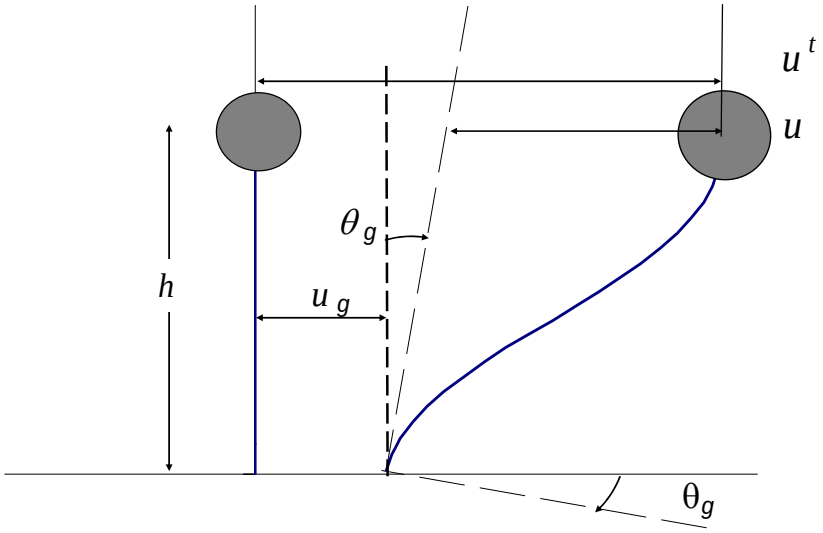

u^t	total top lateral displacement
u	relative top lateral displacement (specimen deformation)
u_g	lateral displacement due to rigid body displacement
θ_g	rotation due to rocking motion
h	measured distance between foundation level and top of specimen

Figure 5.1 illustrates different displacement components recorded during testing. The rocking motion results in a rotation θ_g at the foundation level and contributes to the specimen's total top lateral displacement u^t, with a value of $\theta_g h$, where h= 2000 mm is the height of the frame, measured as the distance from the foundation level to the center of the beam. The specimen's deformation, u, and inertial force f_I is then determined as

$$u = u^t - u_g - \theta_g h \qquad \text{(eq 5.1)}$$

$$f_i = m\ddot{u}^t \qquad \text{(eq 5.2)}$$

Rocking was not always present during the shake table motion, however, the rotation interaction of the shake table with the specimen' motion during testing was always present. Prior to a test, the shake table's four vertical supports are in compression sustaining the distributed weight of the shake table, the specimen and the surcharge assembly. During testing, these vertical supports resist the overturning moment resulting from the specimen's generated inertial force. This overturning moment will produce compression deformations in the vertical supports that result in a rotation of the shake table which will only be small when all the supports remain in compression. The onset of rocking occurs when the overturning moment results in a tension force on one of the vertical supports, which have no resistance to uplift.

The combination of the relative top lateral deformation, u, and the top lateral displacement contribution due to rotation at the foundation level, θ_g h, represents the effect of the resulting dynamic interaction of the specimen and the shake table. This combined displacement was plotted against the top inertial force, f_I, and compared to the hysteretic response of specimen #2, in Figures 5.2 and 5.3, for several of the performed shake table tests. This comparison allowed to study the effect of the interaction of the rocking motion of the shake table with the dynamic deformation of the tested specimen.

For the case of test #01 the inertial forces did not cause uplift of the shake table's vertical supports and the calculated rotation of the shake table was of 0.5×10^{-3}rad. This rotation resulted in a top lateral displacement, θ_g h, of 1.1mm, and the uncorrected measured lateral displacement of the specimen was of 4.25 mm, which indicates a contribution of 26%. For test #19 the calculated rotation was of 4.4×10^{-3}rad and resulted in a contribution of 29% of the maximum lateral displacement of the specimen #2. For

test#22 the calculated rotation was 6.1 $x10^{-3}$rad and resulted in 52% of the maximum measured lateral displacement of the specimen.

As seen from the comparison Figures 5.2 5.3, all the tests where there was observed uplift of the vertical supports of the shake table, such as tests #10, #19, #22, #30 and #31, the hysteretic plots with the combined displacement, $u + \theta_g h$, show larger values of area under the hysteretic loop, than that for displacement u. This suggests that during the rocking motion of the shake table the interaction considerably dissipated the energy generated by the specimen's response.

5.3 Stiffness Degradation

This section shows the resulting values of effective lateral stiffness during the response motion of specimen #2 and #3 for the performed shake table tests. Tracking the variation in stiffness allowed identifying events associated with change in the conditions of the tested specimen that had not been previously observed.

The effective lateral stiffness during the response of the specimen was calculated as a function of the surcharge mass and the frequency of vibration. This frequency of vibration was taken as the frequency that corresponded to the highest value in the power spectral density of the acceleration response.

5.3.1 GLDRC Infilled Frame

Prior to testing the initial effective lateral stiffness was estimated to be K_0=13.4 kN/mm, as a function of the frequency of vibration obtained from the ambient vibration tests described in Section 3.4. Figure 5.4 shows the resulting values of effective lateral stiffness of the GLDRC infilled frame for test Series A through E in the testing program.

Figure 5.2 Rocking motion effects on specimen 2 force vs displacement response

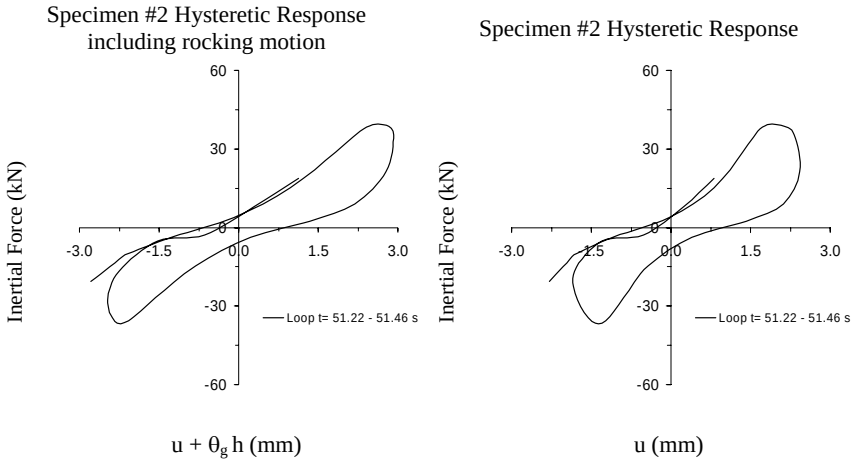

a) Test #01

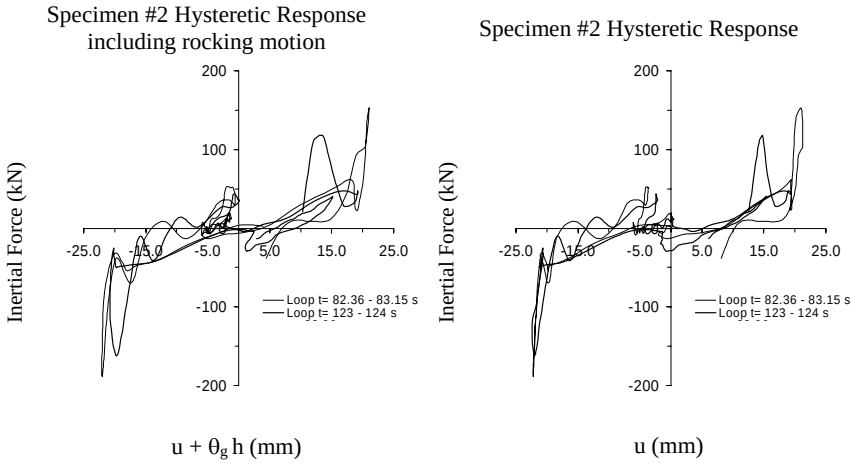

b) Test #10

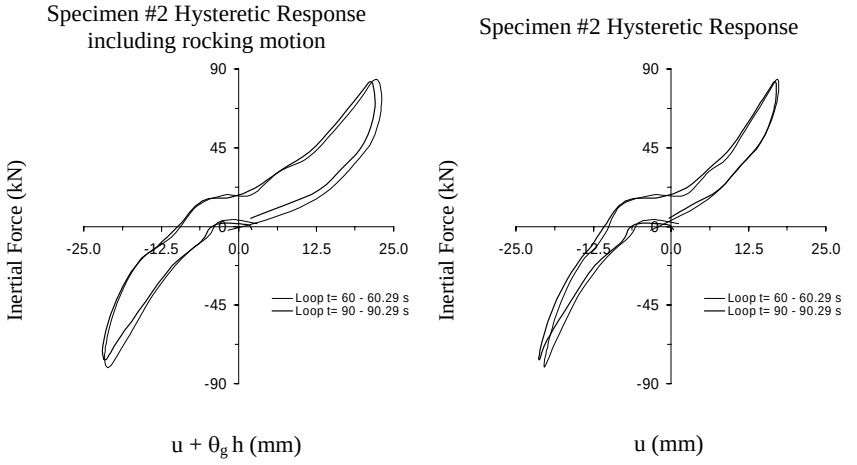

c) Test #19

Figure 5.3 Rocking motion effects on specimen 2 force vs displacement response

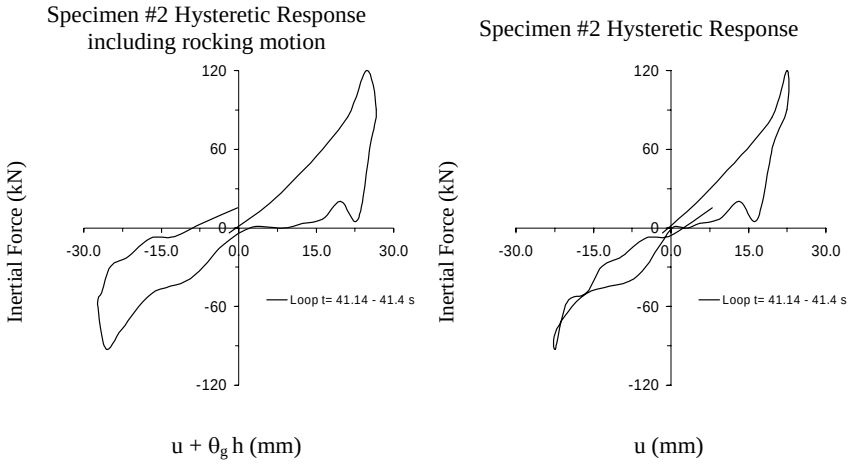

a) Test #22

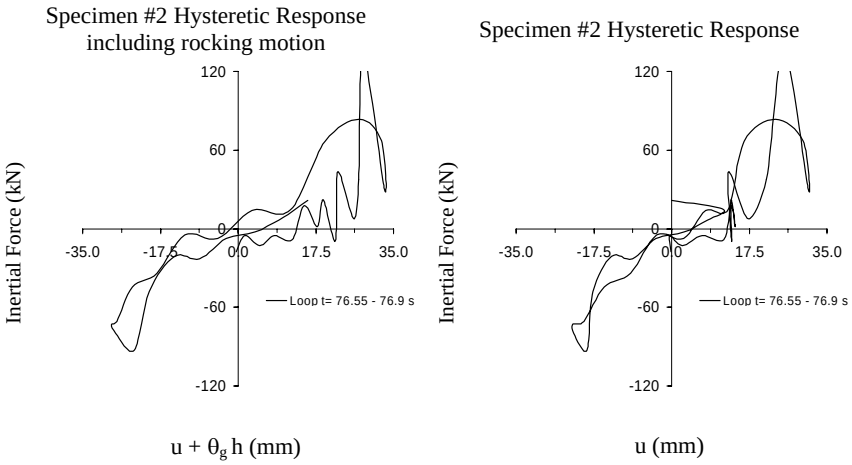

b) Test #30

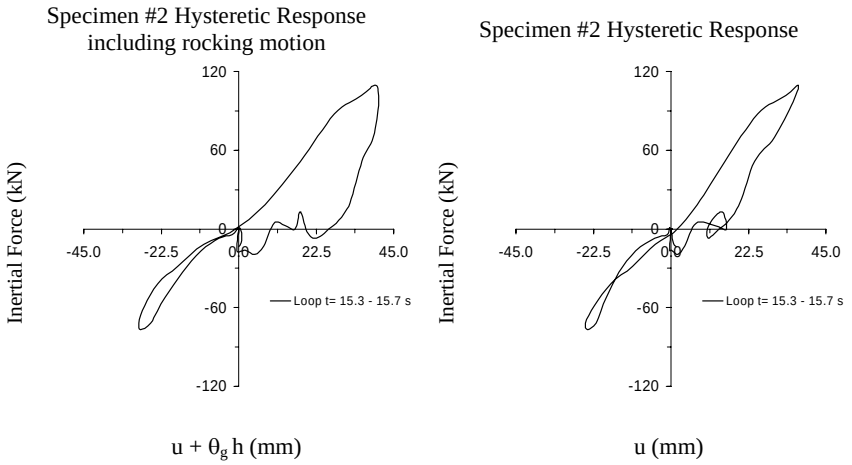

c) Test #31

Figure 5.4 Stiffness degradation through testing program Specimen #2

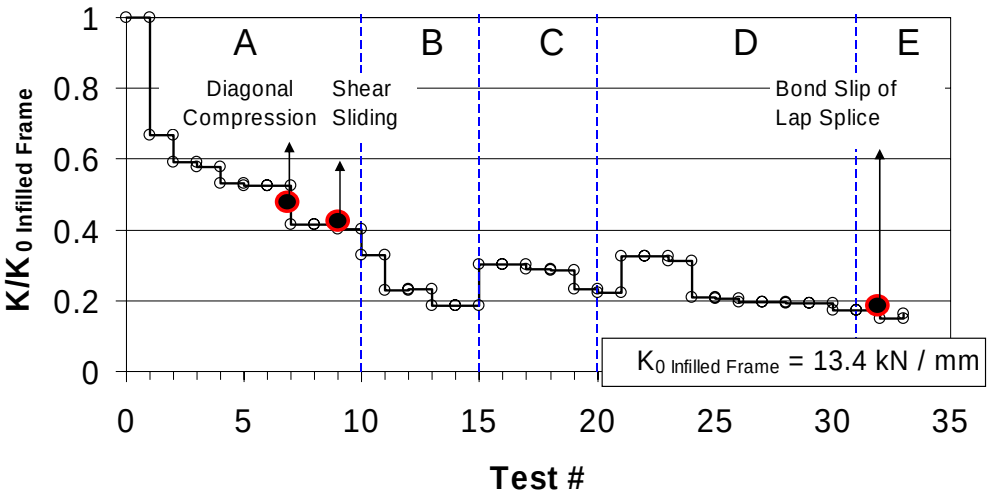

Tracking the variation in stiffness allowed identifying events associated with change in the conditions of the tested specimen. The points in Figure 5.4 that suggest important events in the testing program are tests #1, test#2, test#4, test#7, test#10, test#13, test #19, test #24, and test #30. Many of these points coincide with the observations made in section 4.3 on the evident development of cracks in the test specimen, such as test #7 with the development of diagonal crack patterns, test #13 with the flexural cracks formed on the GLDRC columns, test #19 with the observed shear sliding behavior forcing short column effects on the specimen. The test values #1, #2 and #4 may be better understood by studying the force and displacement time history response of the specimen. After the response to shake table tests #15 and test #21 according to the values observed in Figure 5.4 there would have been a gain in stiffness. For test #15, the first point indicating increase in stiffness, K/K_0 varies from 19% to 30%. For test #21, the second point indicating increase in stiffness, K/K_0 varies from 22% to 32%.

Test #15 was the first test in Series C, and the surcharge weight used for testing was changed from W=4.5 kN to W=31 kN. A change in surcharge weight from W=62 kN to W=4.5 kN also explains the drop in stiffness from 33% to 23% for test #11, the first test in Series B. Test #21 is the second test in Series C, and coincided with a change in the shake table input motion from Extended VERTEQIIZ4 to the SCT1-1985 Modified #1

records. For test #24, the input motion is changed back to Extended VERTEQIIZ4 and the stiffness drops from 31% to 21%.

These gains in stiffness suggest that to track degradation of the effective lateral stiffness, the surcharge weight of the specimen and the frequency content of the input motion should be kept constant for the tests being compared. Based on this observation, association of damage due to observed decrease stiffness was only made for events within a range of tests where these conditions were met.

5.3.2 GLDRC Bare Frame

Prior to testing, the initial effective lateral stiffness was estimated to be K_0=11.8 kN/mm, based on vibration tests described in Section 3.4. Figure 5.5 shows the resulting values of effective lateral stiffness of the GLDRC bare frame for test Series A, including the applied impulse motion identified as test F.

Figure 5.5 Stiffness degradation through testing program Specimen #3

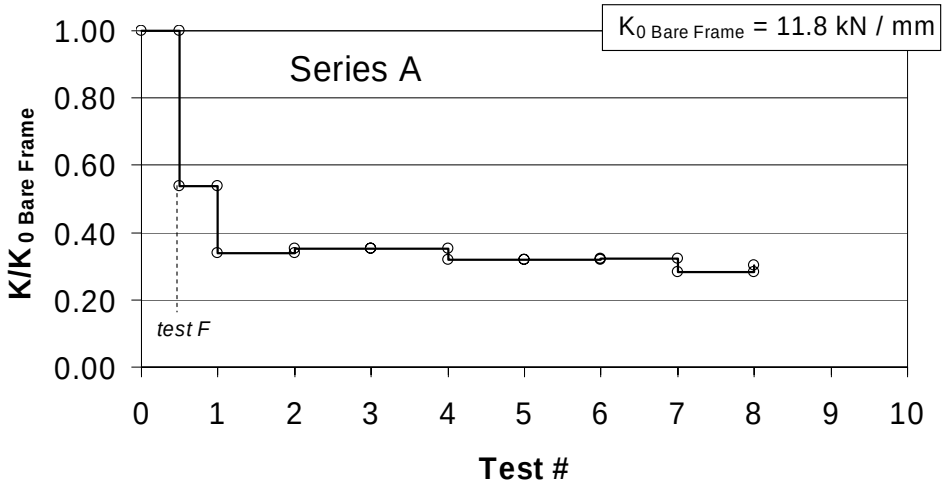

The results presented in Figure 5.5, indicate that after test F, the effective stiffness decreased from 100% to 54% K/K_0 and after test #1, there was a second decrease from 54% to 34% K/K_0. The measured effective stiffness from test # 2 until test #8 show a

small variation from 34% to 30% of K/K_0. These observations indicate that the first two tests were significant events in the testing program for the GLDRC bare frame specimen.

5.4. Inertial Force and Displacement Response

This section presents the observations made from the hysteretic loops formed and the instantaneous displacement during a time interval corresponding to the occurrence of the maximum displacement during the response motion. The instantaneous displacement plot shows the variation in displacement of measured points (y/H) located along the height of the specimen, H, at 100 mm (y/H= 5%) and at 2000 mm (y/H= 100%) from the foundation level at different times during the hysteretic response.

5.4.1 GLDRC Infilled Frame

Test Series A

The results from test #01, presented in Figure 5.6, show the specimen to have responded with a lateral stiffness of 13.4 kN/mm when the applied inertial force was below an absolute value of 15kN, and with higher stiffness as the applied load increased. The resulting deformation response presented inelastic behavior and reached a maximum deformation amplitude of 2.4 mm.

Figure 5.6 Inertial force and displacement response for Specimen #2 test #01

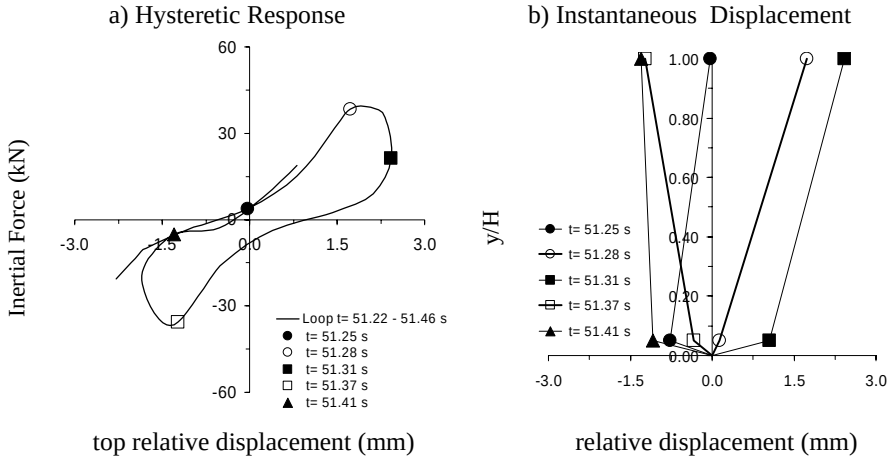

In the hysteretic plot for test#01, when the specimen is in the loading portion of the response for t=51.25 sec, the measured instantaneous displacements show the GDLRC frame to have had small deformations at the base of the columns relative to the top. After the maximum inertial force was reached, at t=51.28 sec, the acting force began to decrease with increasing deformation at the top resulting in a negative slope as observed in the hysteretic plot. The instantaneous displacements for this instance of the response indicates localized concentrated deformations at the base of the GLDRC frame which suggests shear sliding of the column's base at the interface with the foundation and the cause for the drop in stiffness highlighted in Section 5.3.1. This observation is consistent for tests #01 through test #07.

The hysteretic response for test#04, presented in Figure 5.7, shows that as the specimen reached its maximum deformation there was a significant increase in stiffness. For test #07, when the first set of diagonal crack patterns were formed in the URM infill, the hysteretic response shows to have reached a maximum inertial force of 98 KN, with great dissipation of energy. In the hysteretic plot for this test, no negative slope is observed during unloading, as shown in Figure 5.8.

Figure 5.7 Inertial force and displacement response for Specimen #2 test #04

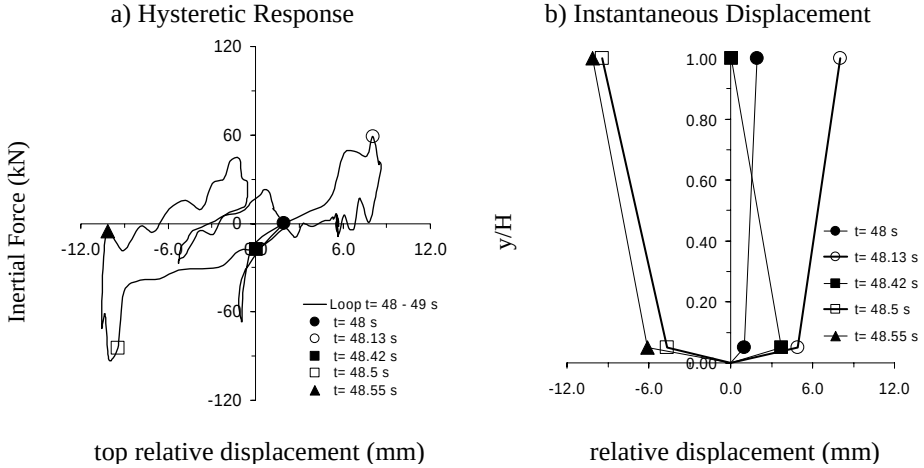

Figure 5.8 Inertial force and displacement response for Specimen #2 test #07

a) Hysteretic Response b) Instantaneous Displacement

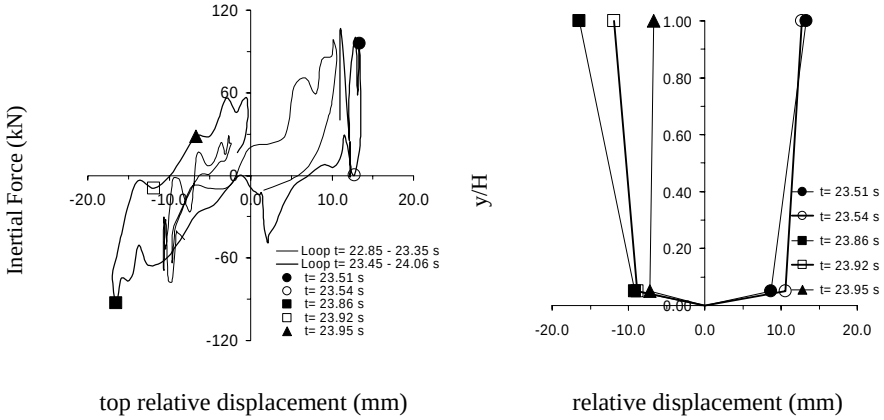

top relative displacement (mm) relative displacement (mm)

Test Series B

The hysteretic plots for tests #13 and #14 show clear pinching effects, as shown in Figure 5.9. This effect is demonstrated to be associated with the local deformations observed at the base of the specimen by following the response through the hysteretic plot and the corresponding instantaneous displacement at different stages of loading.

For test #13, during the unloading part of the hysteretic response for t=43.98 sec, the instantaneous displacements show that while the top deformation decreased, the local deformation at the base of the columns increased. As the specimen was loaded in the opposite direction, the local residual deformation at the base of the columns remained constant. After having reached a value of inertial force of -5.6 kN, the hysteretic response shows a decrease in inertial force and an increase in deformation. This behavior corresponds to the initiation of local deformations at the base of the column in the direction of loading, which reduced the total residual deformation from the previous unloading stage. When the inertial force reached a value of -2.11 kN, the specimen regained stiffness due change in the ground motion direction as an effect of its relative velocity.

Figure 5.9 Inertial force and displacement response for Specimen #2 test#13

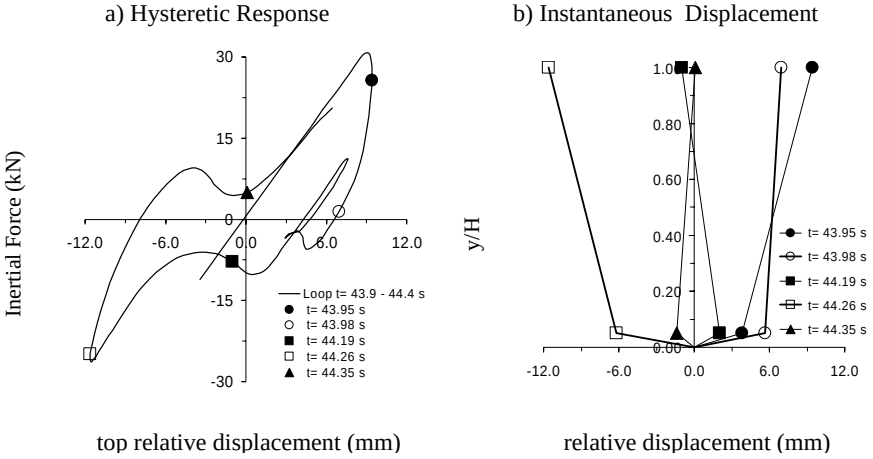

Test Series C

For tests #18 through #20, the hysteretic loops show that during the response the pinching effect was interrupted for a portion of the response thereby the system showed significant stiffness after unloading, as observed in the hysteretic loop for test #19 in Figure 5.10. For test #19, as described in section 4.3.1, there were significant local deformations of the GLDRC columns observed at the location of the sliding plane of the URM wall, 500 mm from the foundation level. The instantaneous displacements shows that at the top of the specimen during the loading stage starting from the negative deformation of -11mm to the positive deformation of +17mm, the specimen deformed 28mm; out of which 14mm are due to deformations at the base of the columns. For the case of loading starting from the positive deformation of +0.1mm to the negative deformation -19mm, the total deformation resulted in 19mm, out of which 3mm are due to deformations at the base of the columns. The initial slopes in the hysteretic plot for these two loading stages studied were 5 KN/mm and 9 KN/mm, respectively. The reduction in the local deformations at the base of the columns, and the increment in stiffness are evidence that the specimen changed its load deformation behavior after the formation of the rotational hinges in the columns located 500 mm above the foundation level.

Figure 5.10 Inertial force and displacement response for Specimen #2 test #19

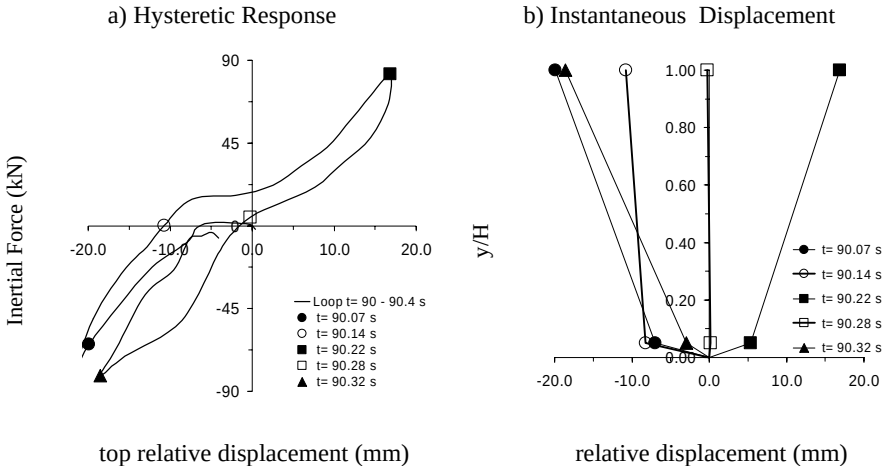

Test Series D

For tests #21 through #23 there was less dissipation of energy through cracking generated than in previous tests, mainly as a result of the large dissipated energy due to rocking motion of the shake table. For these set of tests there is also evidence of local deformation at the base of the specimen that result in a pinched hysteretic plot. For test #22, shown in Figure 5.11, the hysteretic response shows that that a maximum inertial force of 120 kN was applied on the specimen due to an absolute top acceleration of 4.0g, where the applied excitation had a maximum amplitude of 1.80g.

For tests #28 thru #30, the hysteretic plots of the response show the effect of pounding of the GLDRC frame and the URM wall, as shown in Figure 5.12. The observations of pounding indicate a detachment of the URM wall with respect to the GLDRC frame, and as a result the masonry wall was no longer confined by the frame during the dynamic response. For test #30, the hysteretic response shows a maximum inertial force of 135 kN and deformation of +30.8mm. Due to the superimposed effect of pounding on the hysteretic plot it is undetermined whether the observed negative slope in the hysteretic response corresponding to the maximum deformation can be associated with degradation in strength of the lateral system.

Figure 5.11 Inertial force and displacement response for Specimen #2 test #22

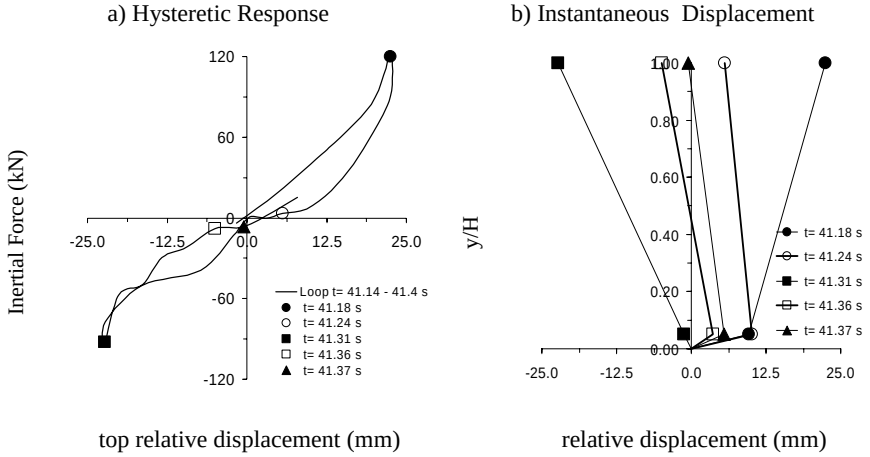

Figure 5.12 Inertial force and displacement response for Specimen #2 test #30

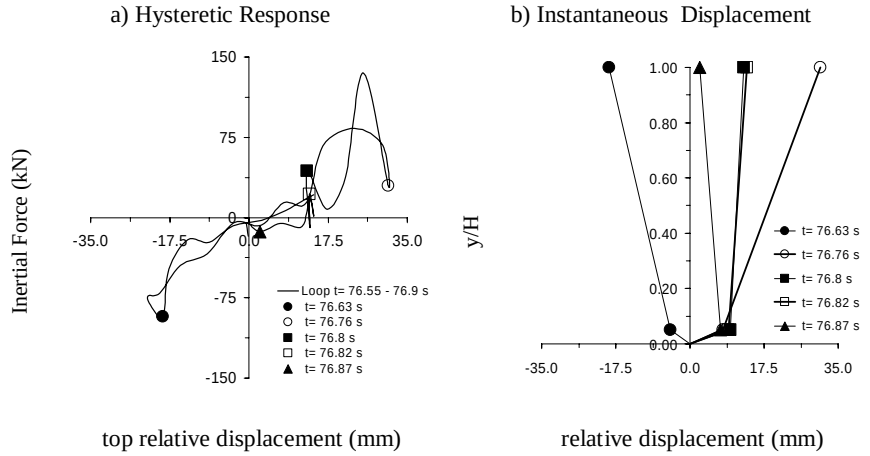

Test Series E

The measured response values for test #31 represent the highest force and deformation demands of this testing series. During test #31, the specimen reached a maximum inertial force of 109 kN and deformation of +37mm, as shown in Figure 5.13. For t=15.57 sec and t=15.65 sec pinching in the hysteretic behavior is observed indicating that during the unloading portion of the response the specimen lost its lateral stiffness. This loss in stiffness corresponds to a residual deformation at the base of the column that had reached a value of +9.5mm at t=15.51 sec. The hysteretic behavior shows increase in stiffness at t=15.69 sec and the residual deformation had reduced to +5.10mm.

Figure 5.13 Inertial force and displacement response for Specimen #2 test #31

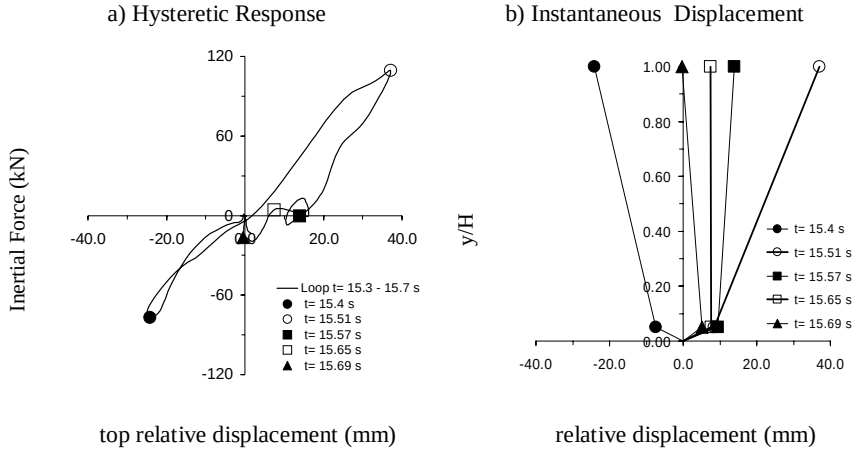

5.4.2 GLDRC Bare Frame

The first dynamic excitation, test F, resulted in the measured inelastic response illustrated in Figure 5.14. The measured maximum relative displacement was -13.0 mm and a maximum inertial force of +66.5 kN.

During the first acceleration pulse at t=39.2 sec, the hysteretic plot shows an initial slope of 9 kN/mm and later presents a variation as a superimposed half sine along the dotted line following the initial slope. This behavior is later observed to be the result of the pounding of the GLDRC bare frame with the unattached URM wall for video recordings for tests 3 through test 8.

This observed pounding effect is seen to have occurred during the first acceleration pulse of the measured time history. The instantaneous displacement plots for instances t=39.2 sec and t= 39.25 sec show that as the specimen displaced with the shake table, the URM wall pounded on the opposite direction of motion resulting in positive displacements at the top and negative displacements at the base of the specimen.

Figure 5.14 Summary of specimen 3 response for test F

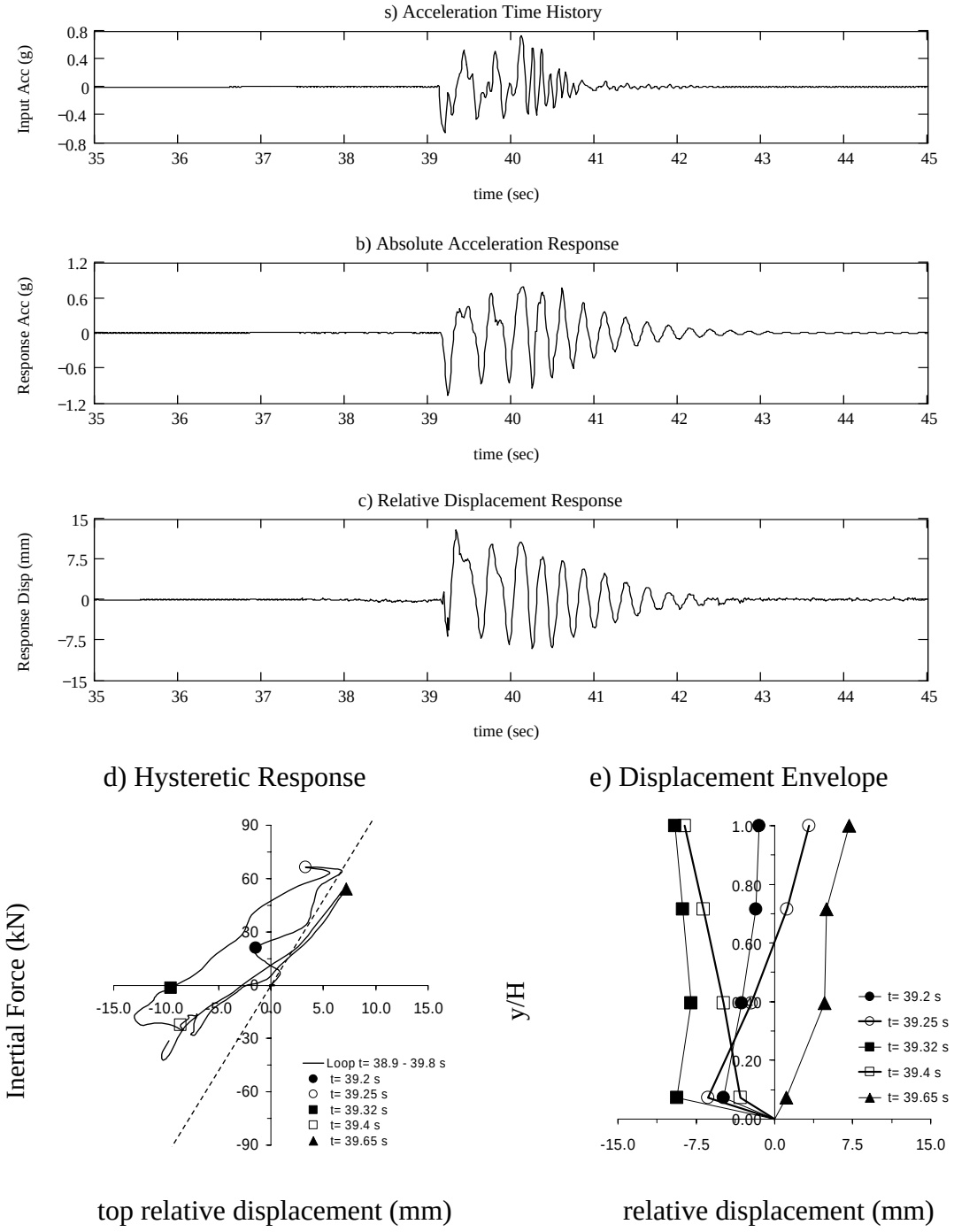

For t=39.32 sec, the instantaneous displacements show that after unloading at the base of specimen there was a residual deformation of -9.3 mm. For t= 39.4 sec, during reloading the hysteretic plot shows a slope equivalent to a low effective stiffness and the corresponding instantaneous displacements present the local deformation at the base of

the specimen returning back to zero deformation. After t=39.5 sec the hysteretic plot shows no additional non linear behavior and a constant slope of 5 kN/mm.

The dynamic response observed for Test #01, presented in Figure 5.15, shows that the GLDRC bare frame dissipated very little energy from nonlinear response. The maximum measured inertial force applied on the specimen was of 26.4 kN, resulting in a maximum deformation of -5.5mm. The average slope of the hysteretic plot was of 4.0 kN/mm and without visible degradation of stiffness. The instantaneous displacements for instances, t=54.23sec, t=54.29sec and t=54.38sec demonstrate small deformations from the base up to midheight of the column indicating high rotational stiffness at the base of the specimen.

Figure 5.15 Inertial force and displacement response for Specimen #3 test #01

a) Hysteretic Response b) Displacement Envelope

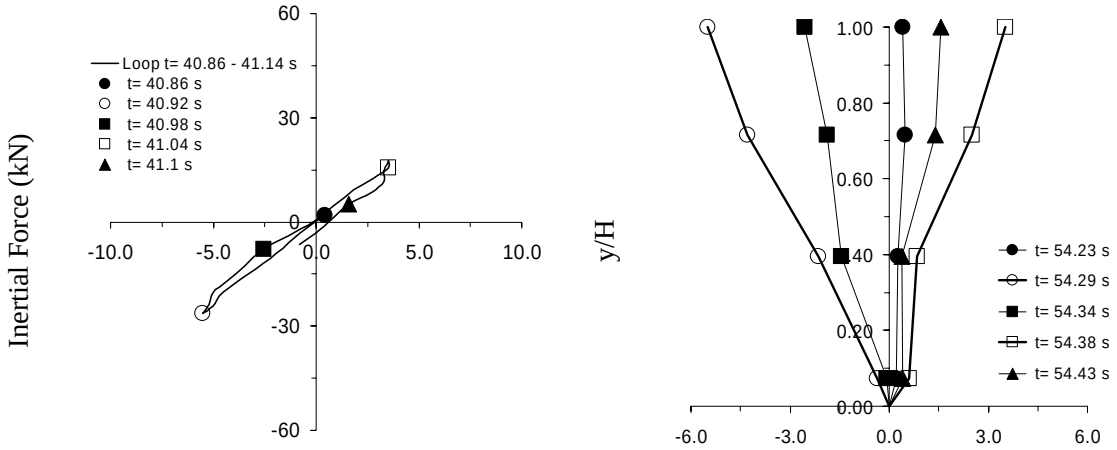

The response to test #2 presented a similar behavior as that described for test #1. The maximum inertial force reached 48.5 kN with a resulting deformation of 8.4mm. The measured response for test #03, shown in Figure 5.16, presents a variation in the response of the specimen observed as a sine wave function superimposed on the hysteretic plot. This effect is first observed for t=28.14 sec, after the response had reached a displacement of -12.6mm at t=28.10 sec. By observing the high speed camera video

recordings it was confirmed that at this stage of testing, the frame and URM wall were coming in contact during the response. The instantaneous displacements for test #3 also show a significant decrease in the rotational stiffness at the base of the specimen compared to test #1, resulting in a variation in the deformed shape of the specimen.

For tests #3 through #8 the hysteretic plot shows the effect of pounding of the URM wall on the GLDRC frame. There is no significant variation in the deformation shape of the specimen's response during these tests, as observed for test #3 in Figure 5.16 and test#8 in Figure 5.17. The deformed shape of the columns of the GLDRC bare frame observed for these tests presents double curvature with a rotation at the base.

Figure 5.16 Inertial force and displacement response for Specimen #3 test#03

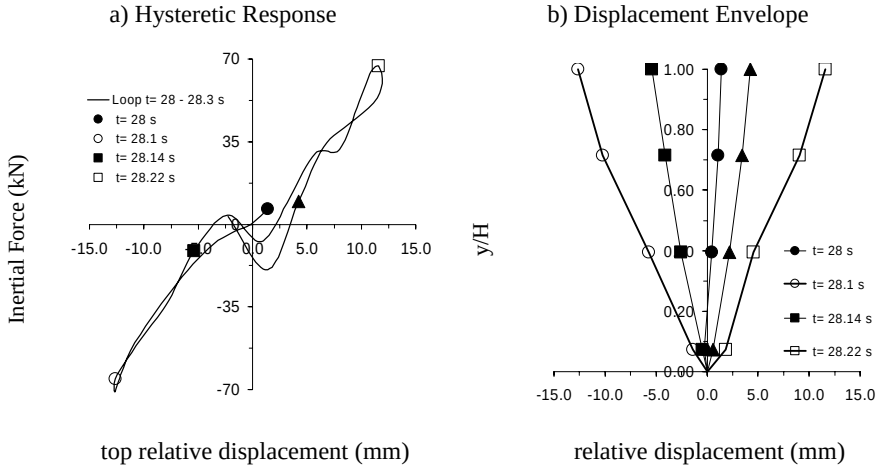

A plot illustrating the variation of base shear and top lateral deformation throughout testing series A is presented in Figure 5.18. It is shown that the base shear reached its maximum at test #6 with a value of 99.1 kN and the maximum displacement was observed at test #5 with a value of 19.4mm. For tests #6 through test #8 the maximum displacement demand was between 18.8mm and 18.1mm. This could indicate that the interaction of the GLDRC bare frame with the URM wall helped to reduce the deformation demands through pounding.

Figure 5.17 Inertial force and displacement response for Specimen #3 test#08

a) Hysteretic Response b) Instantaneous Displacement

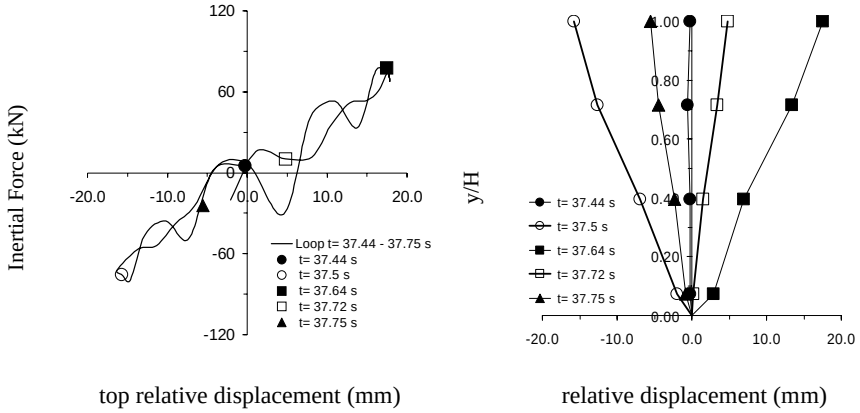

top relative displacement (mm) relative displacement (mm)

Figure 5.18 Maximum response values of specimen 3 for test Series A

a) Test # vs Base Shear b) Test # vs Top lateral deformation

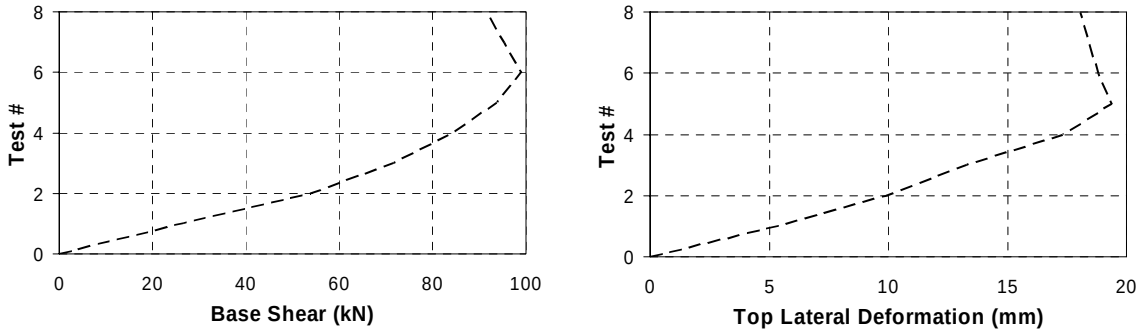

5.5. Damage Prediction Parameters in FEMA 306

In this section, the recorded variation in stiffness and hysteretic behavior of the infilled frame specimen during monotonic and shake table testing are compared to the damage prediction parameters in the FEMA 306 document [ATC, 1999]. This comparison allows determining future retrofit recommendations for GLDRC frames with URM infill walls.

The FEMA 306 document provides a performance-based methodology for the evaluation of earthquake-damaged concrete and masonry buildings. It consists of damage parameters for use in a performance based retrofit design. These parameters are used to modify the structural properties of an undamaged building such as, stiffness and strength,

to evaluate its capacity after reaching a specified performance level. These values are presented for different damage patterns and require an understating of the expected behavior of the existing structure.

The testing program conducted for infilled GLDRC frames provided the required information to compare the monotonic loading curve with the backbone curve of several hysteretic responses. Figure 5.19, presents a comparison between the monotonic load vs drift curve and the backbone of the hysteretic responses during the shake table testing program. The comparison shows that the maximum lateral resistance for the shake table tests was 60% that of the monotonic loading test. Despite the difference in achieved lateral strength, the governing behavior modes, discussed in section 4.2.2, were observed for similar drift demands. It is shown in Figure 5.19 that the undamaged infilled frame under monotonic loading showed a stiffness of $K_{monotonic}$ = 11.5 kN/mm, while the infilled frame under shake table testing, after shake table test #07 showed a stiffness of K_{07}=5.57 kN/mm and damage of diagonal cracks on the URM infill wall. After test #31, the infilled frame had a stiffness of K_{31}=2.34 kN/mm and was severely damaged

Figure 5.19 Comparison of monotonic load vs deformation curve and backbone curve of shake table testing program.

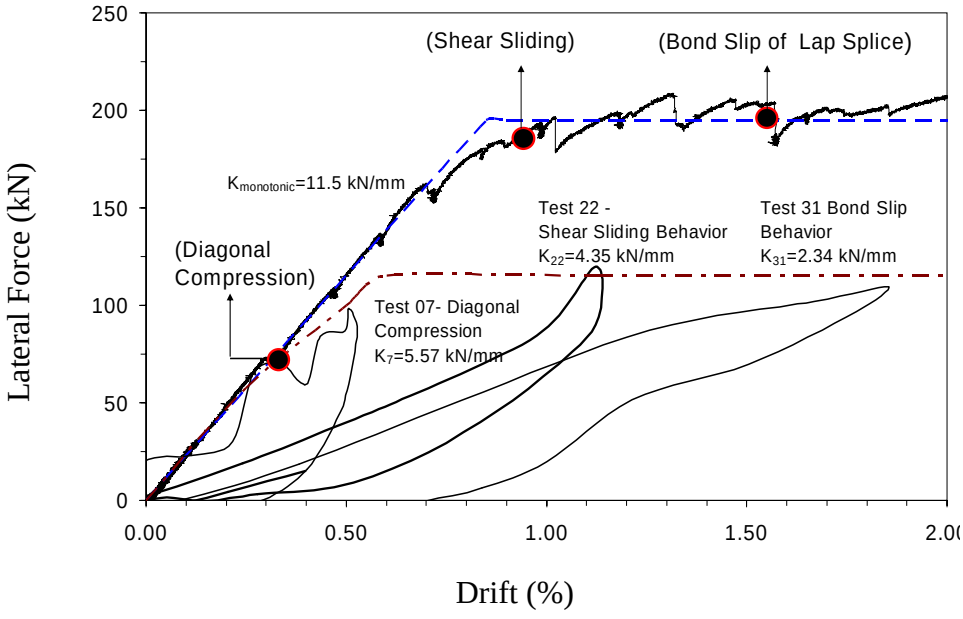

In the FEMA 306, the damage prediction parameters are classified for different categories for a given structure type, depending on the expected behavior mode and damage level. The infilled frame specimen fit into category INPS2 because its response showed cracking along the diagonals, had small damage observed in the reinforced concrete frame and after heavy damage portions of the entire infill wall fell out of plane under cyclic loading. However, FEMA 306 does not specify if this category can be applied directly to existing GLDRC frames. The damage prediction parameters include the estimate in degraded stiffness, λ_K and degraded strength, λ_Q, for different levels of damage. Table 5.1 presents the comparison of the test results and the recommended values in FEMA 306.

Table 5.1. Damage prediction values in FEMA 306 and recorded damage values from shake table testing program

Damage Level – Behavior Mode	λ_K - Degraded Stiffness	λ_Q - Degraded Strength
FEMA 306 – Insignificant	**0.70**	**1.0**
Test #07, Diagonal Compression Behavior	0.60	1.0
FEMA 306 – Moderate	**0.40**	**0.80**
Test #09, Shear Sliding Behavior	0.40	0.60
FEMA 306 – Heavy	**0.20**	**0.50**
Test #31, Bond Slip Behavior	0.20	0.60

In a separate category, INF1C2, suggested for lap splices at hinge zone location that show lack of sufficient lap length, FEMA 306 recommends considering slip of the rebar and the formation of flexural cracks at floor level even for expected insignificant damage level. However, there is no recommendation on the possibility of shear failure of the column at the floor level due to the transferred diagonal load from the URM infill wall to the GLDRC column.

Despite FEMA 306 damage parameters not accounting for shear sliding, they are shown to be in good agreement with the overall results of this testing program. The damage

prediction values in FEMA 306 can be used for GLDRC frames with URM infill walls for similar geometric and material properties as the ones observed for these tests and for a maximum 2.0% drift.

5.6. Column Rotations

For the response of the bare GLDRC frame, one of the columns was instrumented to later calculate column rotations at a location 260mm above the base of the column. Two sets of rotations were determined at this location, one relative rotation, $\theta_{relative}$, which was determined with respect to the base of the column and one total rotation θ_{total}, with respect to the foundation beam. An illustration of these rotations as observed in a deformed column is presented in Figure 5.20.

Figure 5.20 Illustration of column rotations at x=260mm

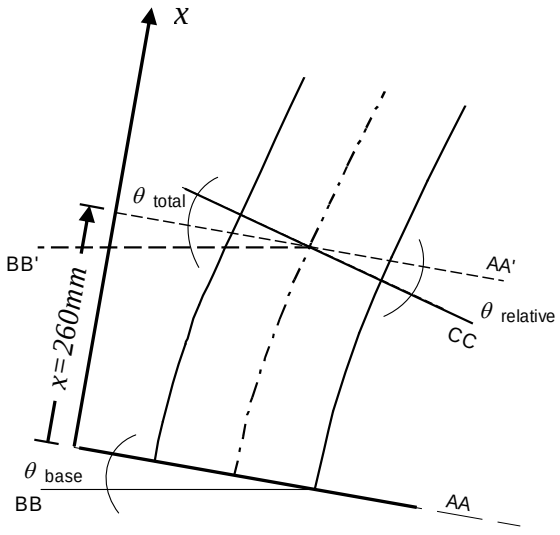

$\theta_{relative}$ =column rotation at x=+260mm with respect to line AA (base of column)
θ_{total} =column rotation at x= +260mm with respect to line BB (foundation)
θ_{base} =column rotation at x= 0mm with respect to line BB (foundation)

The rotation $\theta_{relative}$, is the measure of deformation in bending of the column at x=+260mm with respect to the base of the column. The rotation θ_{total}, includes $\theta_{relative}$ and the rigid body displacement of the column due to a rotation at the base of the column, θ_{base}. The rotation at the base of the column θ_{base} was calculated as the difference between rotation θ_{total} and $\theta_{relative}$ as presented in equation 5.3

$$\theta_{base} = \theta_{total} - \theta_{relative} \qquad \text{(eq 5.3)}$$

Figure 5.20 presents the rotations at x=+260mm from the base of the instrumented column for the dynamic response of the bare frame during test F. These values are evidence that during the dynamic response of the bare frame there were rotations due to deformation (θ_{relative}), as well as due to rigid body motion (θ_{base}) of the column. The maximum value of the base rotation, θ_{base} =2.1e-3 rad, is 70% of the maximum total rotation, θ_{total} =-3.1e-3 rad ,, and 33% of the maximum top drift, Δ=-0.64%. These measurements are additional evidence of a flexible condition at the connection of the GLDRC columns to the foundation

A plot of the variation of the maximum rotations and the maximum relative drifts during the response time histories for tests in testing Series A is presented in Figure 5.21. From this plot of maximum values it can be identified that the base rotation, θ_{base}, is on average, 72% of the total rotation of the column and 51.2% of the top lateral drift of the specimen. This observation indicates that the GLDRC frame can not be analyzed assuming a zero rotation support condition and rather should be modeled as free to rotate.

5.7 Comparison Bbetween Measured Response of GLDRC Infilled Frame and Bare Frame

This section compares response values of the infilled GLDRC frame with the bare GLDRC frame to illustrate in which aspects the interaction between the URM infill wall and the GLDRC frame changed the dynamic behavior of the structure. The comparison of the response of the two specimens is carried out only for tests #01 through test #08 of testing Series A.

Figure 5.22a presents the maximum values of the top lateral deformation responses of the infilled GLDRC frame and the bare GLDRC frame for each test in Series A. This Figure

shows that for the same dynamic excitation the maximum top relative displacement response for the infilled frame was lower than for the bare frame. In addition, it demonstrates that for infilled frame, the URM wall and the frame maintained a constant interaction through the mortar interface during all the testing series A. For the case of the bare frame with the 19mm gap, it is shown that for test #5 with a maximum top relative displacement of 19.4mm, there is a change in the variation of the maximum relative deformation per test, from increasing to decreasing proportionally to the increase in the excitation's amplitude. This behavior can be associated with the effect of pounding with the URM wall observed during testing.

Figure 5.21 Column rotation time histories

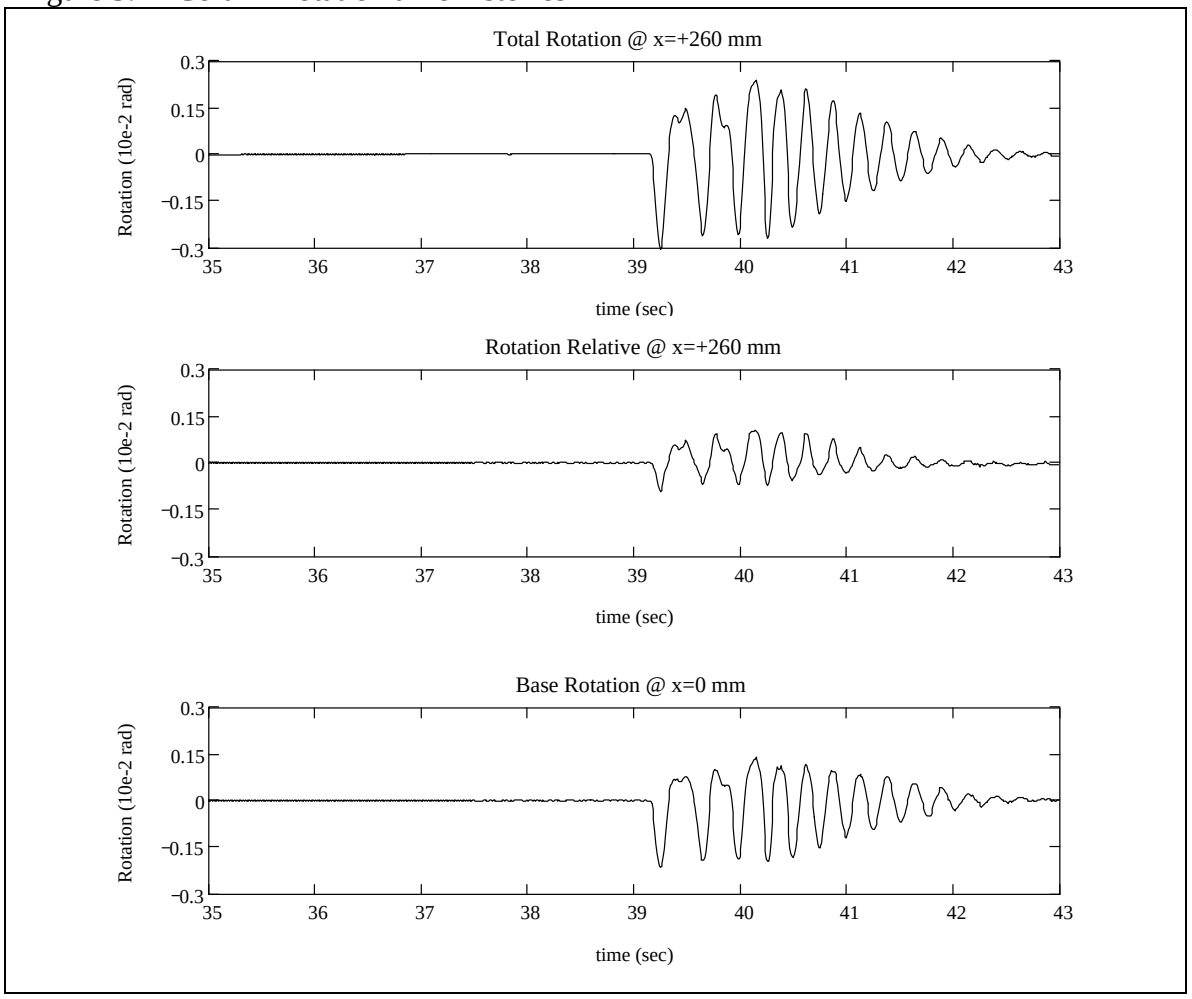

Figure 5.22 Maximum rotations and top lateral drift plot for test Series A specimen #3

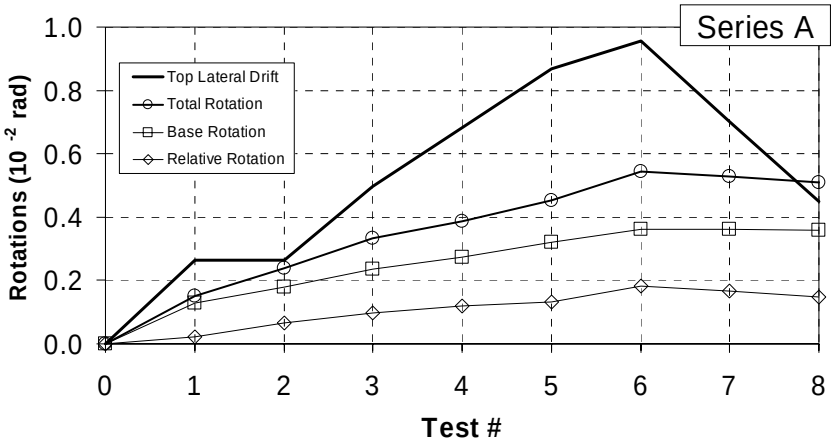

Figure 5.23b presents the effective lateral stiffness of the infilled GLDRC frame and the bare GLDRC frame. This Figure allows observing that the infilled frame presented a higher effective stiffness than the bare frame for all of the tests performed in test series A. For the response of both specimens, the highest degradation in effective stiffness occurred after their first dynamic response and little variation after tests #02 through #06.

5.8 Discussion on the Observed Response of Gravity Load Designed RC Frames with Unreinforced Masonry Infill Walls

The results of this experimental test program suggest that the gravity load designed RC frames have a weak connection to the foundation that changes its lateral load deformation behavior. The masonry infill contributes by increasing the shear stress at the column to foundation interface while reducing the top lateral deformations. Overall, this flexible connection reduces the deformation of the reinforced concrete frame elements.

Figure 5.24 presents a comparison of the instantaneous relative displacements for both the infilled frame and the bare frame for tests #01 and #06. The first visible difference is in the top displacement, which is lower in the infilled frame than in the bare frame, however, what is more important to observe is the difference in the measured

displacements at the base of the columns. In the case of the infilled frame, the measured value at the base indicates that sliding of the column at the interface with the foundation took place, while for the case of the bare frame; the measured values indicate the effect of rotation, described in Section 5.5. Figures 5.24a and 5.24b indicate that the columns in the infilled frame had less deformation along the height compared to the bare frame which is consistent with the observations for the two compared tests.

Figure 5.23 Maximum response values for specimens 2 and 3 for test Series A

a) Max Top Lateral Deformation Response

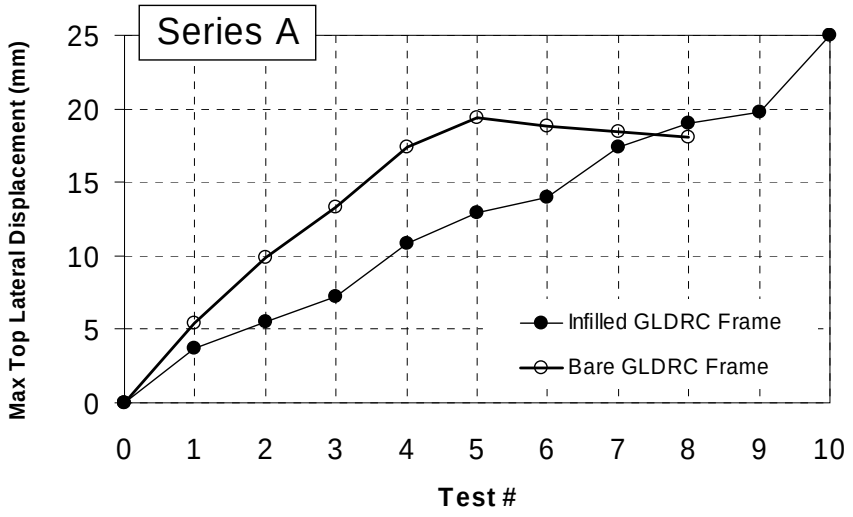

b) Effective Lateral Stiffness

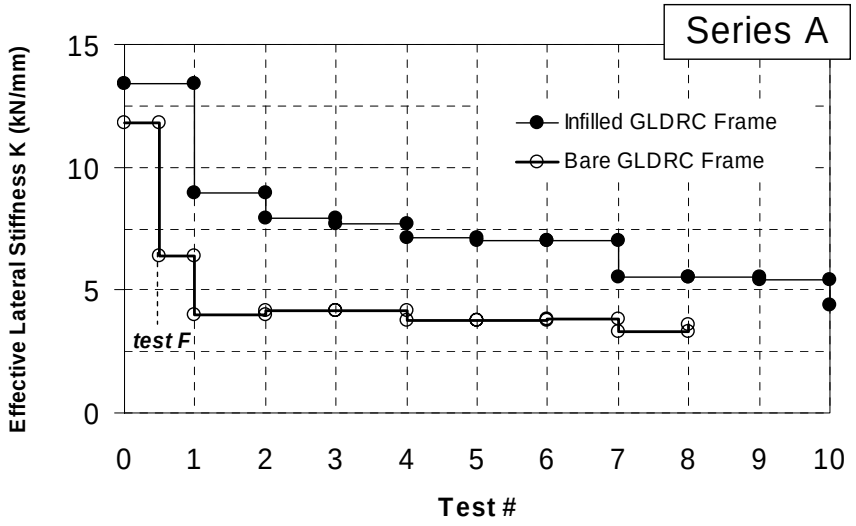

Figure 5.24 Deformed shapes for test Series A

a) Instantaneous Displacements test #1 b) Instantaneous Displacements test #6

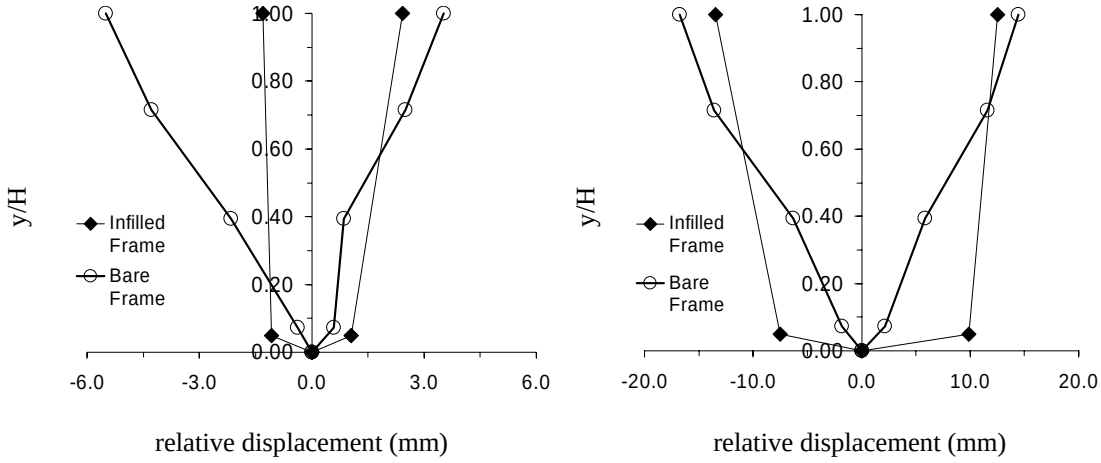

The column-to-foundation interface has a weak bond strength due to a cold joint formed in the construction process. When this bond fails in shear during dynamic response, its shear and bending load-deformation capacity is obtained from friction and the lap spliced rebar, where the latter will slip under high normal stress due to its inadequate development length.

For the seismic response of an infilled GLDRC frame, the masonry infill contributes with lateral stiffness which reduces the deformation demand on the top of the structure, while applying a concentrated shear stress at the lower portion of one column, causing a shear slip of the column at the foundation interface. The system responding under shear slip will have a significant nonlinear behavior thus reducing the input energy from the ground motion.

For the seismic response of a bare GLDRC frame, there is no evidence of local shear deformations at the column-to-foundation interface, but there are rotations at the base. This flexibility prevents the formation of a plastic hinge at the bottom of the RC columns thus avoiding the premature failure of the inadequate lap spliced rebar. The overall behavior becomes similar to that of a simply supported frame with moderate ductility.

For both the bare and infilled frame the flexible connection to the foundation prevents the formation of high flexural or shear deformations at the lower portion of the column. A flexible moment connection at the base of the columns does not affect the system negatively. High shear deformations at the column foundation interface may result in shear failure of the lap splice resulting in an undesirable failure mechanism. Therefore, the maximum deformation capacity of this existing system is controlled by the shear strength at the column-to-foundation interface.

Chapter 6 Conclusions and Recommendations

6.1 Summary

This research project was performed to observe and establish the mechanical characteristics that influence the dynamic response of GLDRC frames with unreinforced masonry walls. The project comprised one monotonic test on a GLDRC infilled frame and shake table testing on one GLDRC infilled frame and one bare frame.

For the monotonic testing of the GLDRC infilled frame, specimen #1, as the top lateral drift demand was increased 3 distinct behavior modes were observed: diagonal compression, shear sliding and bond slip. Diagonal compression was observed as the behavior mode for the linear response of the system, with a constant stiffness of K_L=11.5 kN/mm. Horizontal shear sliding behavior was initiated as the lateral load vs. drift curve indicated yielding at 1.0% drift and 195 kN lateral resistance was not observed beyond 1.65% drift. This mechanism resulted in several horizontal mortar cracks on the bed joints extending all along the length of the URM wall. Bond Slip of the longitudinal rebar at the lap splice was observed as longitudinal splitting cracks in concrete at the base of the GLDRC columns. The bond slip behavior resulted in large rotations at the base of the columns without the formation of plastic hinges. The tested structure reached a maximum drift of 3.55% without loss in lateral strength.

For the shake table testing of the GLDRC infilled frame, specimen #2, a total of 33 tests were performed. The levels of shaking followed the established testing program. The response of the specimen showed three behavior modes: diagonal compression, horizontal shear sliding and bond slip. Diagonal compression was observed for the first set of tests. The shear sliding behavior was observed during test #09, with the formation of a mortar cracking along the bed joints extending along the full length of the URM wall. For tests #15 through #19, the shear sliding behavior resulted in the knee braced effect on the GLDRC columns which generated plastic rotations above the expected

location for plastic hinges in columns. The URM wall failed at test #30 due to loss of mortar bond of the concrete blocks in the center and the corners of the wall. After test #33, longitudinal splitting cracks in the concrete were found at the base of the GLDRC columns. At the end of the shake table tests, no plastic hinges or flexural cracks were found along the location of the lap splice of the longitudinal rebar for the GLDRC columns.

A total of 8 shake table tests were performed on the bare frame, specimen #3, following the same testing program as for specimen #2. Due to an unexpected response of the shake table system, prior to starting the test protocol two large pulse motions were applied to the specimen which resulted in flexural cracks at the ends of the GLDRC beam. The response to test #01 showed cracking in the GLDRC columns and beam. The behavior was observed to have larger amplitudes of vibration.

6.2 Conclusions

The overall results of the testing program showed 3 distinct behavior modes through different stages in the response of the infilled specimens: diagonal compression, shear sliding and bond slip. The test results also indicated large measured rotations and concentrated shear sliding at the base of the GLDRC columns. The change in the specimens measured structural properties after different levels of shaking confirmed the damage values recommended by FEMA 306 for performance based retrofit design.

.

For the diagonal compression behavior mode the infilled frame showed a linear elastic behavior with some dissipation of energy. The URM wall in diagonal compression increased the lateral stiffness of the system and thereby prevented cracking in the bounding frame. Significant shear sliding displacements were found at the base of the infilled frames due to the infill wall's diagonal compression transferring of the inertial load to the base of the adjacent column and to the foundation. Shear sliding of the URM wall occurred due to the low bond strength of mortar joints and the high compression

strength of concrete blocks. When the URM wall changed to a shear sliding behavior, it resulted in softening of the wall, and produced a knee braced effect on the GLDRC frame. This knee braced effect was observed as the formation of a plastic hinge in each GLDRC columns. The column's plastic hinge location along its length coincided with the sliding plane of the cracked URM wall. These observed plastic hinges coincided with the recorded reduction in sliding at the base of the columns. The bond slip of the columns' longitudinal reinforcement at the location of the lap splice resulted in large rotations at the base and prevented yielding of the longitudinal rebar at the base of the columns.

At the base of the columns of the three tested GLDRC frames there were observed and measured rotations and concentrated shear sliding. Rotations were measured for a bare frame and were found to represent on average 51.2% of the top lateral drift of the specimen. The shear sliding of the columns was measured from the first shake table test and resulted in a pinched hysteretic plot and the highest decrease in lateral stiffness for the response of the structure.

High shear deformations at the column foundation interface may result in shear failure of the lap splice resulting in an undesirable failure mechanism. Therefore, the maximum deformation capacity of this infilled frame is controlled by the shear strength at the column-to-foundation interface.

For both the bare and infilled frame the flexible connection to the foundation prevents the formation of high flexural or shear deformations at the lower portion of the column. A flexible moment connection at the base of the columns does not affect the GLDRC frame negatively except, it reduces its redundancy.

6.3 Recommendations for Further Studies

This study recommends a testing program to determine an efficient retrofit strategy of a GLDRC frame with a URM infill wall using Fyber Reinforced Polymer (FRP) technology. The study would determine the effect of the location and alignment of the FRP sheets on the failure mechanism. This study should also determine the dynamic response of the retrofitted system to out of plane motions.

An additional testing program would require studying the shear strength and deformation capacity of the GLDRC column-to-foundation connection. This information would allow presenting a more accurate retrofit strategy for GLDRC frames with URM infill walls.

6.4 Recommendations for Retrofit Solutions for Gravity Load Designed Frame Structures with Unreinforced Masonry Walls

Based on the observed results in this research program, a recommended 1.0% drift capacity should be considered for unretrofitted GLDRC frames with URM infill walls. This value is set to ensure that the URM infill wall will not fail in shear, thus avoiding the shear sliding behavior of the URM concrete block infill wall and avoiding short column effects on the GLDRC columns.

The URM walls require a retrofit strategy that will increase the shear strength of the masonry wall. This strategy would allow for the URM wall to behave in diagonal compression for larger deformations and avoid shear sliding behavior. Additional testing is required to recommend an effective retrofit strategy for GLDRC frames with URM infill walls.

In addition, this testing program observed that the slip due to short lap splices at the column to foundation connection were beneficial to the response of the specimen.

Retrofitting this connection to increase the flexural strength and stiffness may result in significant difference in the resulting deformation behaviors.

It is recommended to increase the shear strength of the column-to-foundation connection based on the results of this testing program. The selected retrofit strategy for the shear resistance of the column-to-foundation connection must only restrain the sliding deformations and not increase the rotational stiffness at the base of the columns.

References

ACI Committee 318, 1963, “Building Code Requirements for Reinforced Concrete (ACI 318-63),” American Concrete Institute, Detroit Michigan.

Al-Chaar G., Issa M., and Sweeny S., 2002, “Behavior of Masonry-Infilled Nonductile Reinforced Concrete Frames” Journal of Structural Engineering Vol 128, No 8, August.

ATC, 1999a, “Evaluation of Earthquake Damage Concrete and Masonry Wall Buildings, Basic Procedures Manual” Applied Technology Council (ATC 43 Project) for the Partnership for Response and Recovery, published by the Federal Emergency Management Agency, Report No. FEMA 306, Washington, DC.

Axley J., and Bertero V.V., 1979, “Infill Panels- Their Influence on Seismic Response of Buildings” UCB/EERC-79/28.

Avendano R., 2007, “Experimental Study on Mechanical Properties of Masonry Infill Walls” Report No 07-05 Department of Civil Engineering School of Construction and the Environment British Columbia Institute of Technology Burnaby, BC, Canada.

Brincker R., and Larsen J. A., 2007, “Obtaining and Estimating Low Noise Floors in Vibration Sensors,” Proceedings of the XXV International Modal Analysis Conference, Orlando, Florida.

Brincker R., Ventura, C.E., and Larsen, J.A., 2007, “A General Purpose Digital System of Field Vibration Testing,” Proceedings of the XXV International Modal Analysis Conference, Orlando, Florida.

Brincker R., Zhang, L., and Andersen P., 2000, “Modal Identification from Ambient Responses using Frequency Domain Decomposition”, 18th International Modal Analysis Conference ,San Antonio, Texas, pp 625-630.

Brokken S., and Bertero V.V., 1981, “Studies on Effects on Infills in Seismic Resistant R/C Construction” UCB/EERC-81/12.

Canadian Standards Association, 2004, Canadian Standard: Design of Masonry Structures (S304.1-04). Mississauga ON: CSA

Cho J.-Y, and Pincheira J.A., 2006, “Inelastic Analysis of Reinforced Concrete Columns with Short Lap Splices Subject to Reversed Cyclic Loads”, ACI Structural Journal, V. 103, No. 2, pp. 280-290.

Drysdale R. G., Hamid A. A., and Baker, L. R., 1999, “Masonry Structures: Behavior and Design”, Second Edition Prentice Hall, Englewood Cliffs, New Jersey.

El-Dakhakhni W.W., Elgaaly M., and Hamid A.A., 2003, “Three Strut Model for Concrete Masonry-Infilled Steel Frames”, ASCE Journal of Structural Engineering, Vol. 129, No. 2, 2003, pp.177–185.

Eligehausen R.; Popov E. P., and Bertero V. V., 1983, “Local Bond Stress- Slip Relationships of Deformed Bars under Generalized Excitations,” UCB/ EERC-83-23, University of California, Berkeley, Calif., 1983, 169 pp.

Fiorato A. E., Sozen, M. A., and Gamble, W. L., 1970, ‘‘An investigation of the interaction of reinforced concrete frames with masonry filler walls.’’ Civil Eng. Studies, Structural Research Series Rep. No.370, Univ. of Illinois, Urbana, Ill

Hashemi A, and Mosalam KM. 2006, “Shake-table experiment on reinforced concrete structure containing masonry infill wall.” Earthquake Engineering and Structural Dynamics 2006; 35:1827–1852.

Holmes, I. L. 1965, "Concrete Masonry Buildings in New Zealand." Proceedings of the 3rd World Conference on Earthquake Engineering.

Jaiswal K., Sinha R., and Goyal A., 2003, “Reinforced Concrete Frame Building with Masonry Infill Walls designed for Gravity Loads”. World Housing Encyclopedia (www.world-housing.net). Earthquake Engineering Research Institute and International Association for Earthquake Engineering, India/Report 19.

Kharrazi, M. H., 2001, “Vibration Characteristics of Single-Familiy Woodframe Buildings,” M.A.Sc. Thesis, Department of Civil Engineering, The University of British Columbia, Vancouver, BC, Canada

Mehrabi A., Shing P. Benson Armin, 1996, “Experimental Evaluation of Masonry-Infilled RC Frames” Journal of Structural Engineering Vol 122 No3.

Melek M.; Wallace J. W.; and Conte J. P., 2003, “Experimental Assessment of Columns with Short Lap Splices Subjected to Cyclic Loads,” Report No. PEER 2003/04, University of California-Berkeley, Berkeley, CA.

Murty, C. V. R., and Jain, S. K., 2000, Beneficial influence of masonry infills on seismic performance of RC frame buildings, Proceedings, 12th World Conference on Earthquake Engineering, New Zealand, Paper No. 1790.

NRC, 2005 “National Building Code of Canada, 2005, Part 4 Structural Design” National Research Council, Ottawa, ON, Canada.

Nan Su, 2002 “structural evaluations of reinforced concrete buildings damaged by Chi-Chi earthquake in Taiwan” Practice Periodical on Structural Design and Construction, Vol. 6, No. 3.

Öztürk M. S., 2005, “Effects Of Masonry Infill Walls On The Seismic Performance Of Buildings” Middle East Technical University, Ankara Turkey

Paulay T., and Priestley M. J. N., 1992, Seismic Design of Reinforced Concrete and Masonry Buildings, John Wiley & Sons, Inc., New York.

Pincheira Jose A., and James O. Jirsa., 1995 "Seismic Response of RC Frames Retrofitted with Steel Braces Or Walls." Journal of Structural Engineering 121.8: 1225-35.

Pinto A., and Taucer F., 2006, “Assessment And Retrofit Of Full-Scale Models Of Existing Reinforced Concrete Frames” Advances in Earthquake Engineering for Urban Risk Reduction pp 353-367.

Polyakov, S. V., 1960, "On Interaction between Masonry Filler Walls and Enclosing Frame when Loaded in-plane of Wall." Earthquake Engineering Research Institute -- Translations in Earthquake Engineering: 36-42.

Saatcioglu M., Serrato F., and Foo S., 2004, “Seismic Performance Of Masonry Infill Walls Retrofitted With CFRP Sheets” Research Report No: OCCERC 04-31, pp. 105.

Sezen H., Whittaker A. S., Elwood K. J., and Mosalam K. M., 2003, “Performance of Reinforced Concrete and Wall Buildings during the August 17, 1999 Kocaeli , Turkey Earthquake, and Seismic Design and Construction Practice in Turkey.” Engineering Structures. Vol 25, No. 1, 103-114.

Stafford-Smith, B. 1966. “Behaviour of square infilled frames” ASCE Journal of the Structural Division, 92(ST1): 381–403.

Telcordia Technologies, “Network Equipment-Building Systems (NEBS) Requirements: Physical Protection”. Telcordia Technologies Generic Requirements, GR-63-CORE, Issue 1, October 1995.

Turek, M., 2002. “In-Plane Shake-Table Testing of Unreinforced Masonry Walls Strengthened with Fibre-Reinforced Plastics”, M.A.Sc. Thesis Department of Civil Engineering, The University of British Columbia, Vancouver, BC, Canada.

Appendix A: Monotonic Test Setup

1) Reaction Column
Verification of Acceptable Stress and Deformation

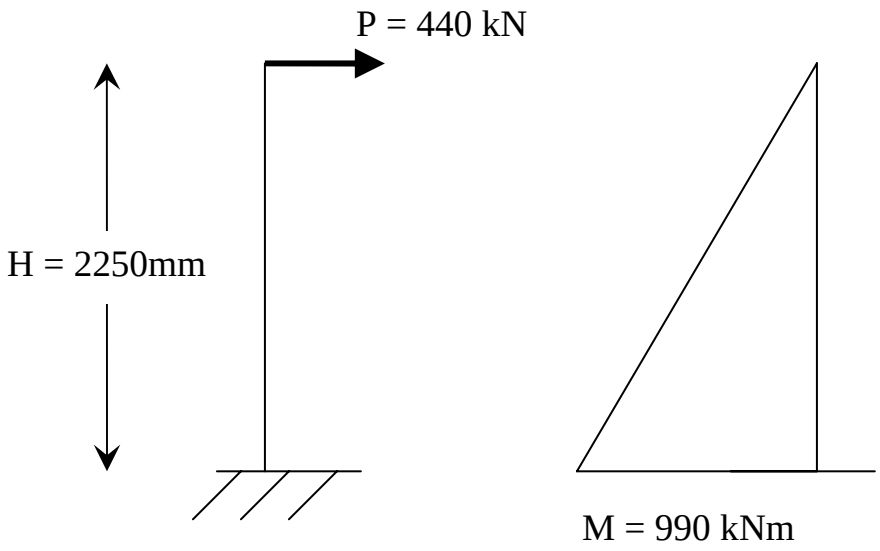

Prior Information=

$\sigma_y = 350 MPa$

$E = 200 GPa$

$I_x = 1.725 x 10^{10} mm^4$

$S_x = 2.61 \; x 10^{7} \; mm^{3}$

$\sigma = \frac{M}{S_x}$		$\Delta = P\frac{H^3}{3EI}$
$\sigma = \frac{990 kNm}{2.61 x 10^7 mm^3}$		$\Delta = \frac{440 kN(2250 mm)^3}{3(200 x 10^3 MPa)(1.725 x 10^{10} mm^4)}$
$\sigma = 37.9 MPa \le \sigma_y$		$\Delta = 0.05 mm$

2) Vertical Supports
Verification of Acceptable Stress and Deformation

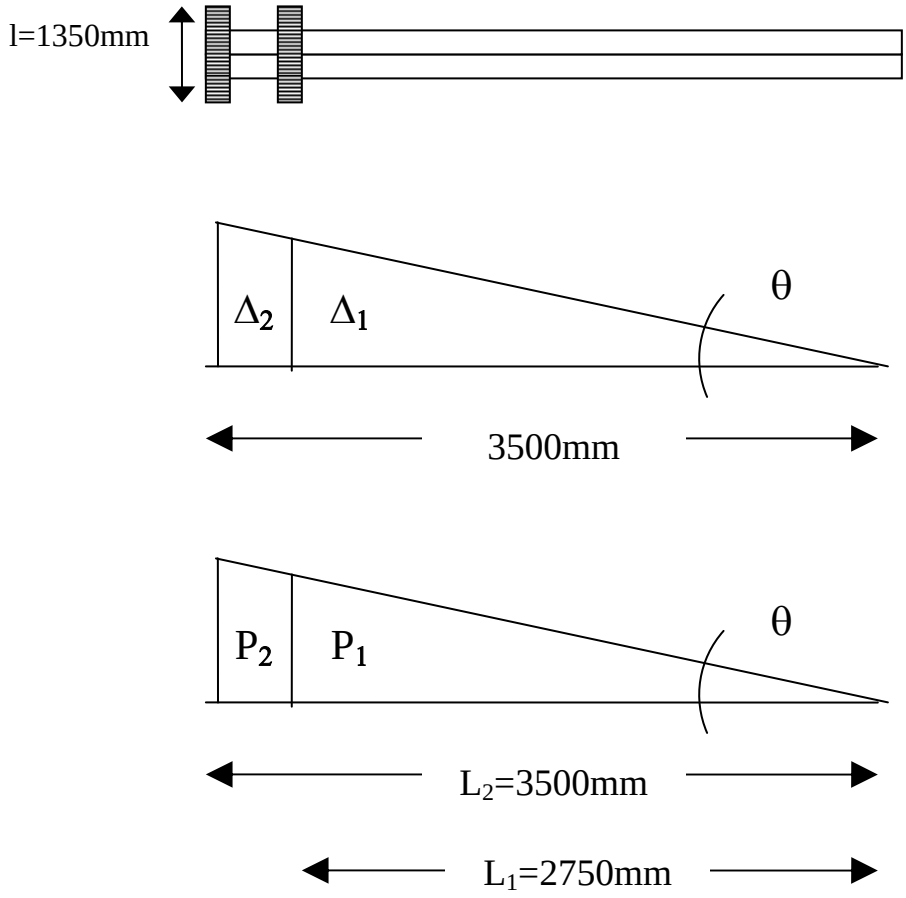

Prior Information=

$M = 990\,kNm$

$\sigma_y = 517\,MPa$

$E = 200\,GPa$

$l = 1350\,mm$

$A = 1963\,mm^2$

$$M = P_2 L_2 + P_1 L_1$$

$$M = (2\frac{AE}{l}\Delta_2)L_2 + (2\frac{AE}{l}\Delta_1)L_1$$

$$M = 2\frac{AE}{l}[\Delta_2 L_2 + \Delta_1 L_1]; \qquad \frac{\Delta_1}{L_1} = \frac{\Delta_2}{L_2}$$

$$M = 2\frac{AE}{l}\left[\Delta_2 L_2 + \left(\Delta_2 \frac{L_1}{L_2}\right)L_1\right]$$

$$M = 2\frac{AE}{l}\left[L_2 + \left(\frac{L_1^2}{L_2}\right)\right]\Delta_2$$

$$990\,kNm = 2\left(\frac{(1963\,mm)(200\,x10^3\,MPa)}{1350\,mm}\right)\left[3500 + \left(\frac{3500^2}{2750}\right)\right]\Delta_2$$

$$990\,kNm = 2\left(290.8\frac{kN}{mm}\right)\left[3500\,mm + \left(\frac{2750^2}{3500}\right)mm\right]\Delta_2$$

$$\Delta_2 = 0.30\,mm\,; \ \frac{\Delta_2}{l} = 2.3x10^{-4} \le \varepsilon_y$$

$$\Delta_1 = 0.24\,mm\,; \ \frac{\Delta_1}{l} = 1.85x10^{-4} \le \ \varepsilon_y$$

Monotonic Test Setup and Dimensions

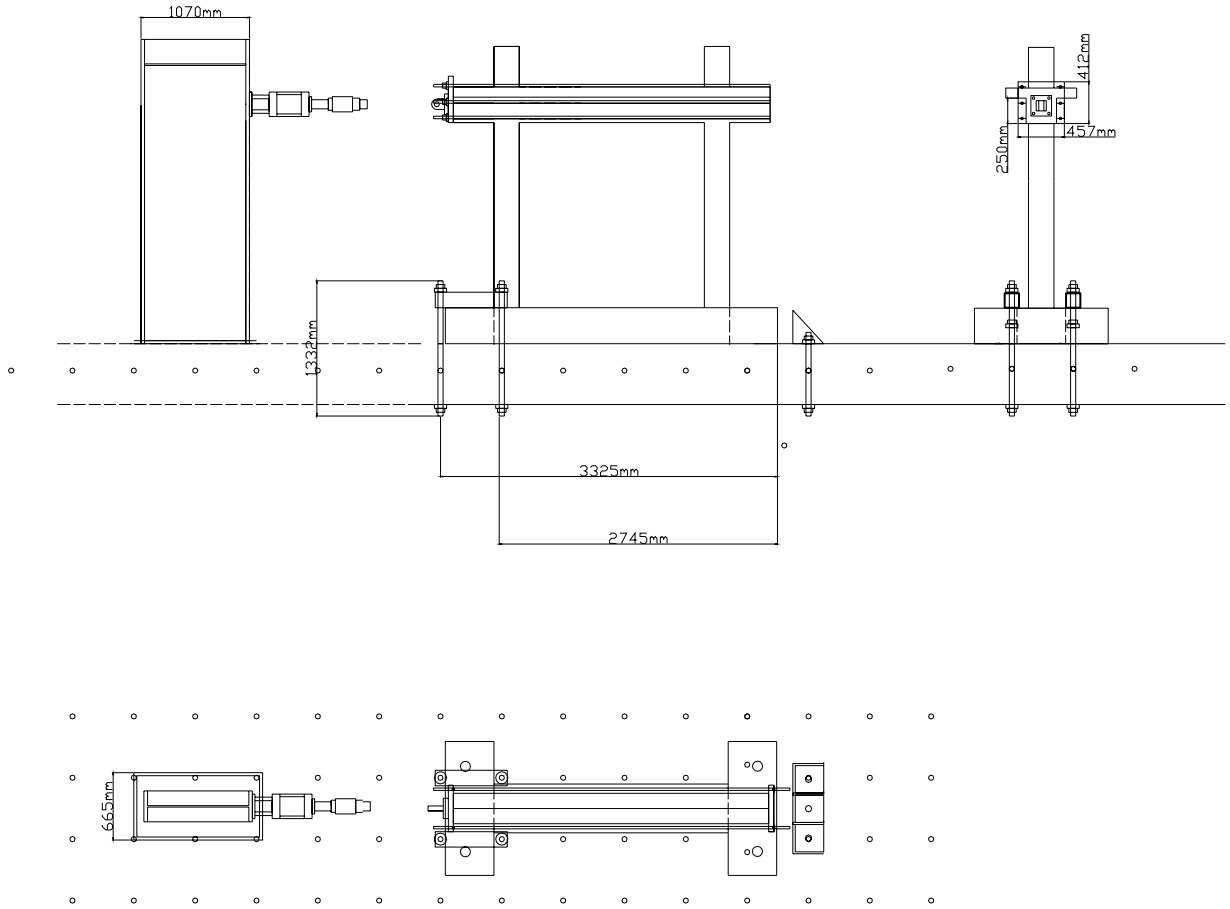

Appendix B: Measured Response from Shake Table Tests on Infilled Frame

Test Series	test #	Earthquake Record	Amplitude	PGA (g)	NOTE
A	01	VERTEQII Z2	50%	0.25	Surcharge Weight = 62 kN
	02		100%	0.50	
	03		150%	0.75	
	04		200%	1.00	
	05		250%	1.25	
	06		300%	1.50	
	07		320%	1.60	
	08		340%	1.70	
	09		400%	2.00	
	10	VERTEQII Z2 Sequence of 3	400%	2.00	3 records are run with 30 secs waiting time
B	11	VERTEQII Z4	100%	0.50	Steel Plates Removed Surcharge Weight = 4.46 kN
	12		150%	0.75	
	13		200%	1.00	
	14		250%	1.25	
C	15		100%	0.50	6 Steel Plates Added Surcharge Weight = 31 kN
	16		150%	0.75	
	17		200%	1.00	
	18		250%	1.25	
	19	VERTEQII Z4 Sequence of 3	225%	1.13	3 records are run with 30 secs waiting time
D	20	Extended VERTEQII Z4	300%	1.50	
	21	Modified SCT1-1985-#1	300%	1.50	
	22		300%	1.50	
	23		300%	1.50	
	24	Extended VERTEQII Z4	200%	1.00	
	25		225%	1.13	
	26		250%	1.25	
	27		275%	1.38	
	28		300%	1.50	
	29		300%	1.50	
	30		300%	1.50	
E	31	Modified SCT1 1985 #2	400%	2.00	
	32	Extended VERTEQII Z4	200%	1.00	
	33		200%	1.00	

Table B1: Dynamic Loading protocol for all the tests performed on Specimen 2

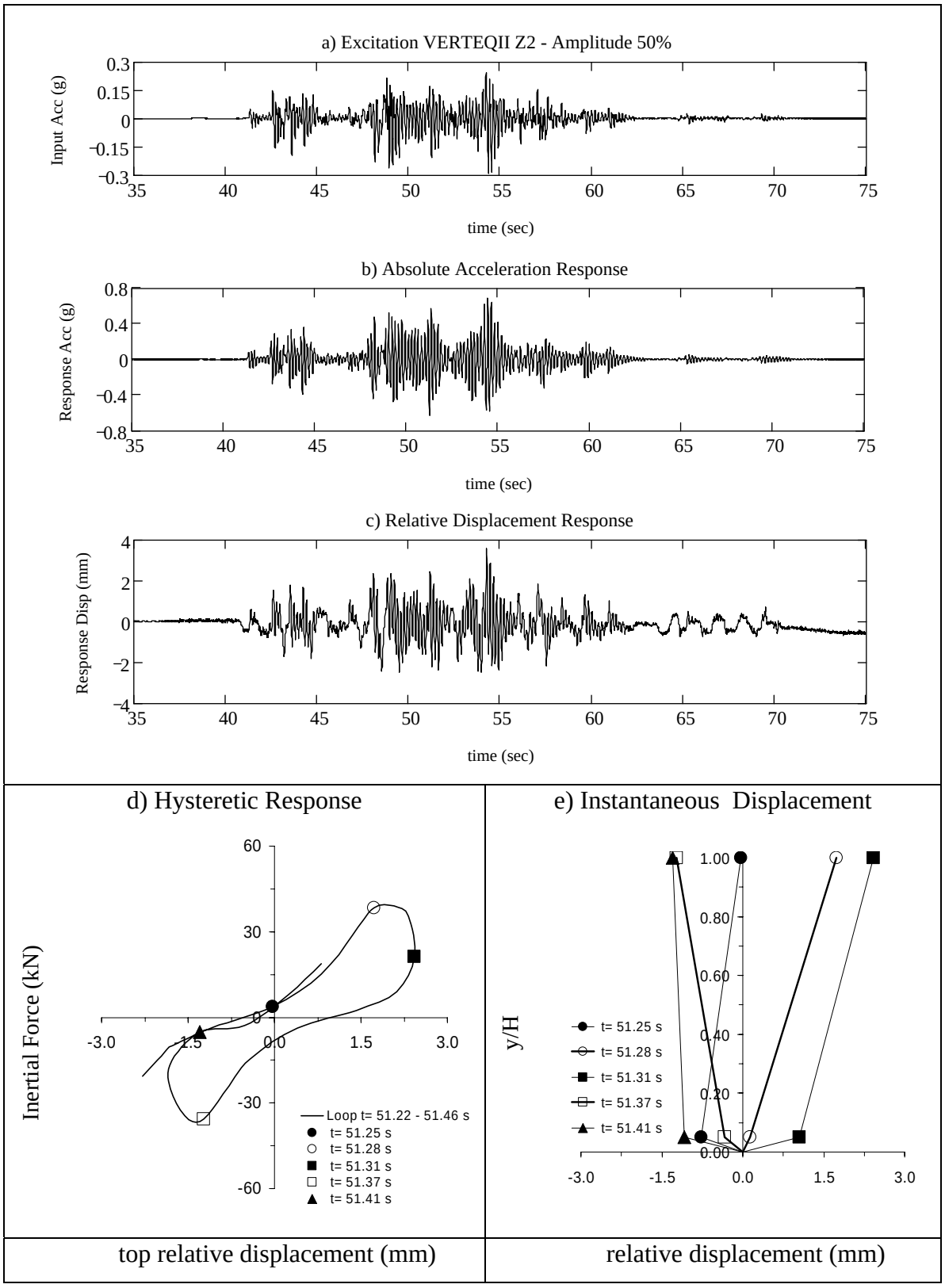

Figure B..1 Summary of Specimen 2 Response for Test#1

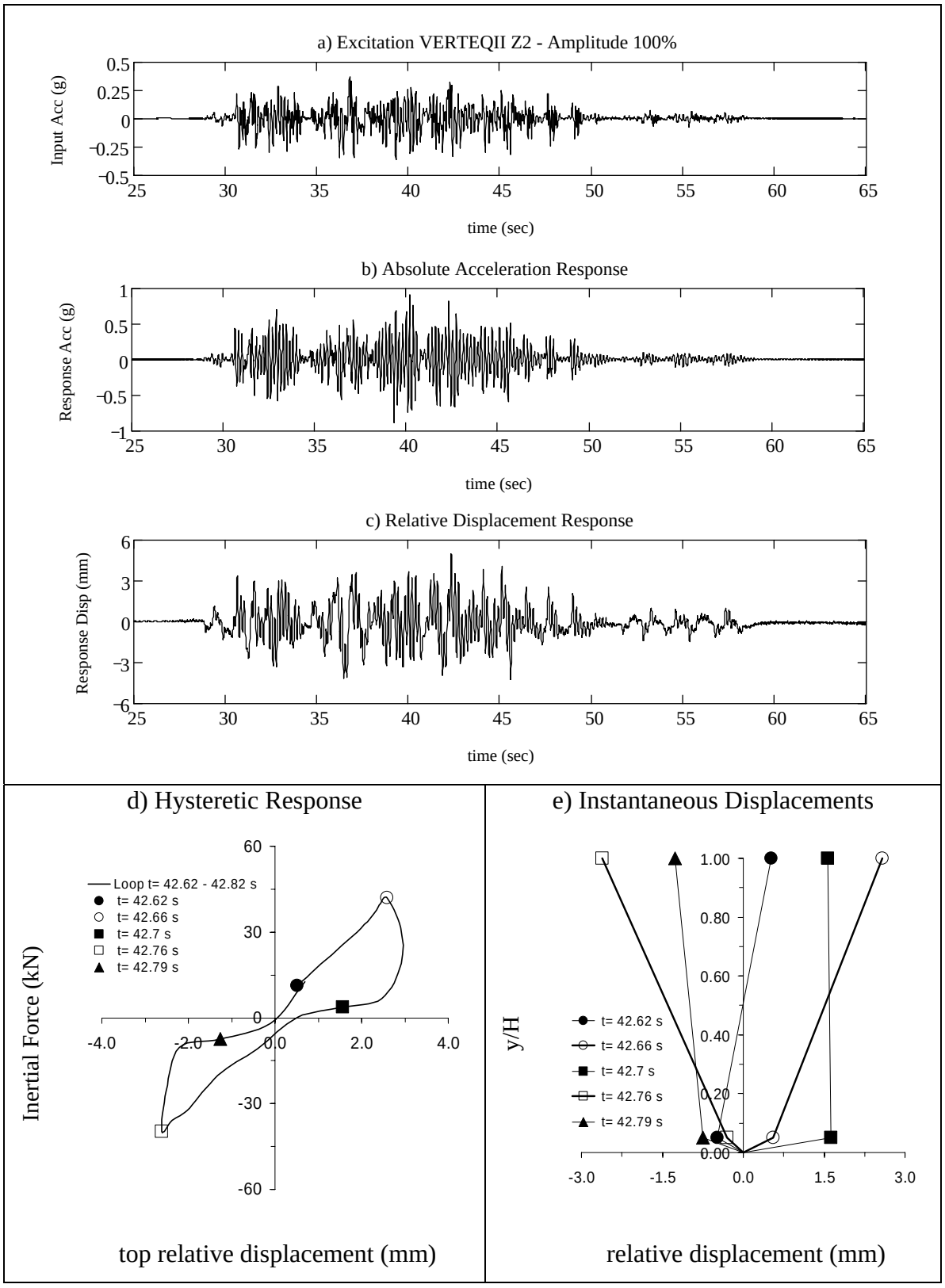

Figure B..2 Summary of Specimen 2 Response for Test#2

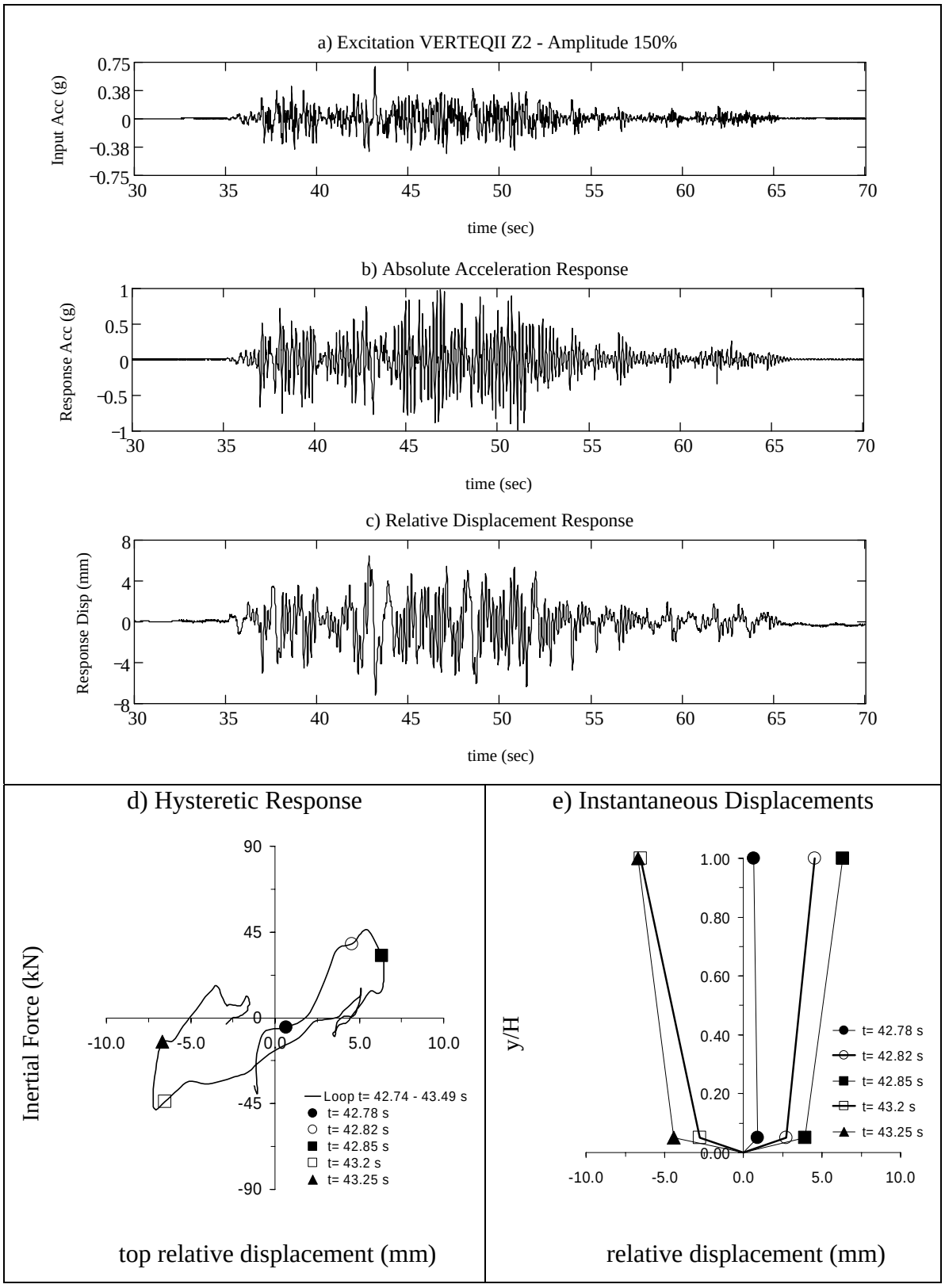

Figure B..3 Summary of Specimen 2 Response for Test#3

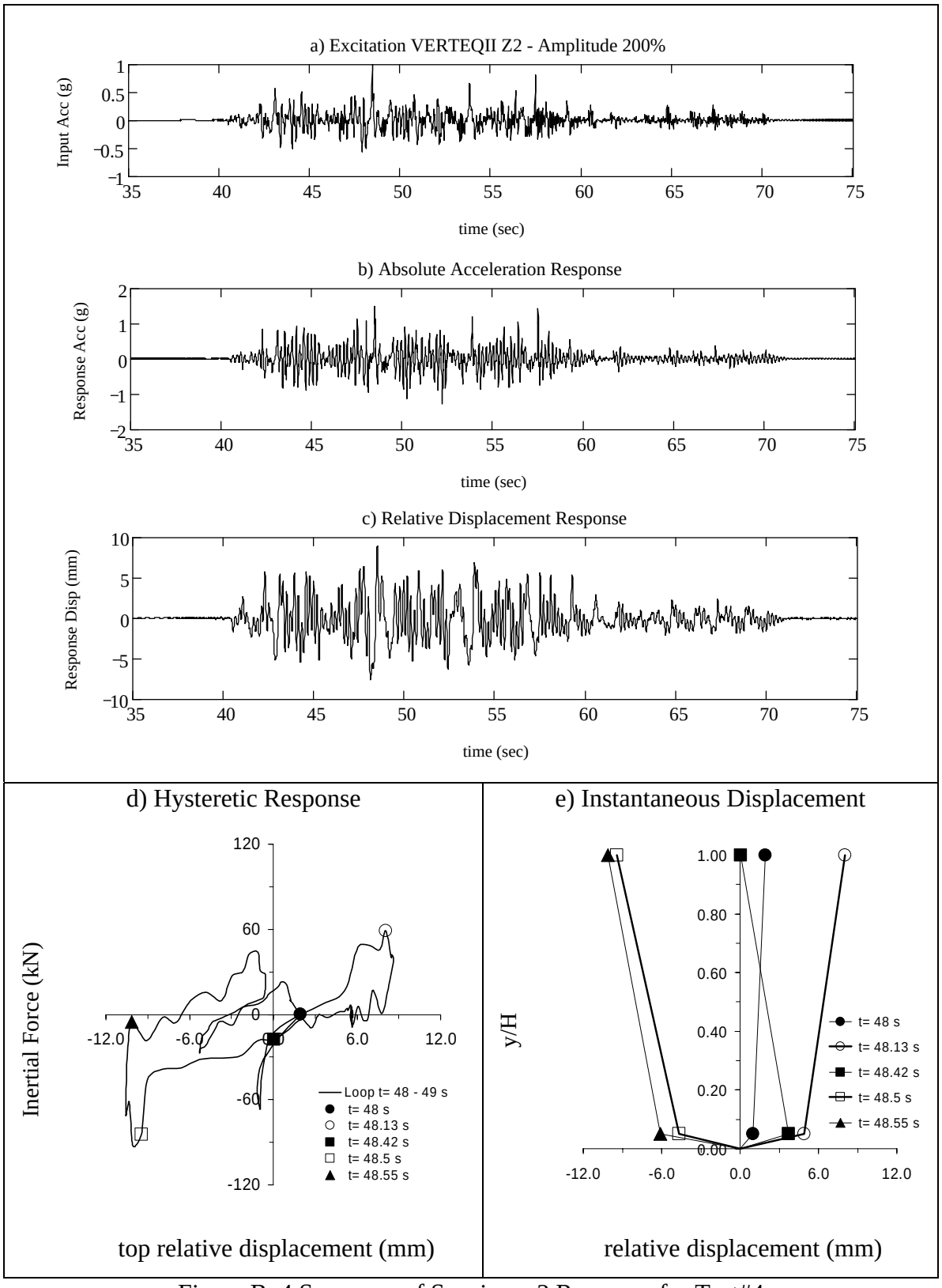

Figure B..4 Summary of Specimen 2 Response for Test#4

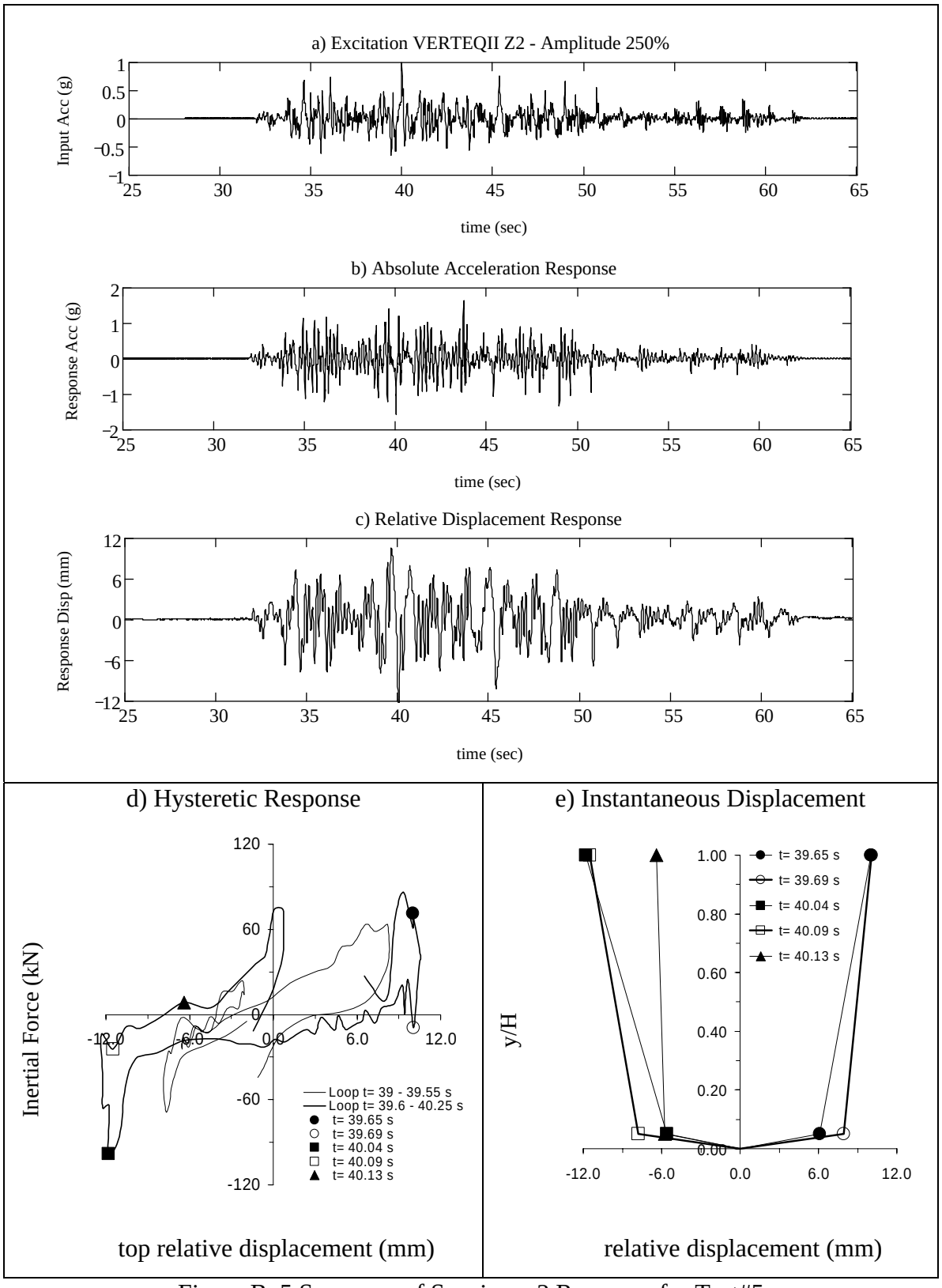

Figure B..5 Summary of Specimen 2 Response for Test#5

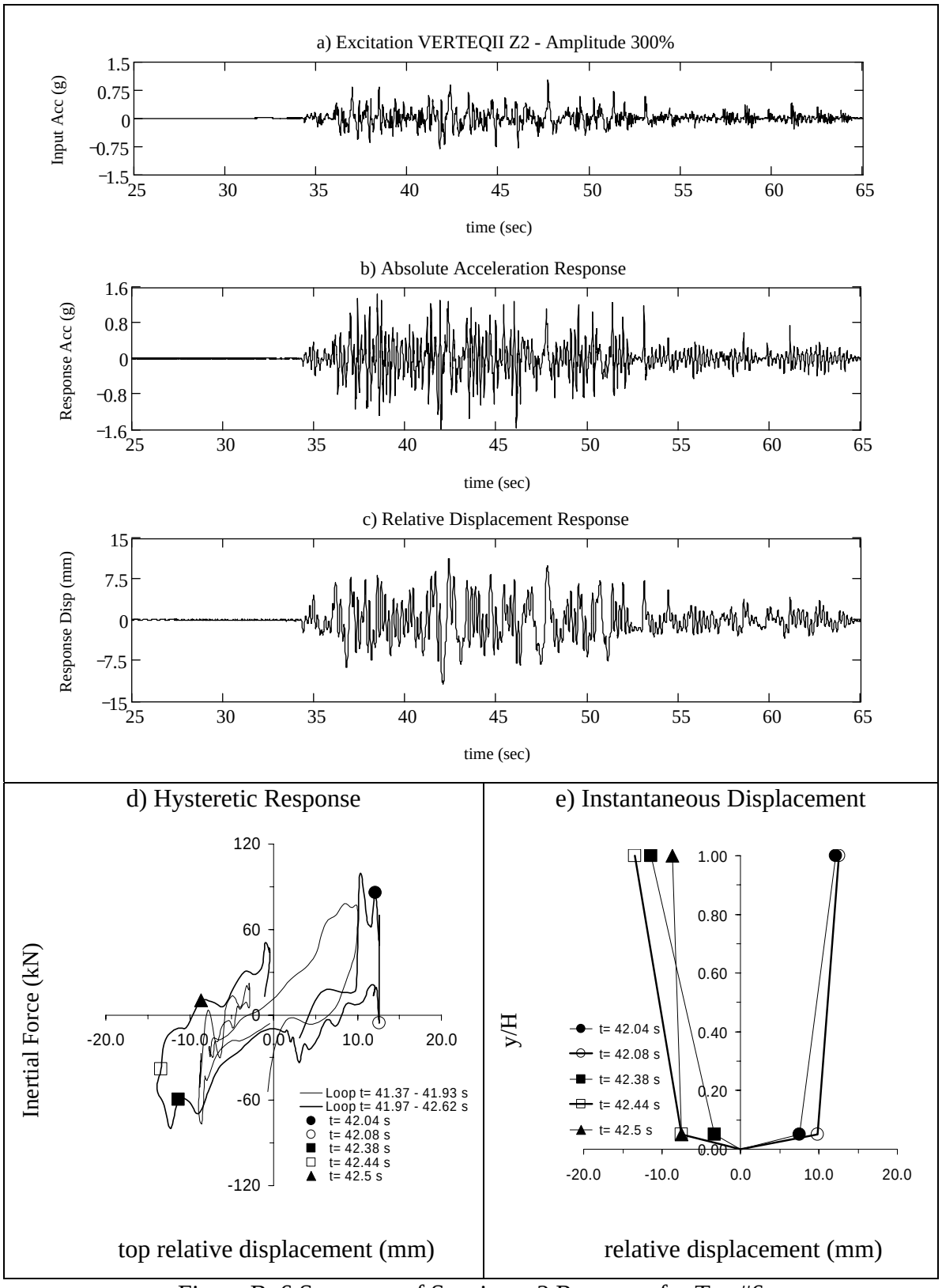

Figure B..6 Summary of Specimen 2 Response for Test#6

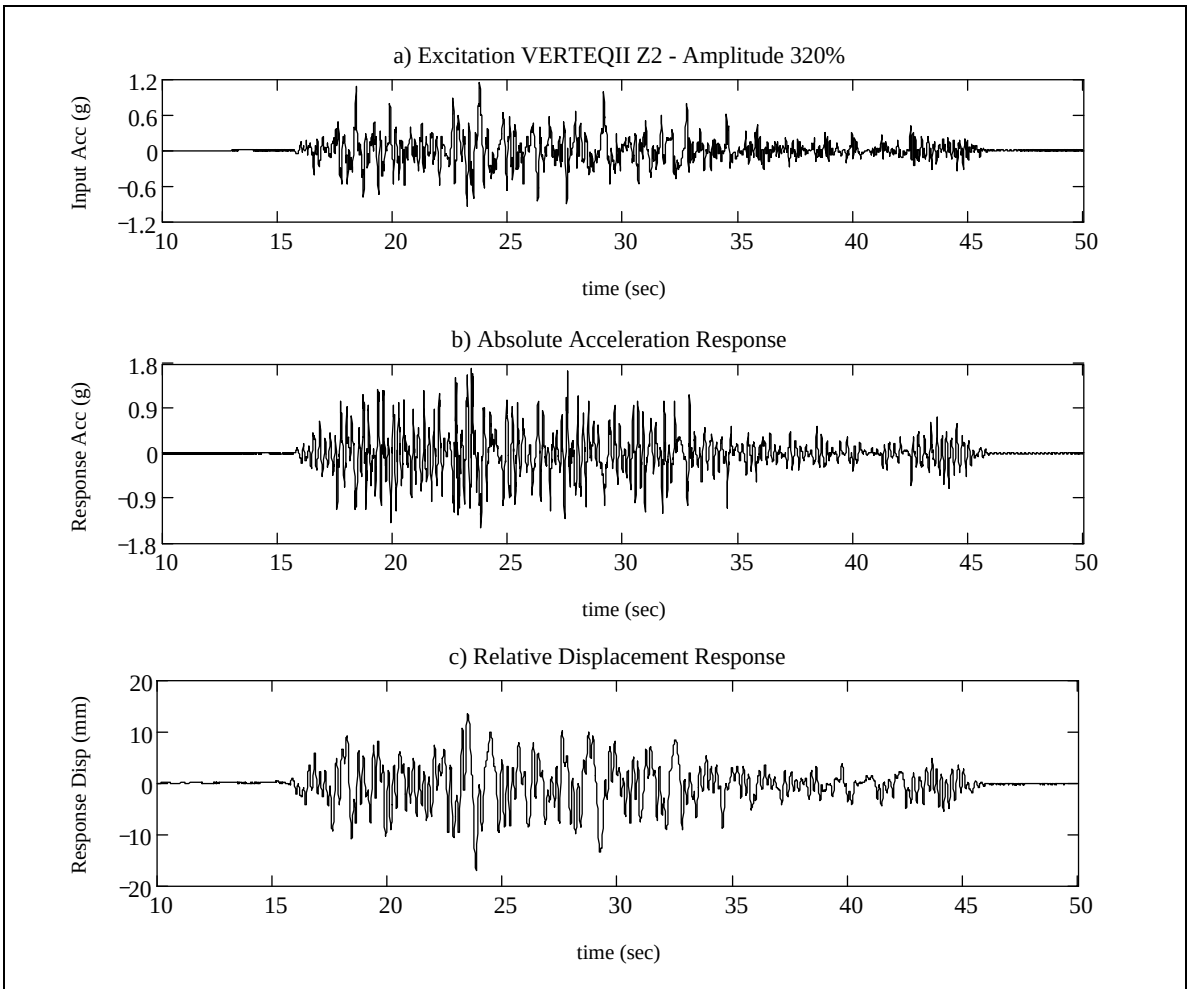

d) Hysteretic Response

e) Instantaneous Displacement

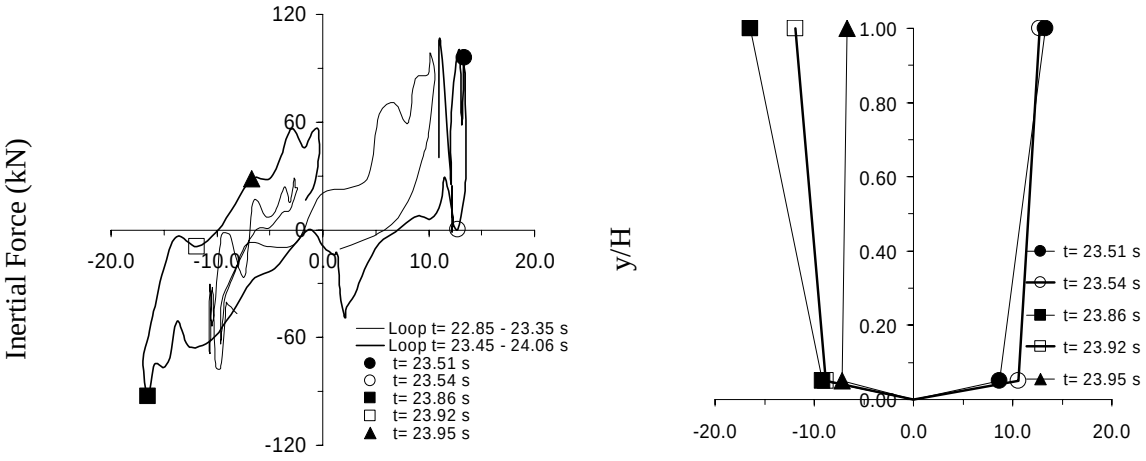

Figure B..7 Summary of Specimen 2 Response for Test#7

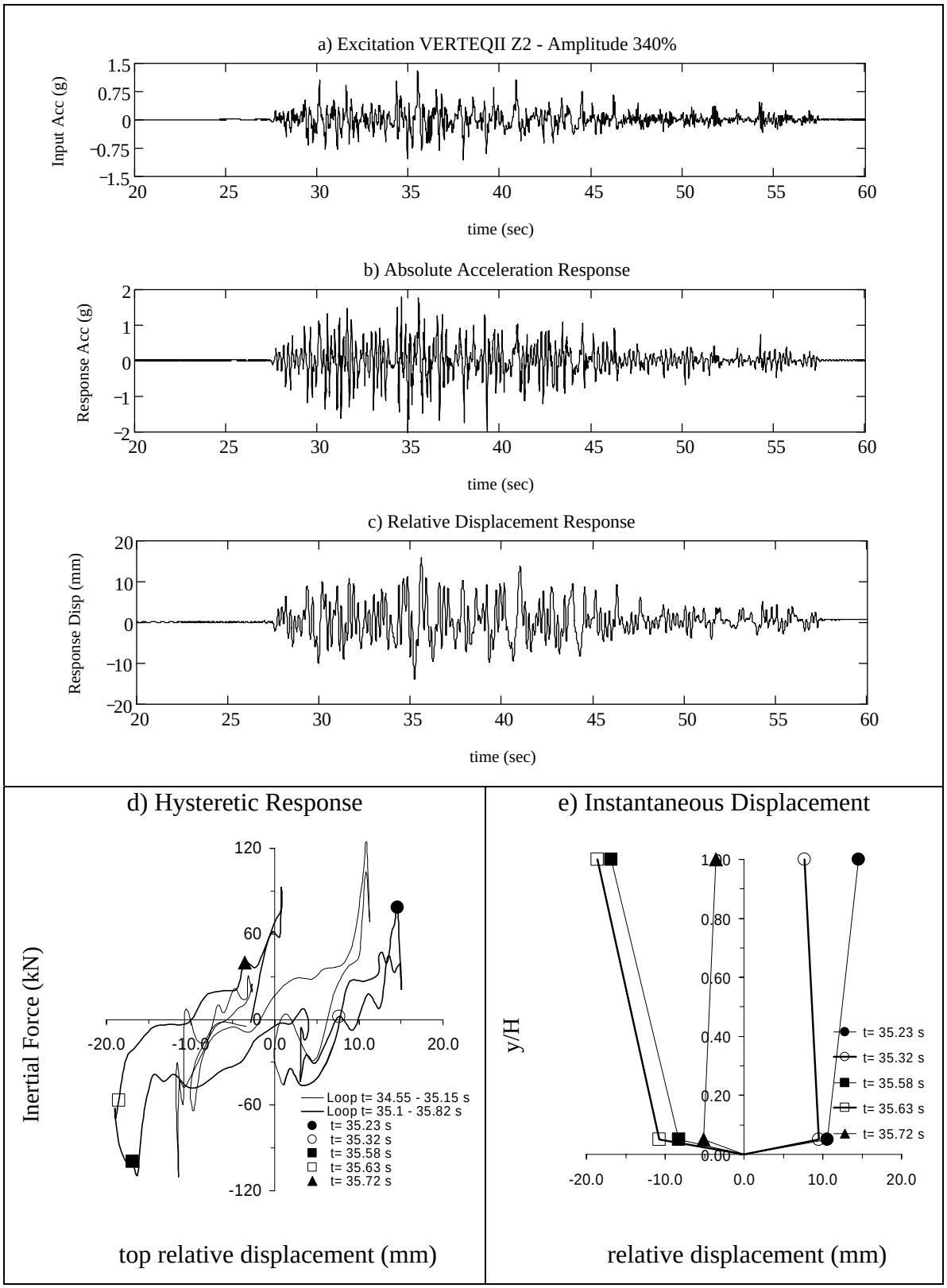

Figure B.8 Summary of Specimen 2 Response for Test#8

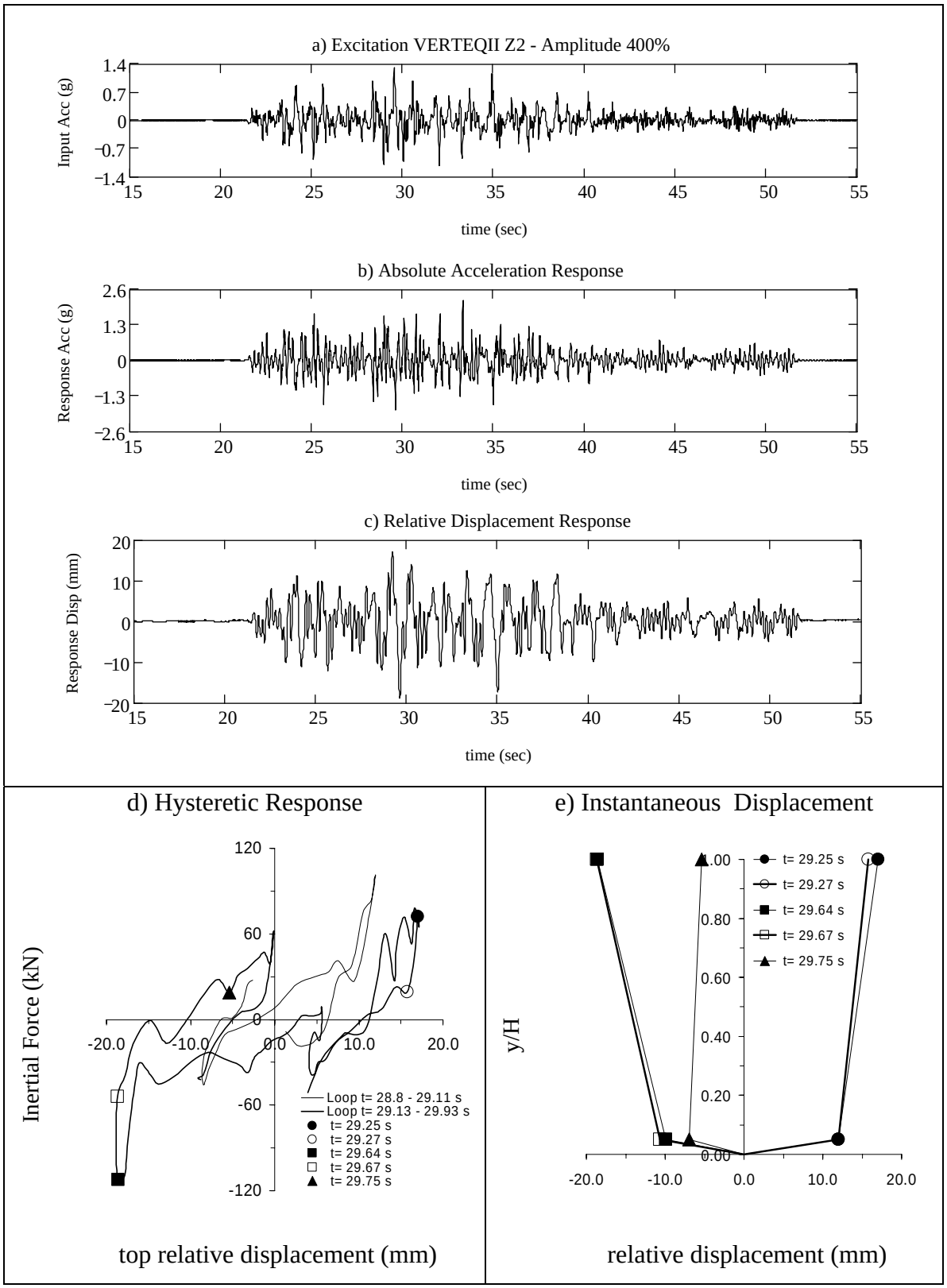

Figure B.9 Summary of Specimen 2 Response for Test#9

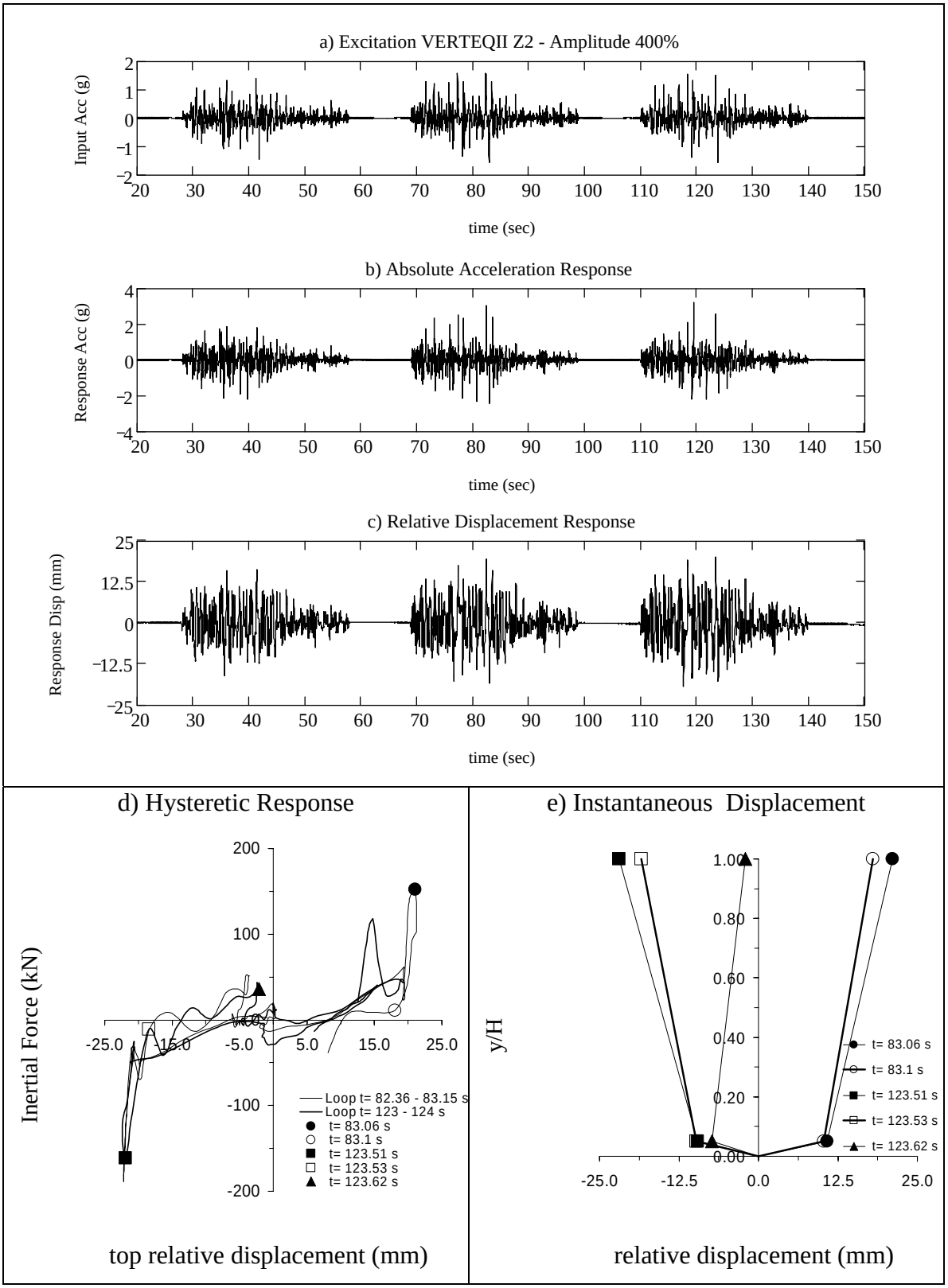

Figure B.10 Summary of Specimen 2 Response for Test#10

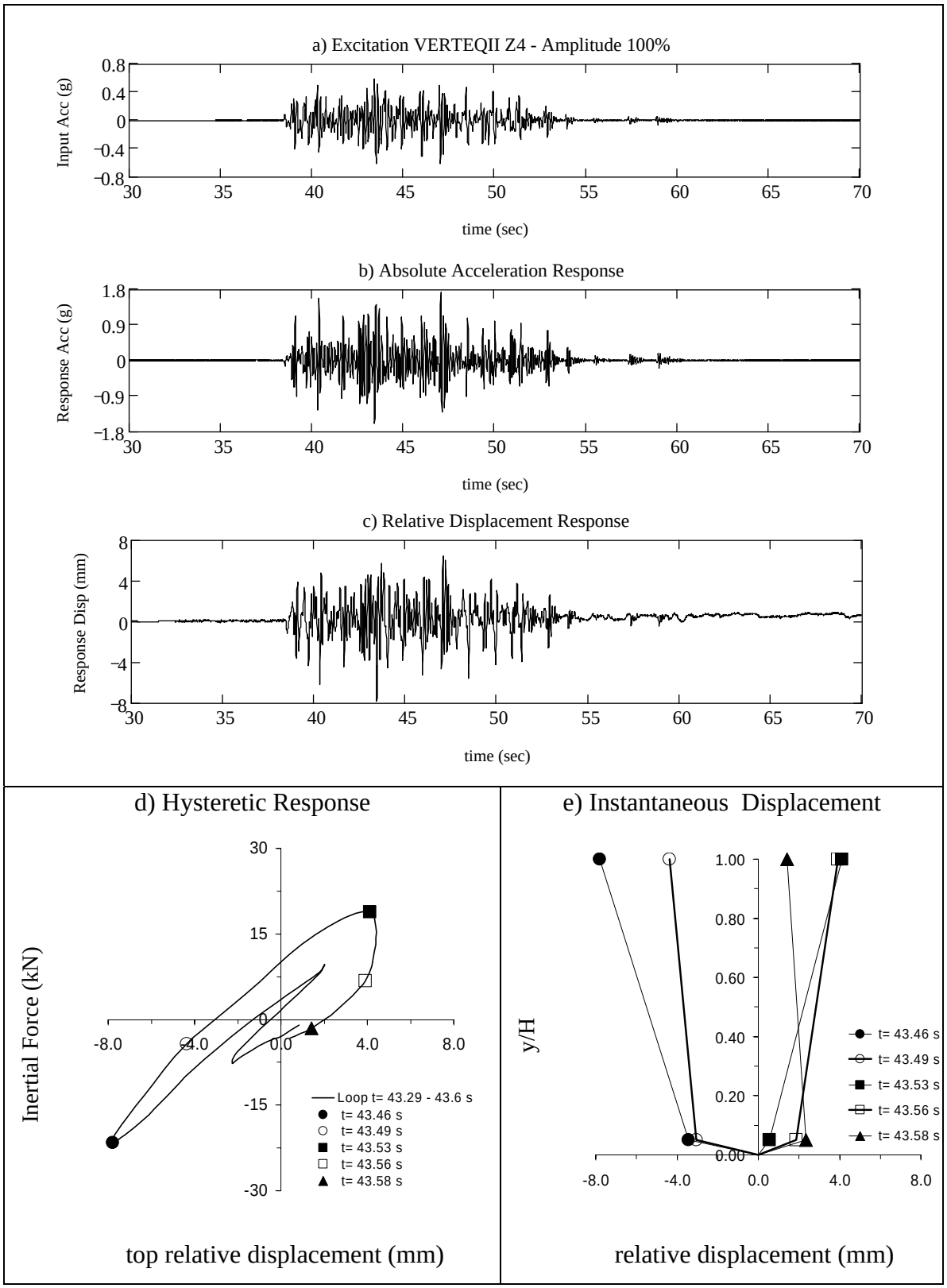

Figure B.11 Summary of Specimen 1 Response for Test#11

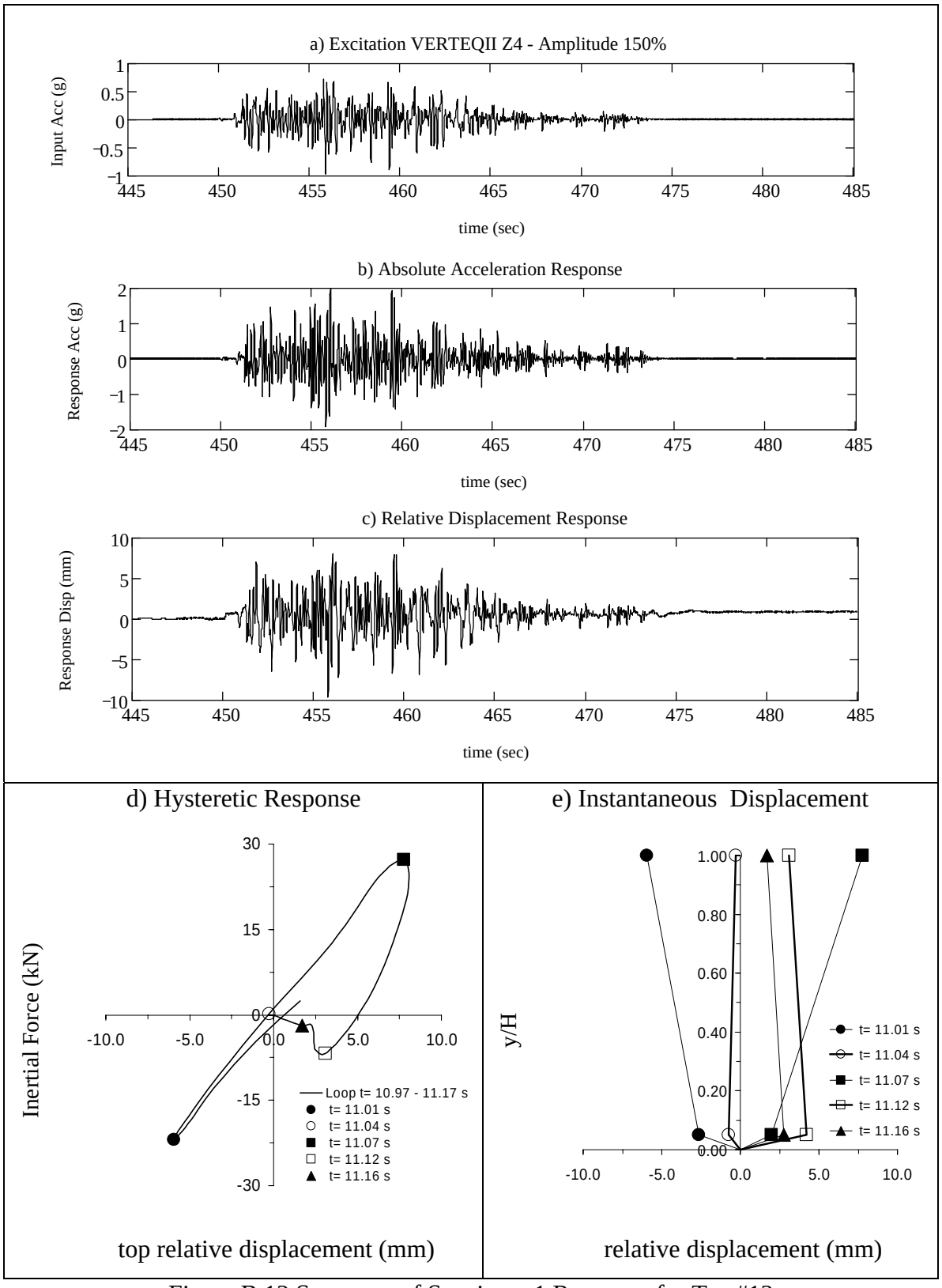

Figure B.12 Summary of Specimen 1 Response for Test#12

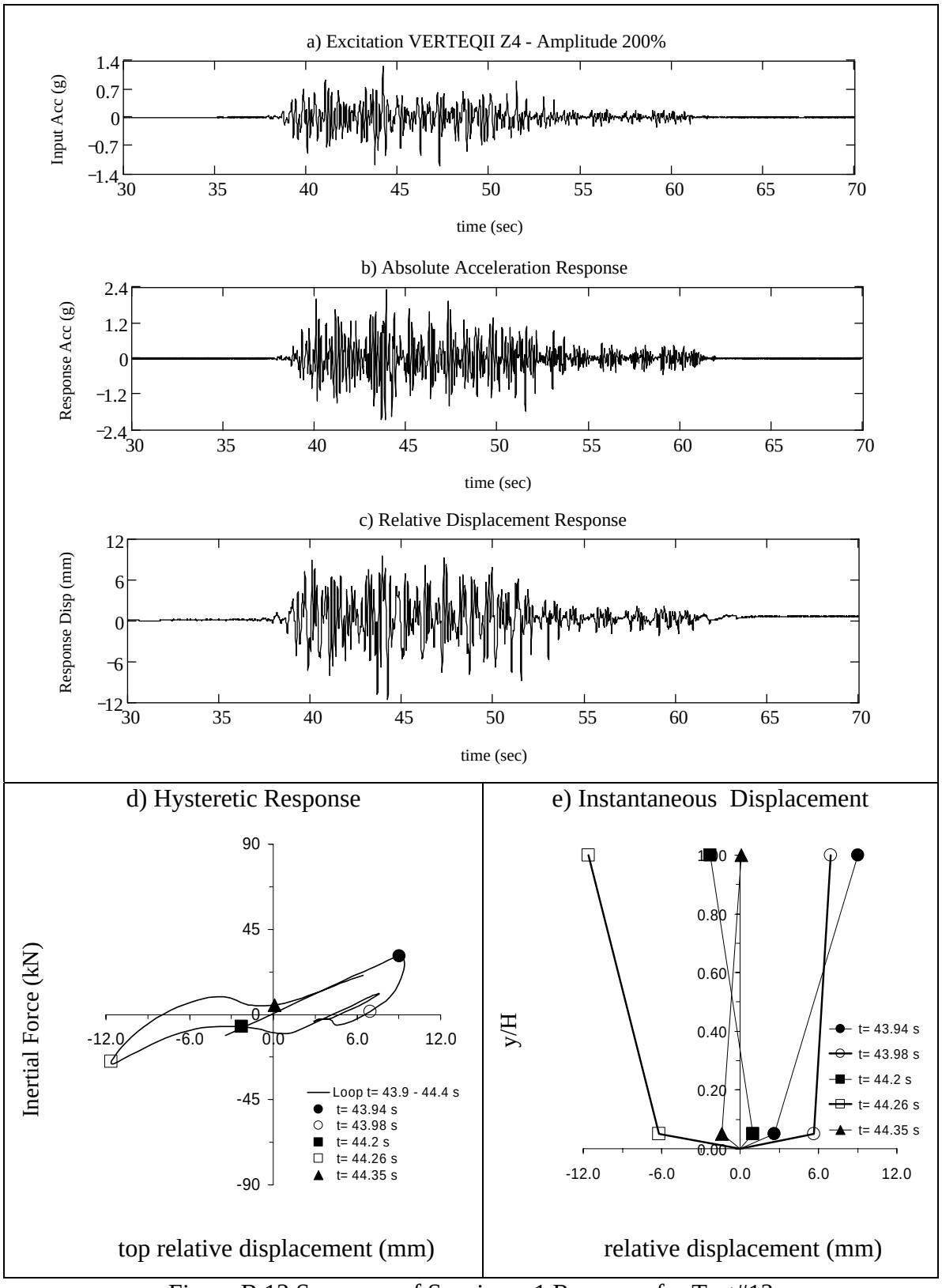

Figure B.13 Summary of Specimen 1 Response for Test#13

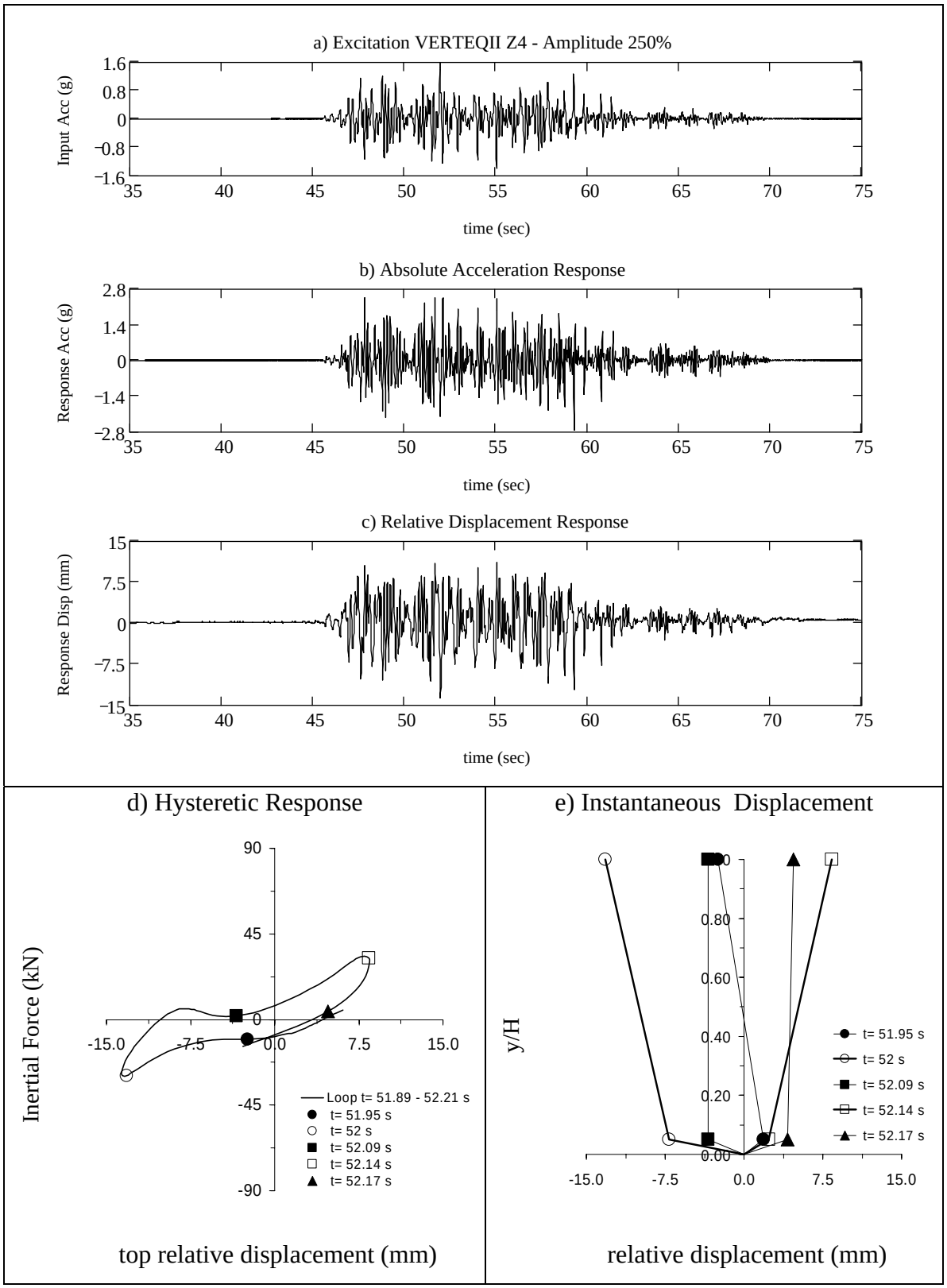

Figure B.14 Summary of Specimen 1 Response for Test#14

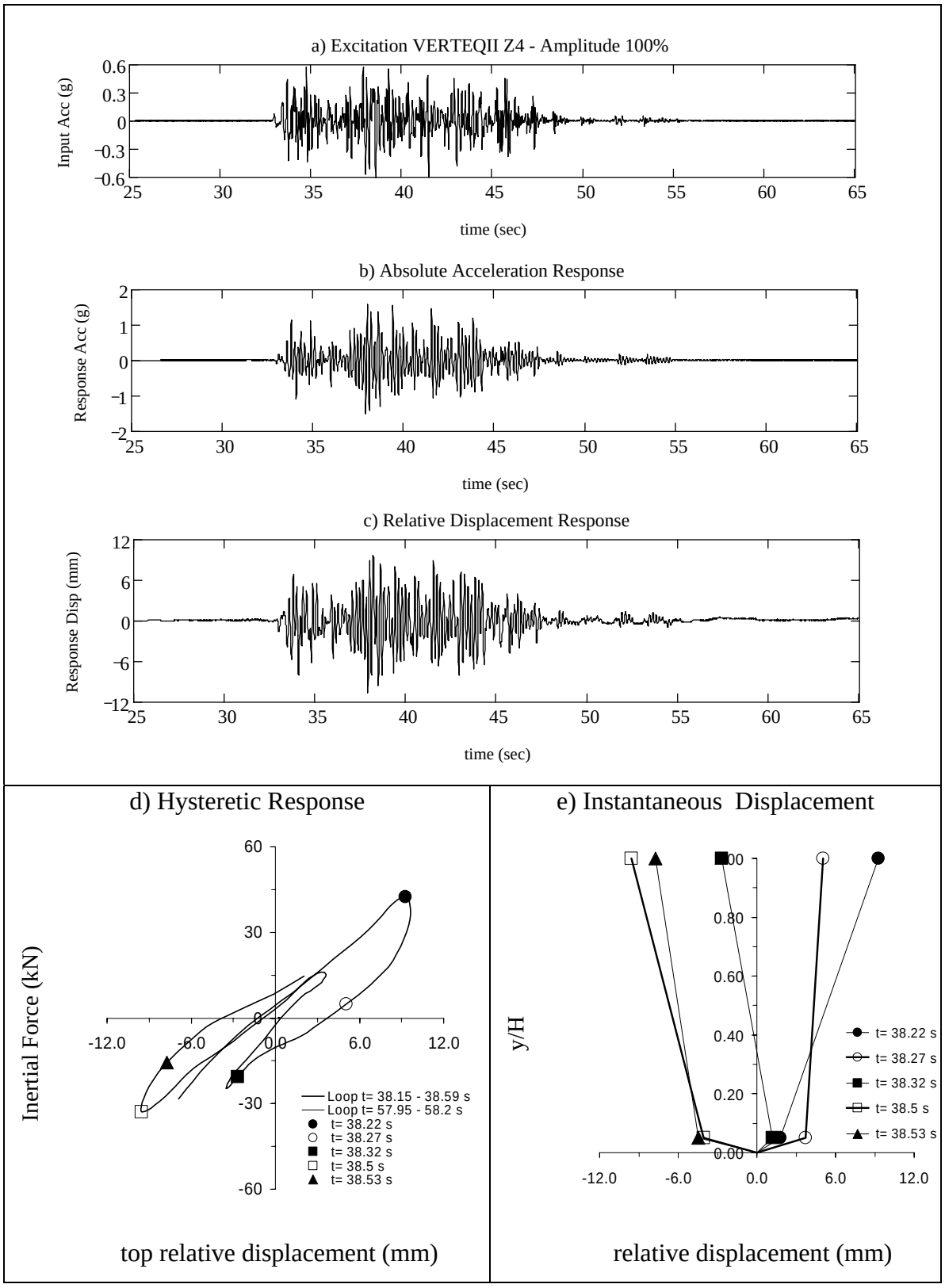

Figure B.15 Summary of Specimen 1 Response for Test#15

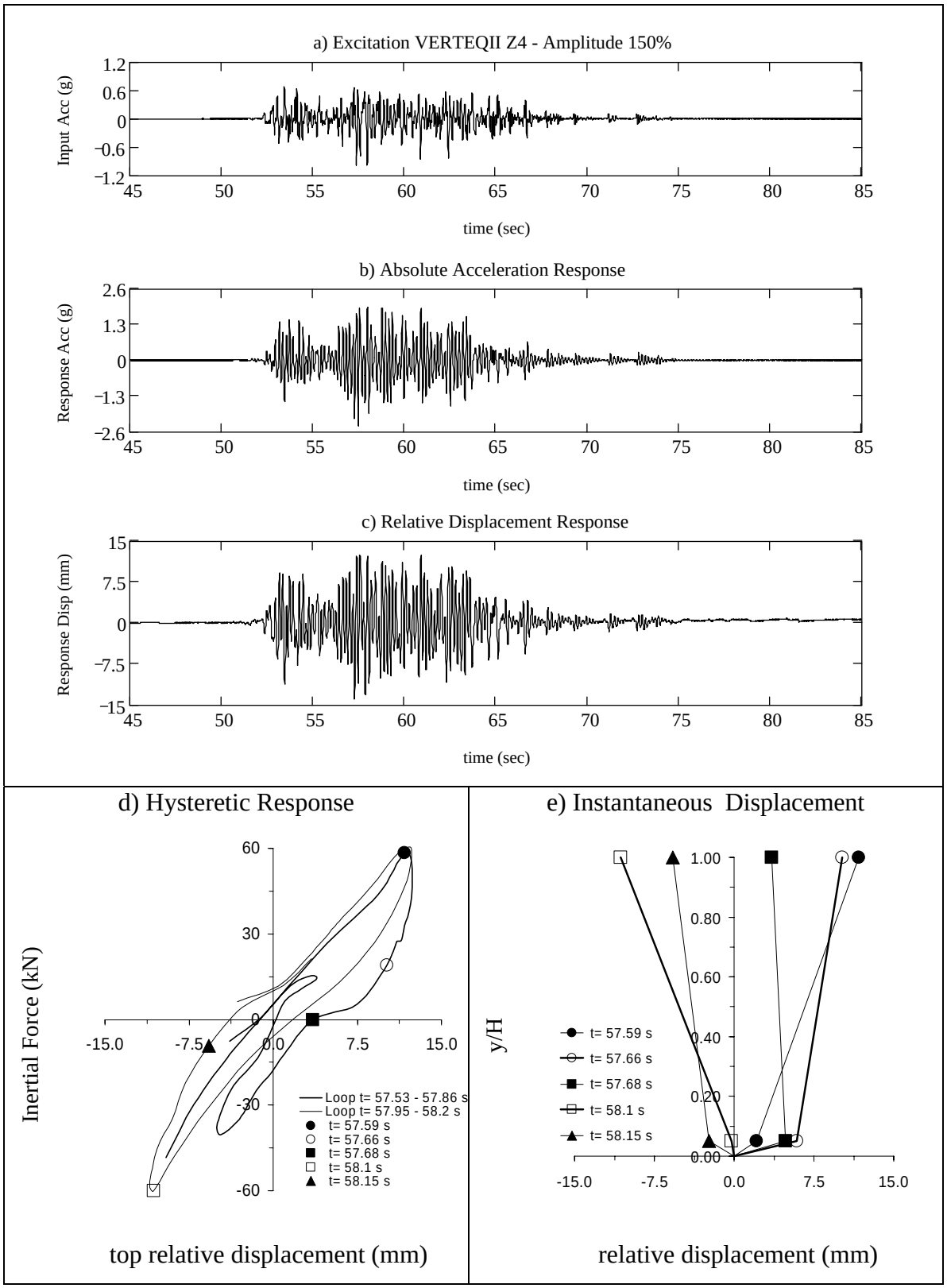

Figure B.16 Summary of Specimen 1 Response for Test#16

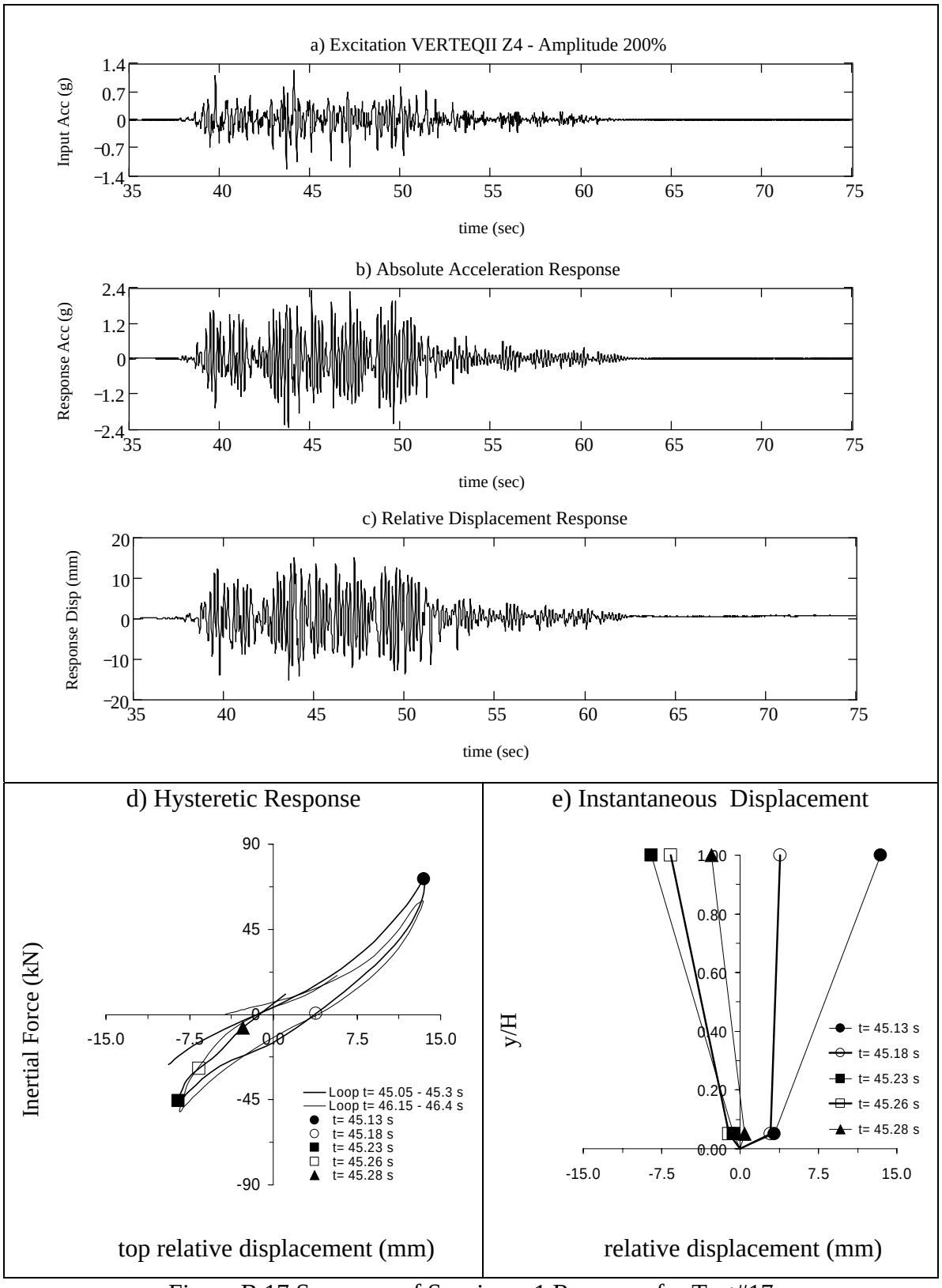

Figure B.17 Summary of Specimen 1 Response for Test#17

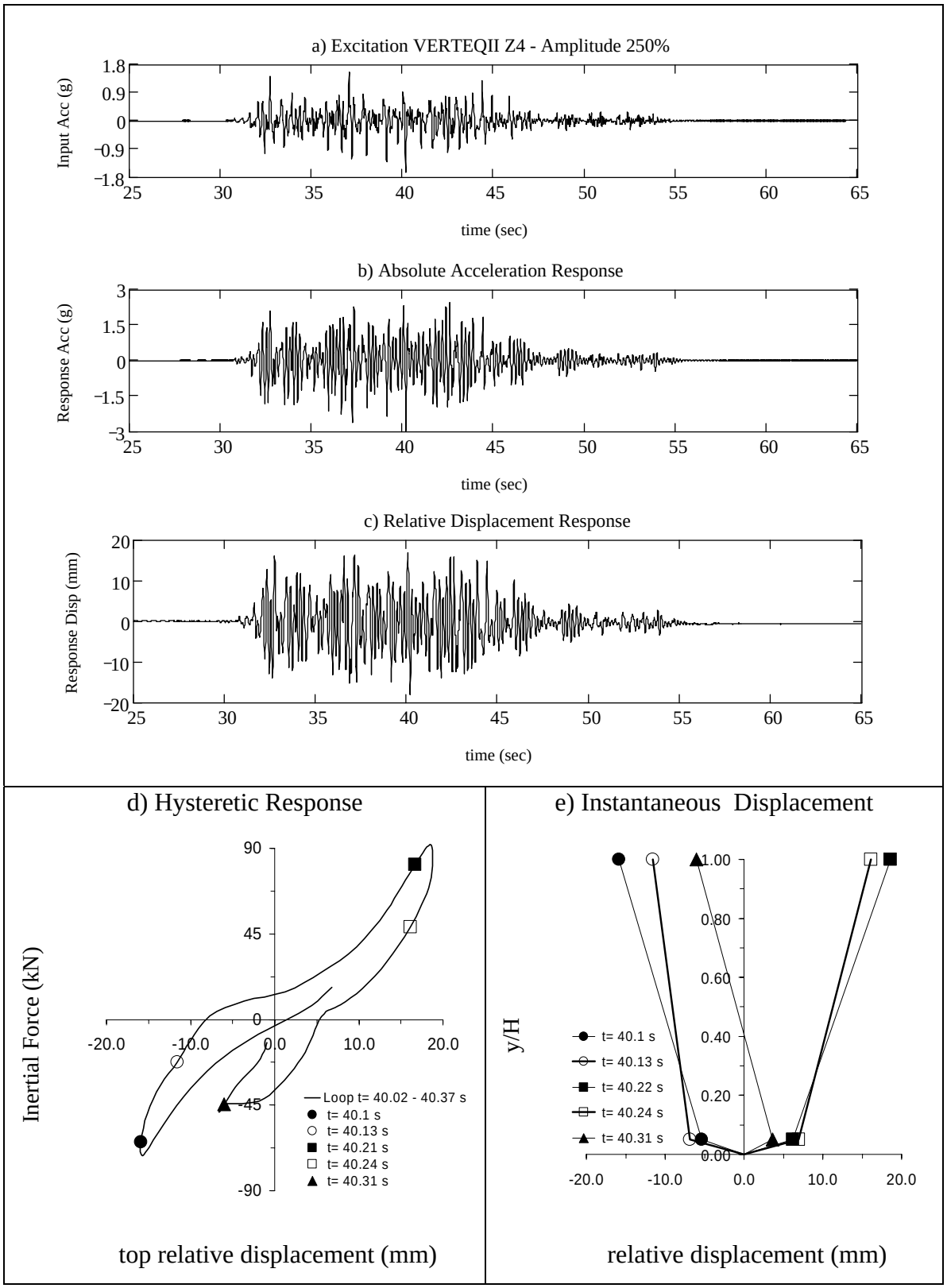

Figure B.18 Summary of Specimen 1 Response for Test#18

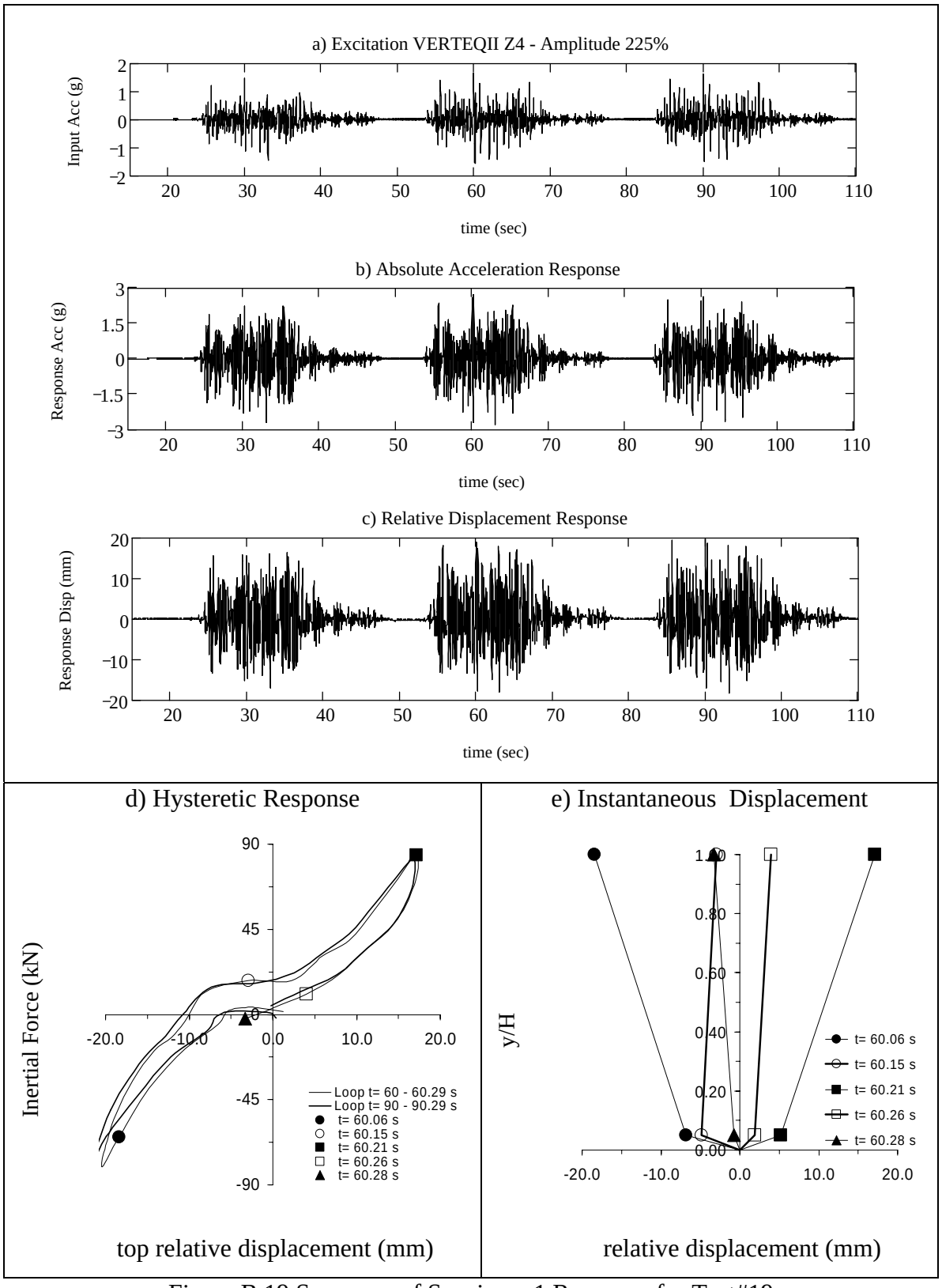

Figure B.19 Summary of Specimen 1 Response for Test#19

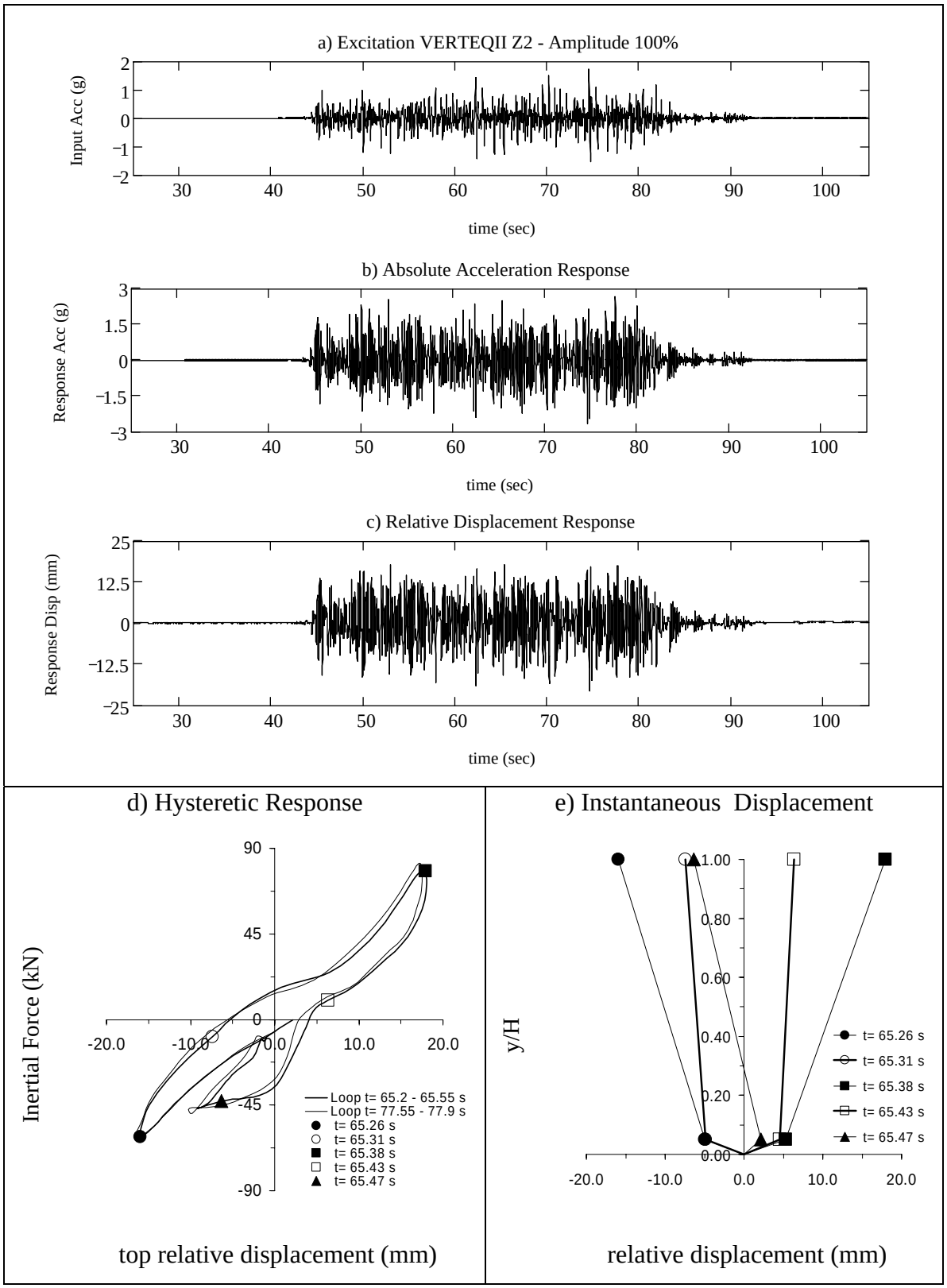

Figure B.20 Summary of Specimen 1 Response for Test#20

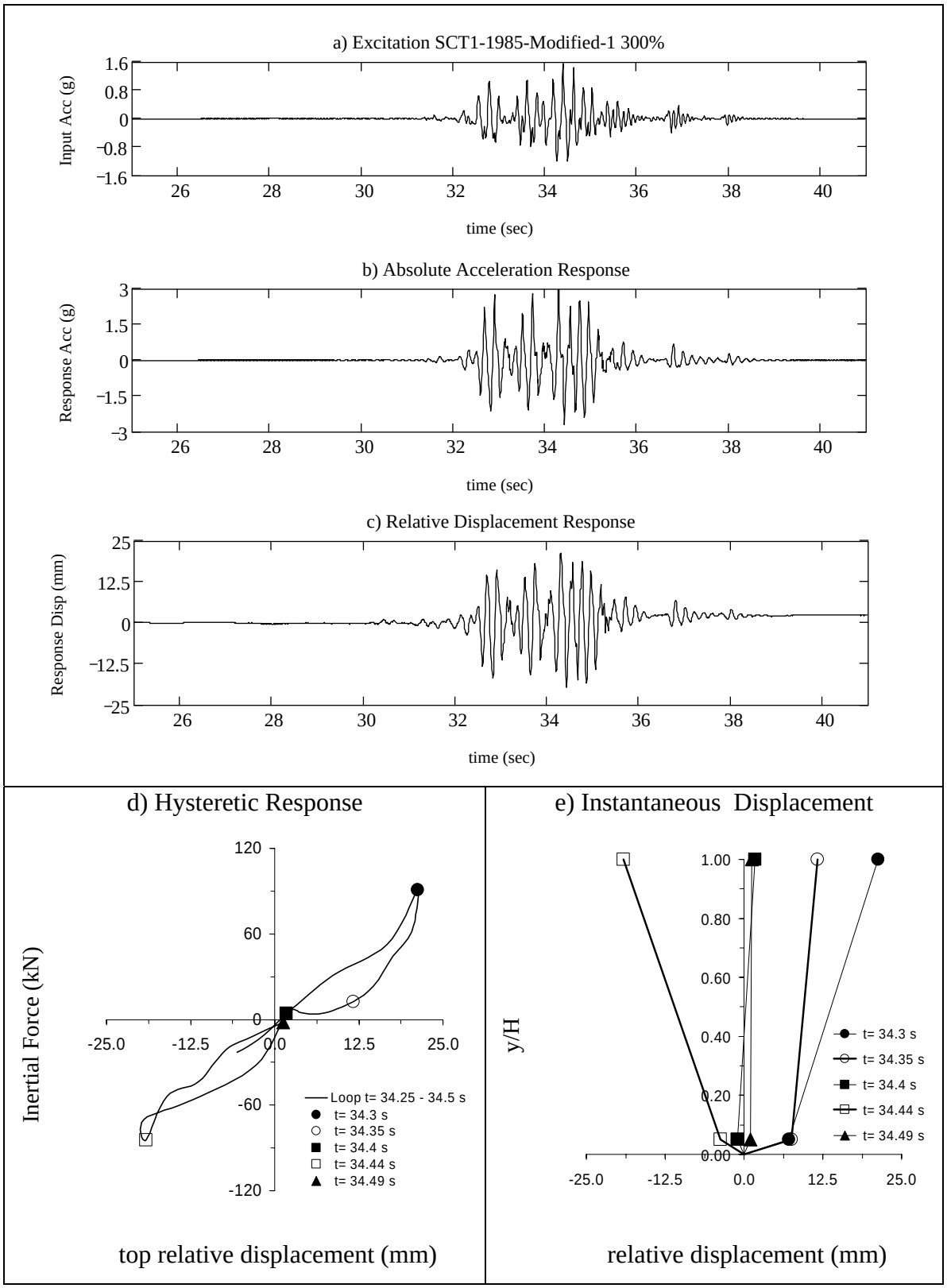

Figure B.21 Summary of Specimen 1 Response for Test#21

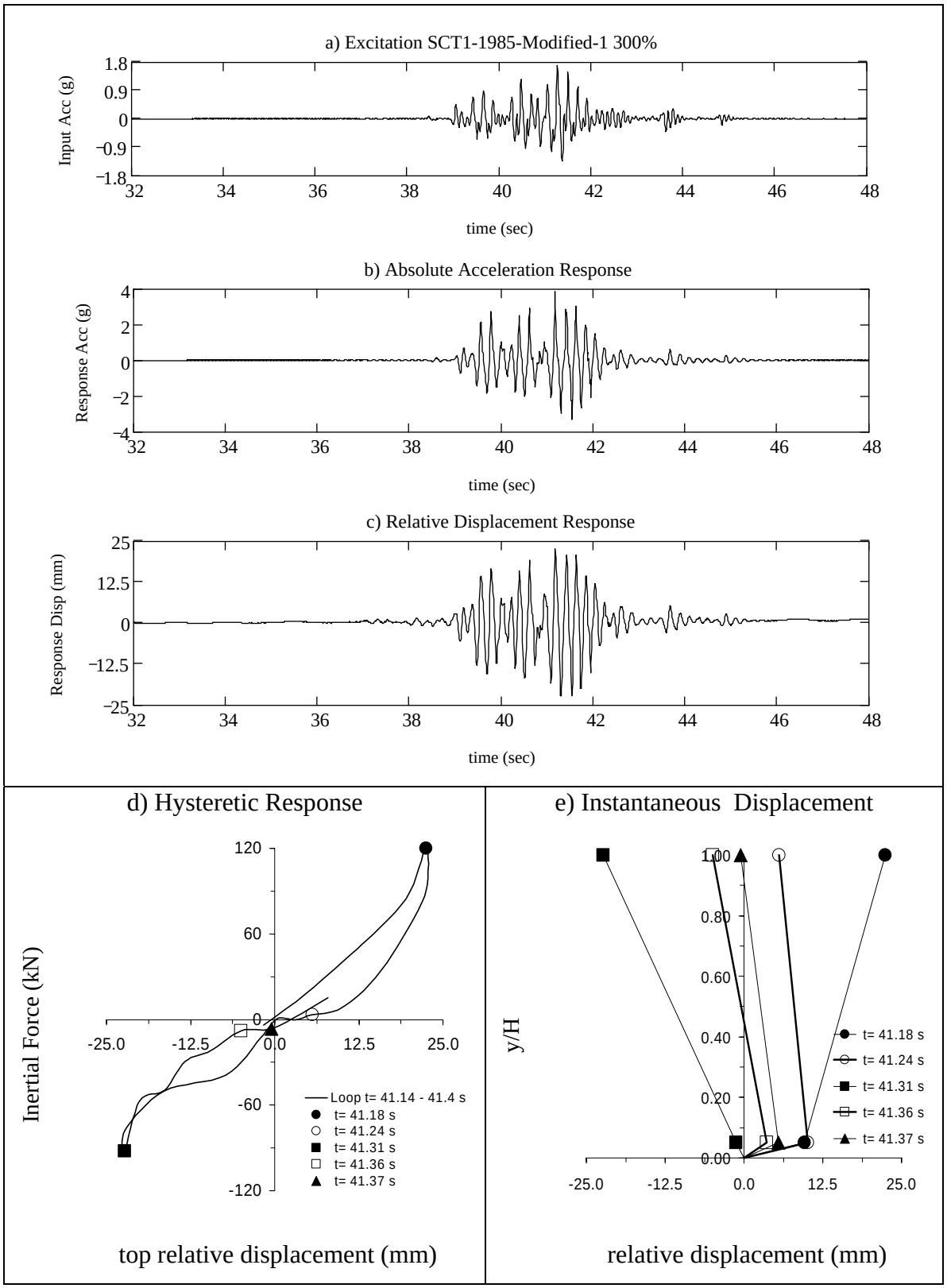

Figure B.22 Summary of Specimen 1 Response for Test#22

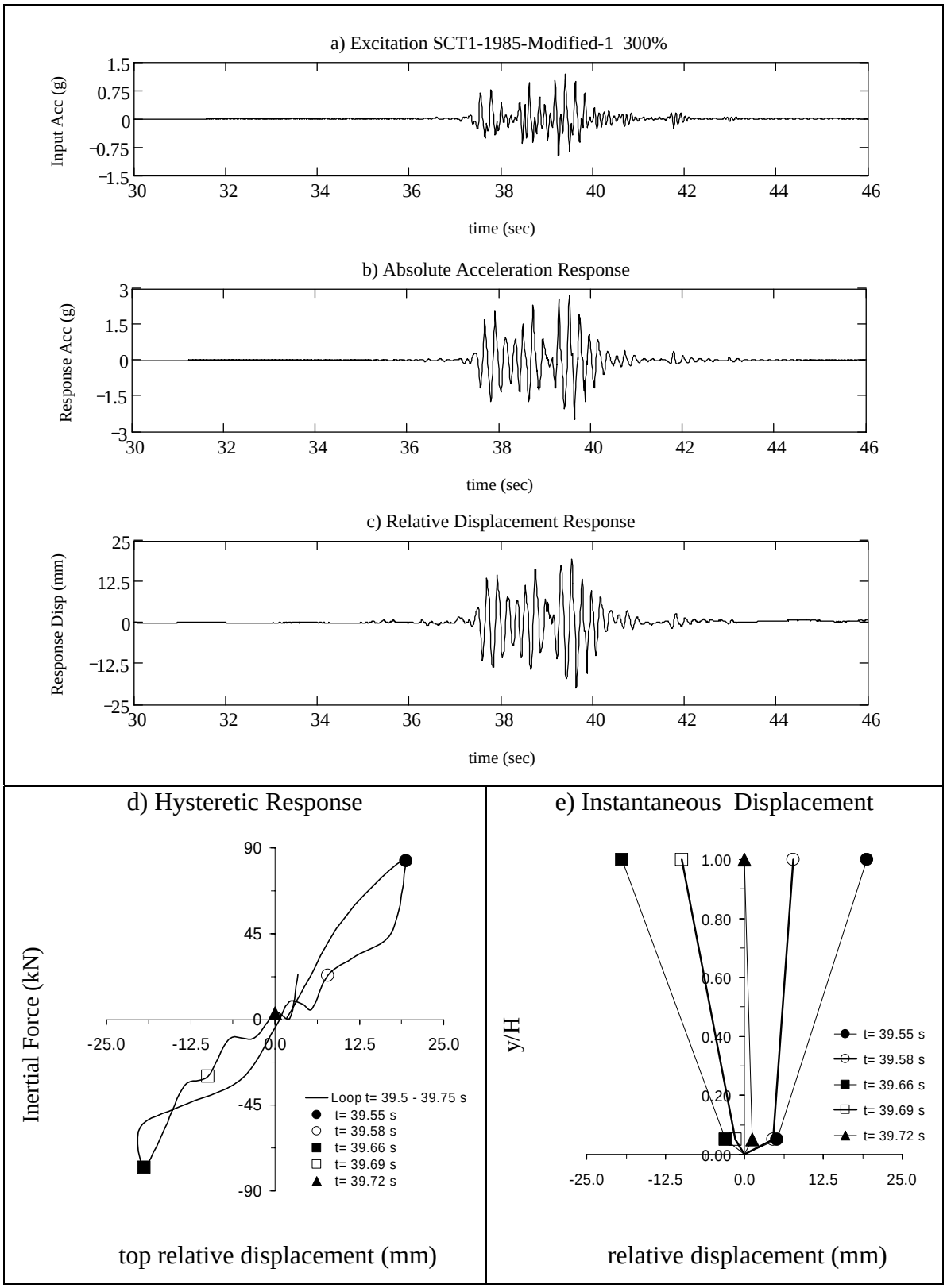

Figure B.23 Summary of Specimen 1 Response for Test#23

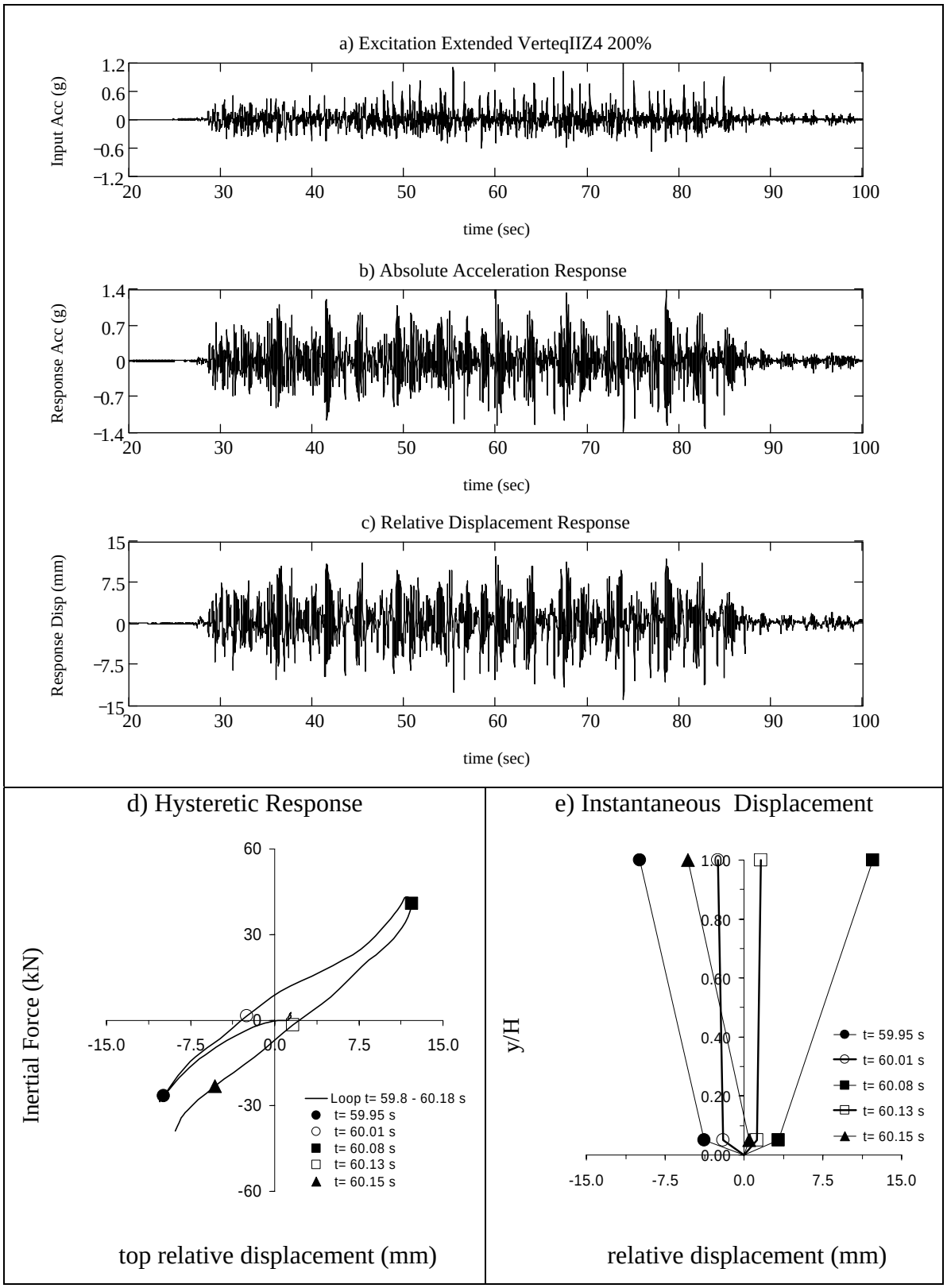

Figure B.24 Summary of Specimen 1 Response for Test#24

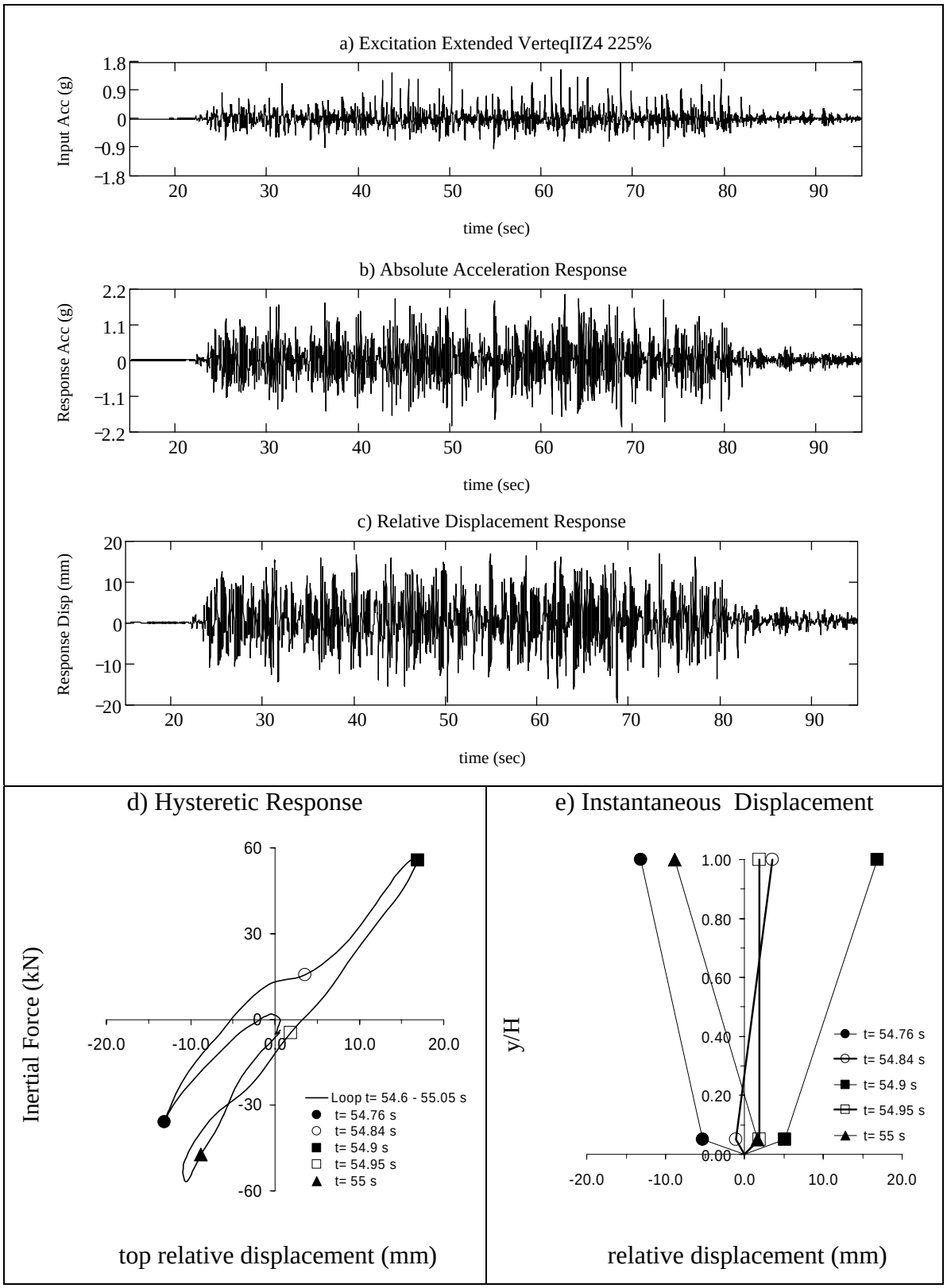

Figure B.25 Summary of Specimen 1 Response for Test#25

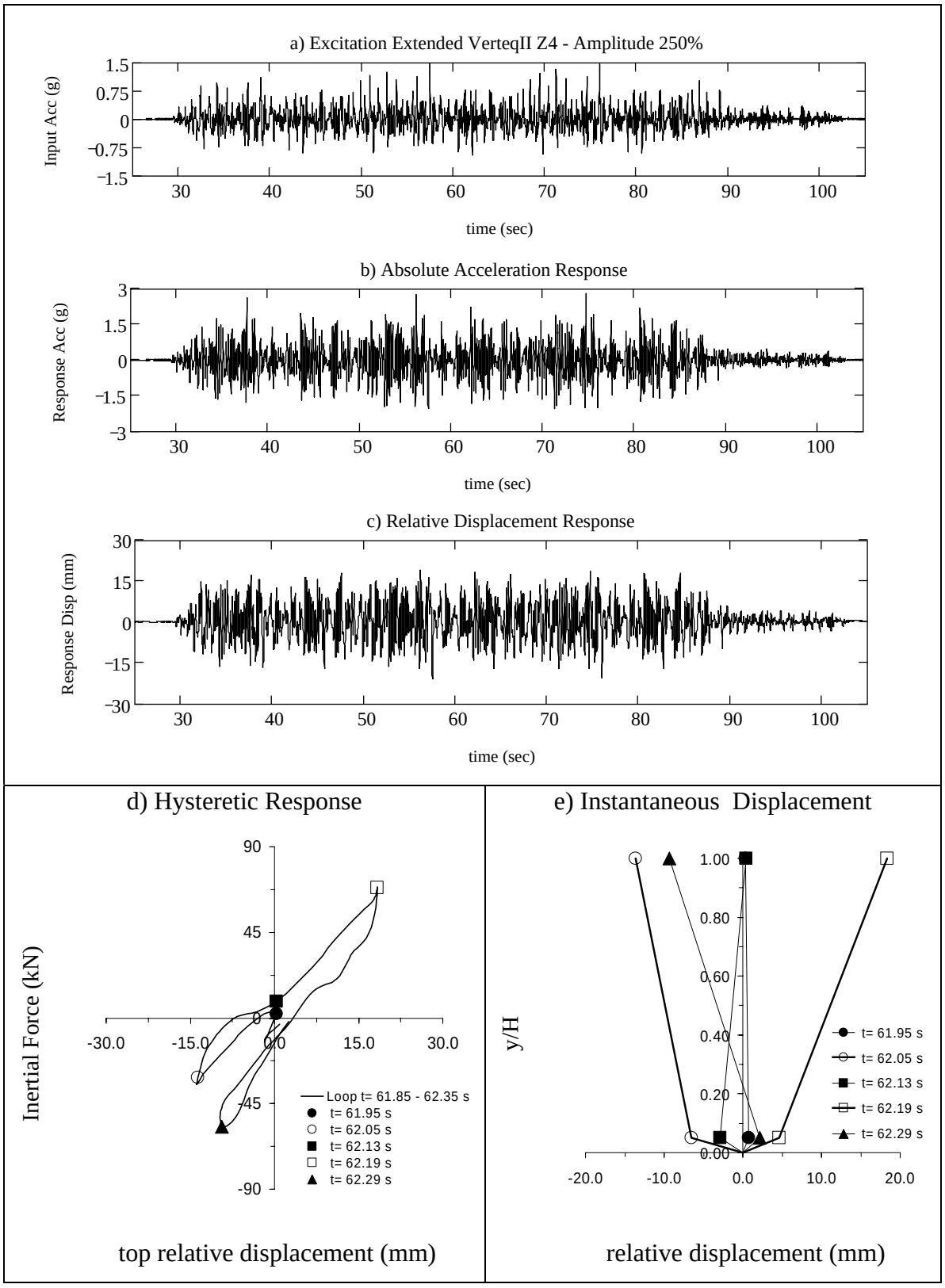

Figure B.26 Summary of Specimen 1 Response for Test#26

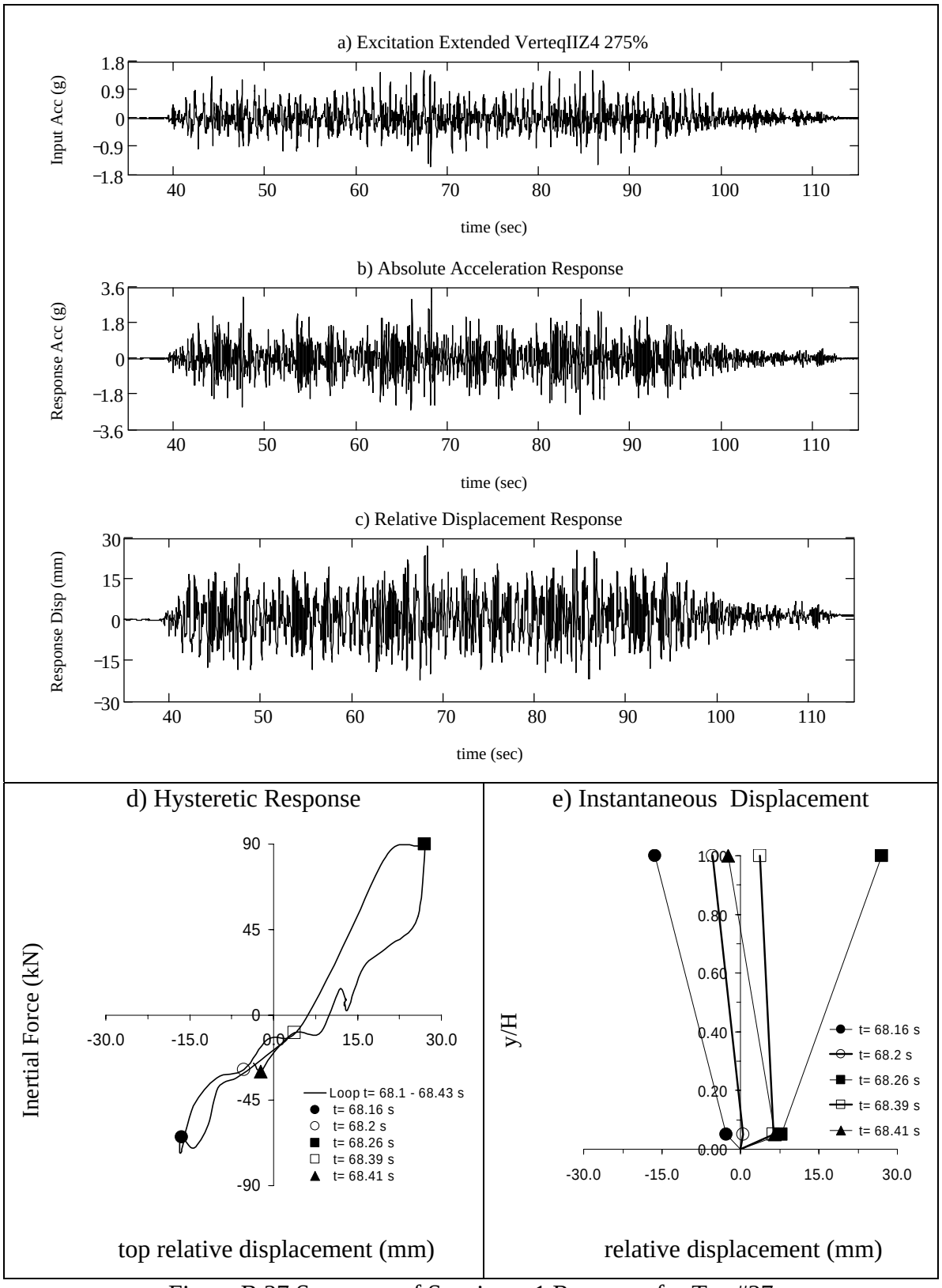

Figure B.27 Summary of Specimen 1 Response for Test#27

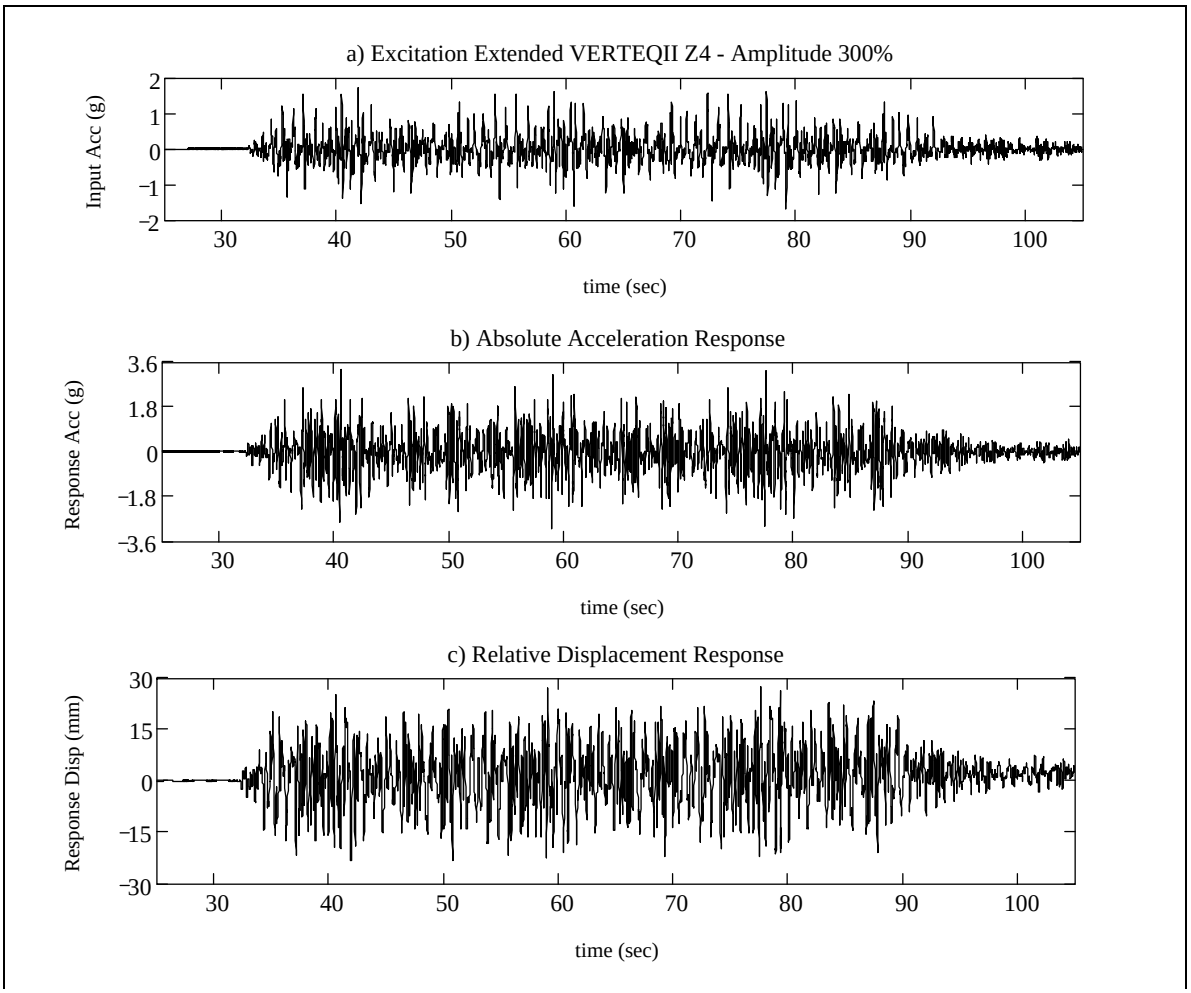

a) Hysteretic Response

b) Instantaneous Displacement

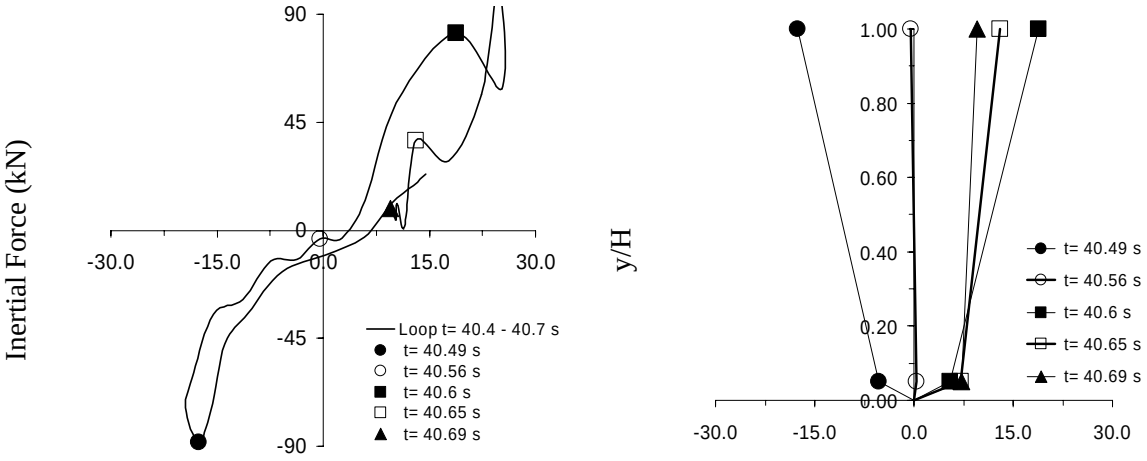

top relative displacement (mm)

relative displacement (mm)

Figure B.28 Summary of Specimen 1 Response for Test#28

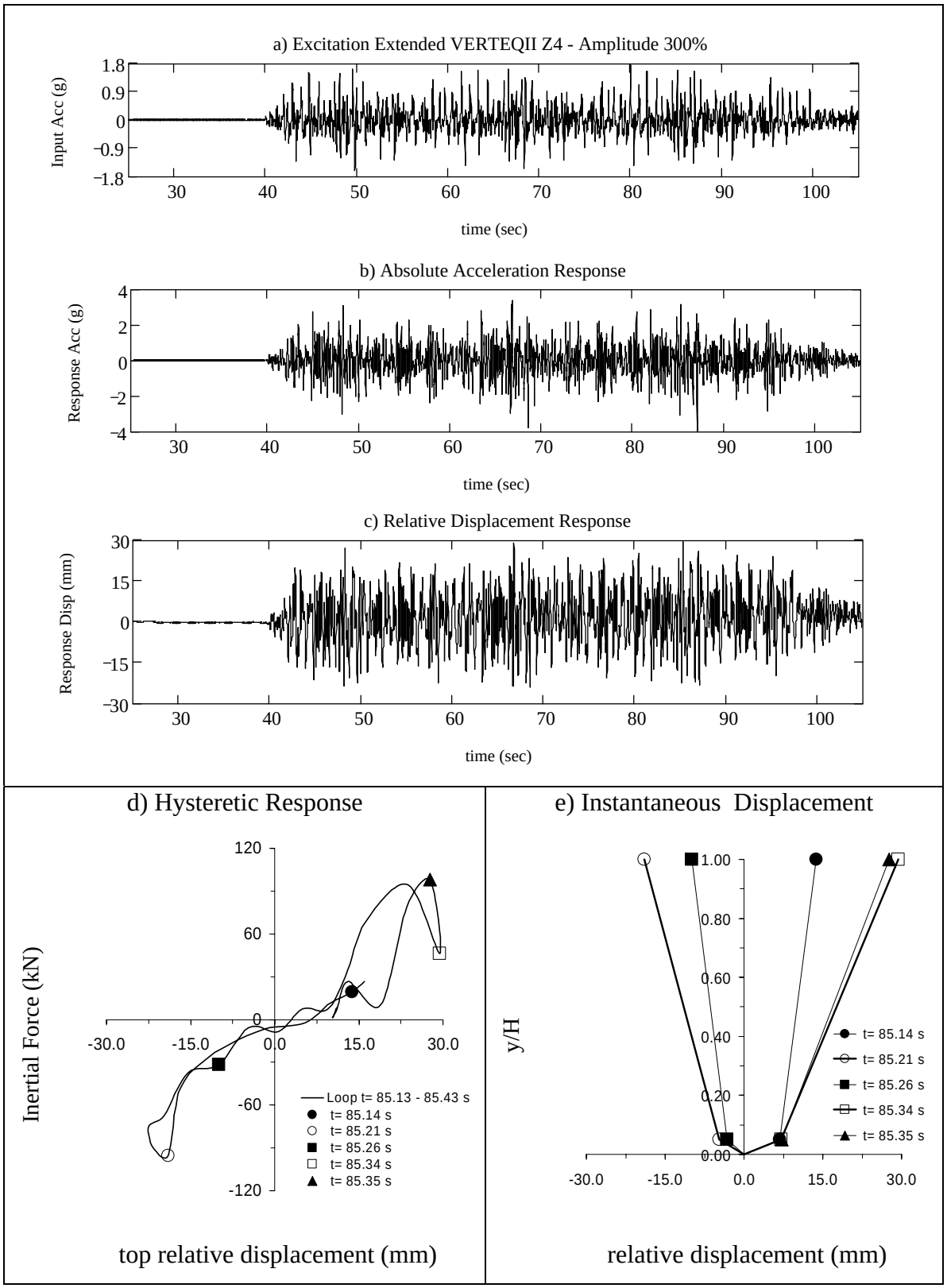

Figure B.29 Summary of Specimen 1 Response for Test#29

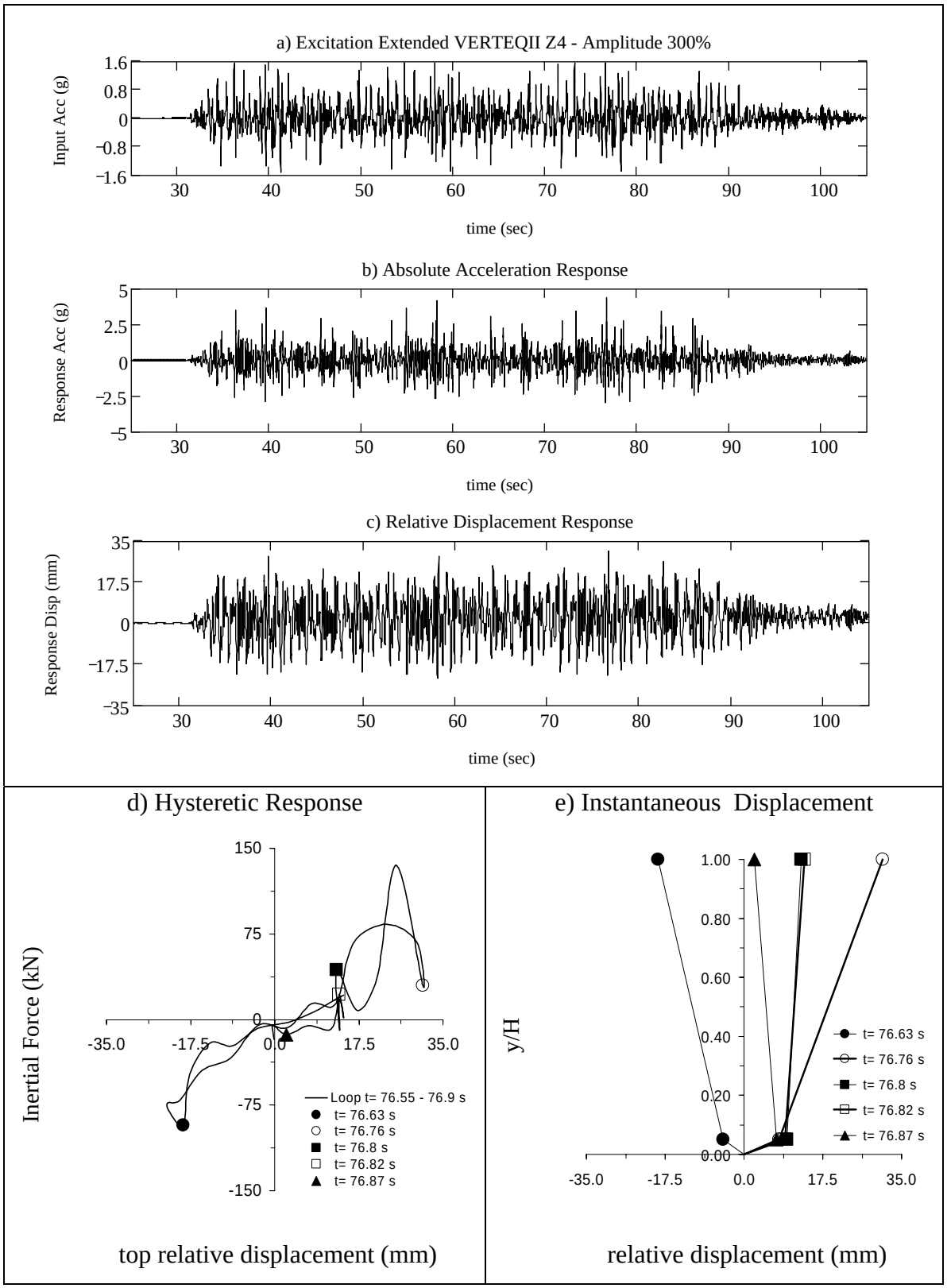

Figure B.30 Summary of Specimen 1 Response for Test#30

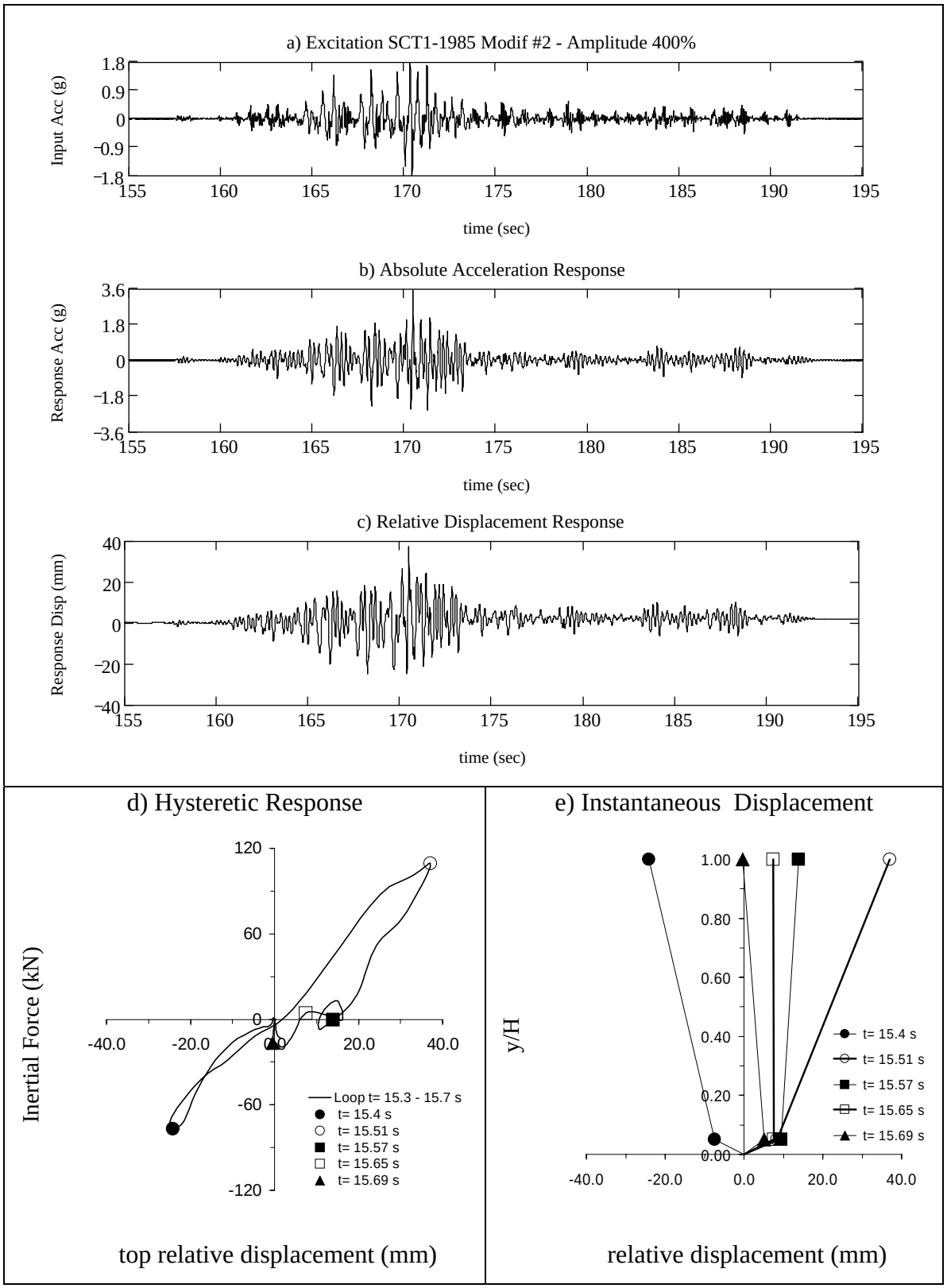

Figure B.31 Summary of Specimen 1 Response for Test#31

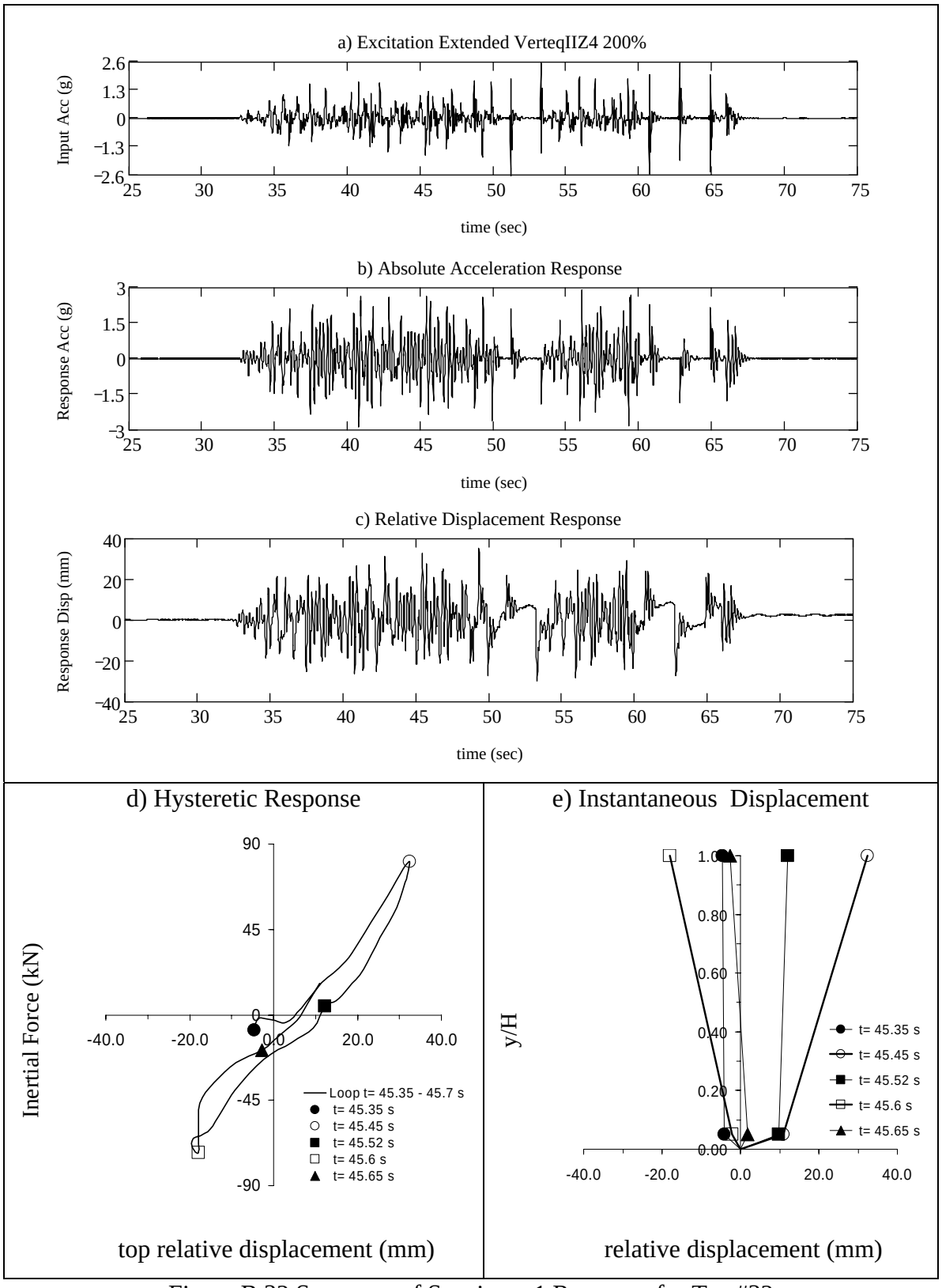

Figure B.32 Summary of Specimen 1 Response for Test#32

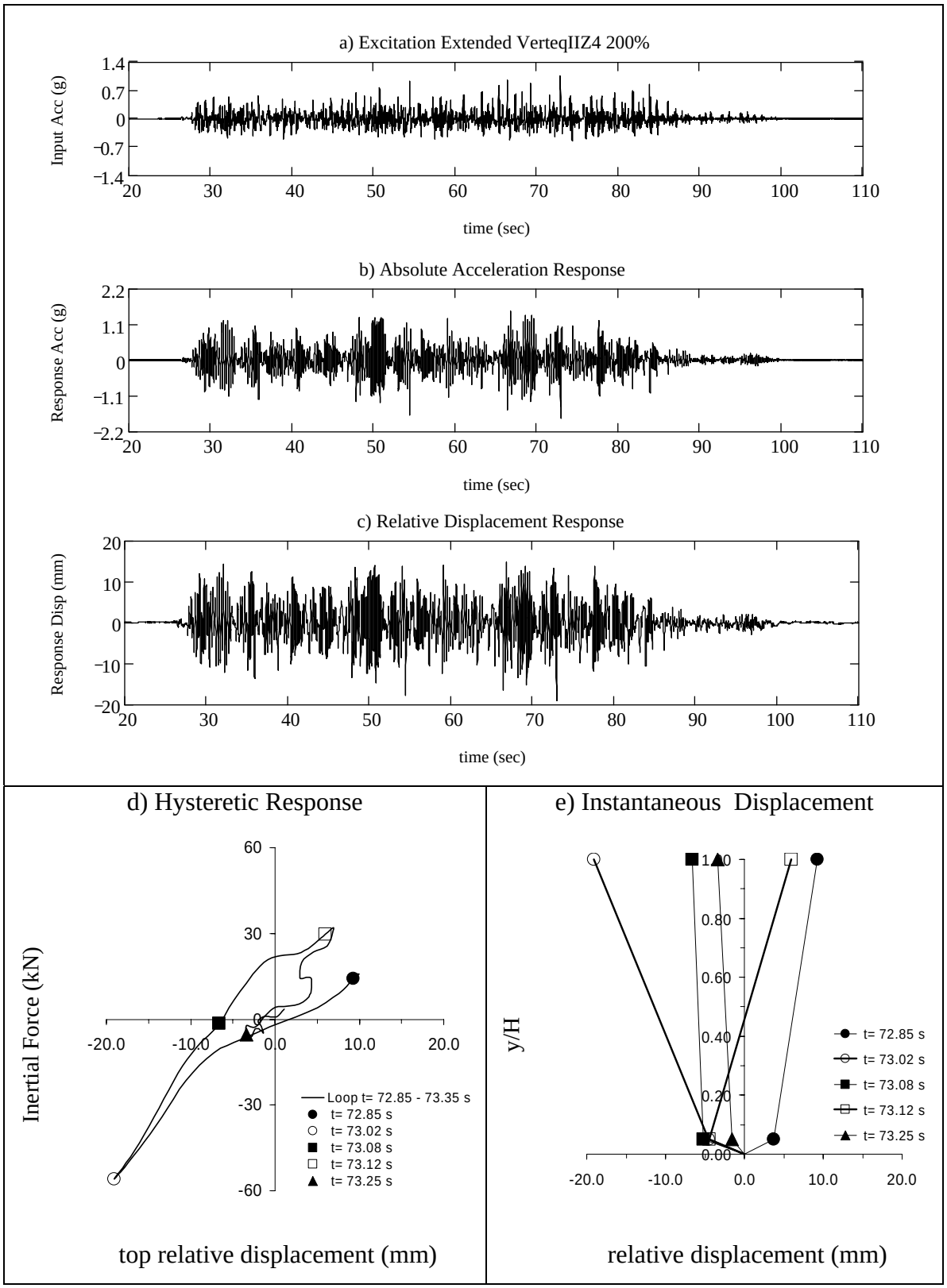

Figure B.33 Summary of Specimen 1 Response for Test#33

Appendix C: Measured Response from Shake Table Tests on Bare Frame

TESTS	EQ RECORD	Amplitude	PGA (g)	NOTE
F	Loss of Control	N/A	0.80	Surcharge Weight = 62 kN
01	VERTEQII Z2	50%	0.25	
02		100%	0.50	
03		150%	0.75	
04		200%	1.00	
05		250%	1.25	
06		300%	1.50	
07		320%	1.60	
08		340%	1.70	

Table C.1: Dynamic Loading protocol for all the tests performed on Specimen #3

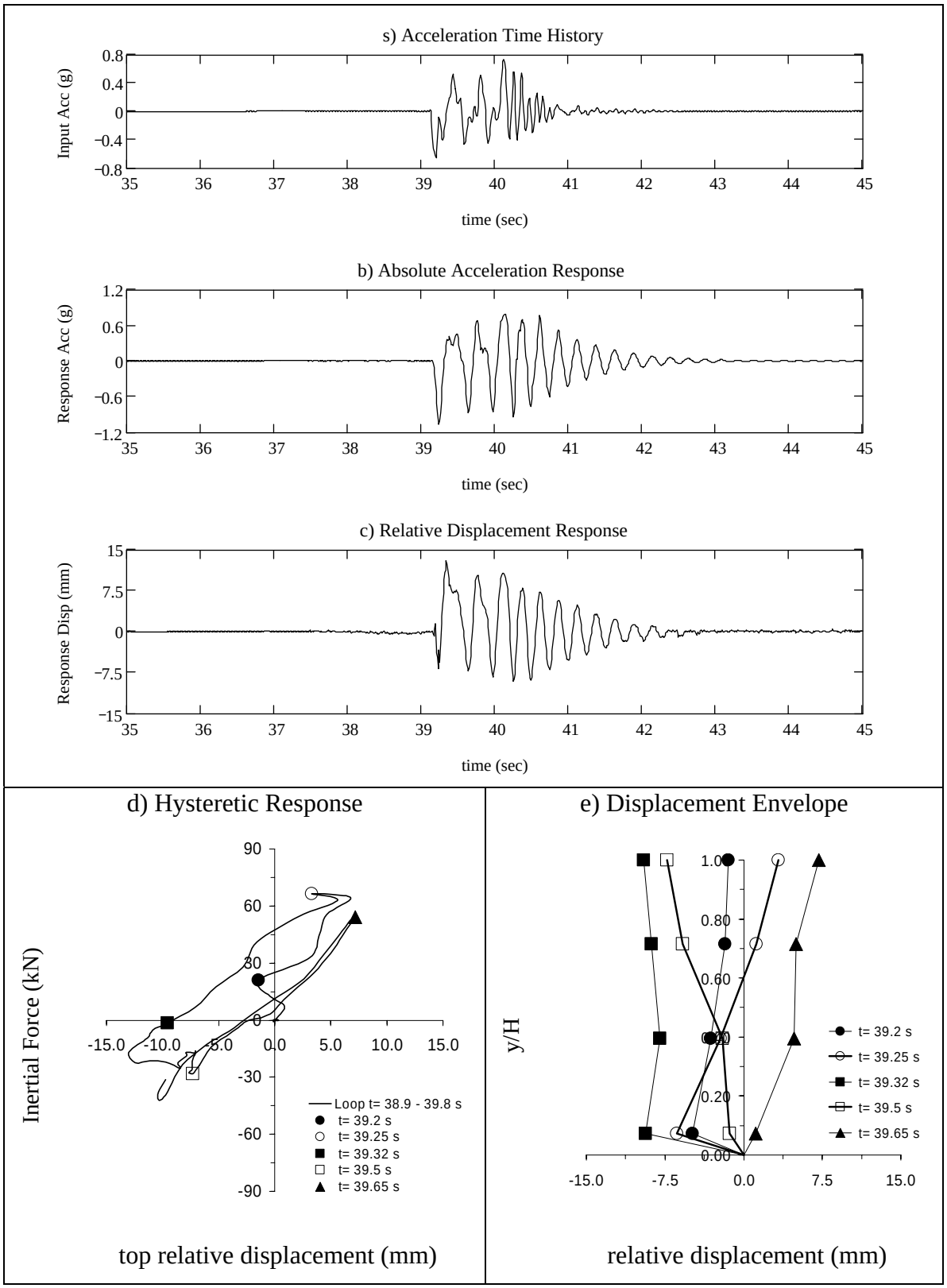

Figure C.1 Summary of Specimen 3 Response for Test F

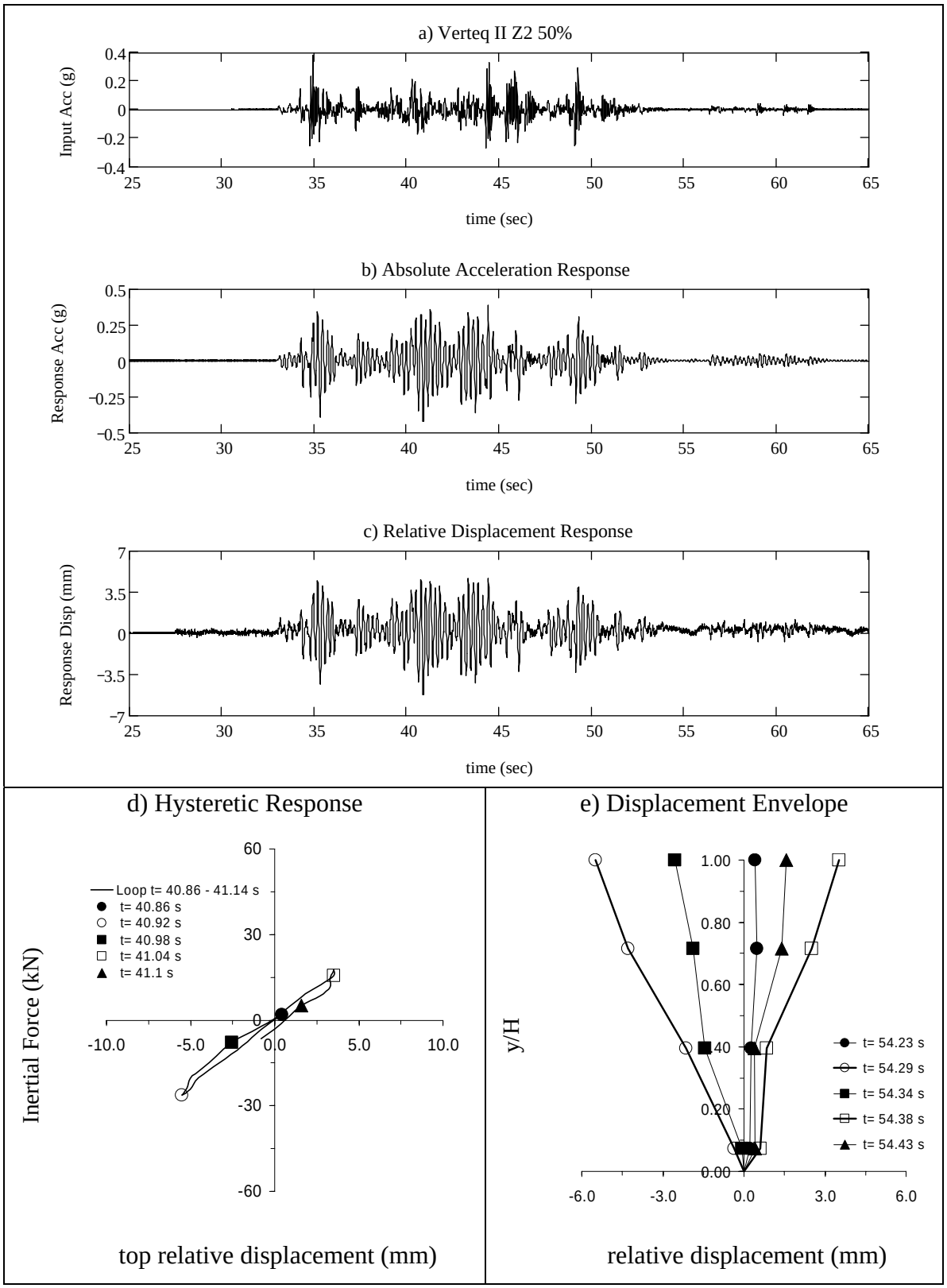

Figure C.2 Summary of Specimen 3 Response for Test#1

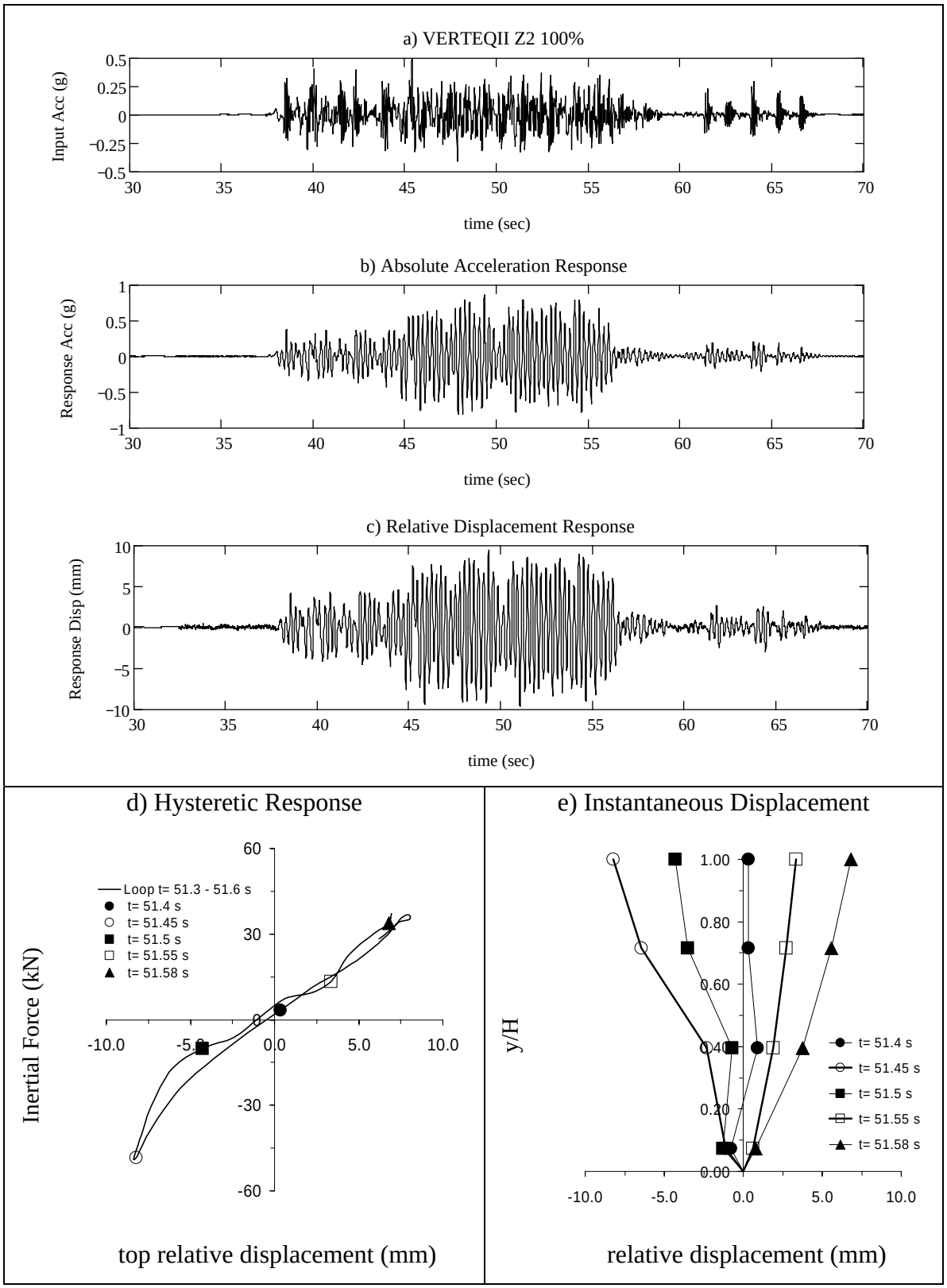

Figure C.3 Summary of Specimen 3 Response for Test#2

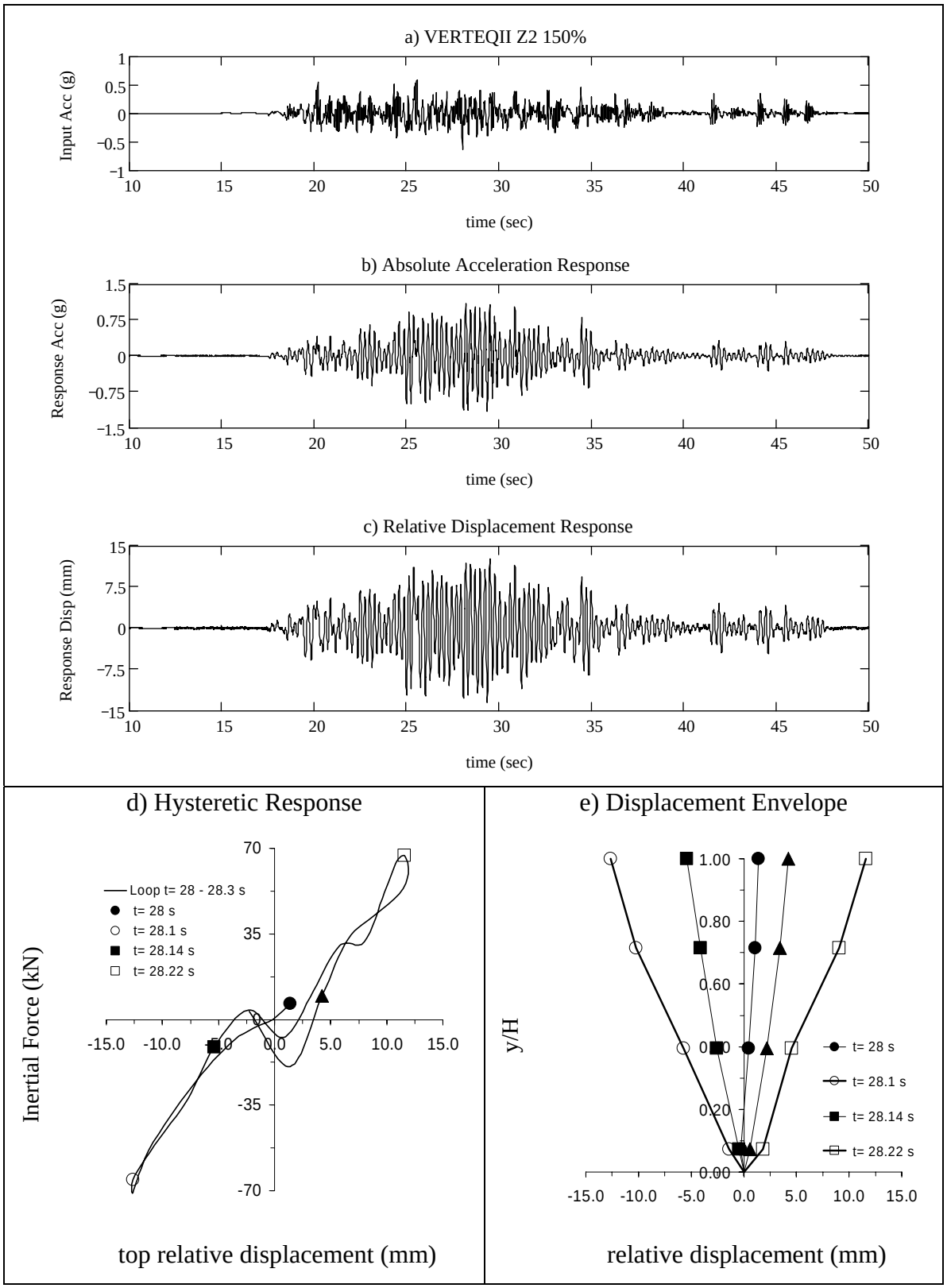

Figure C.4 Summary of Specimen 3 Response for Test#3

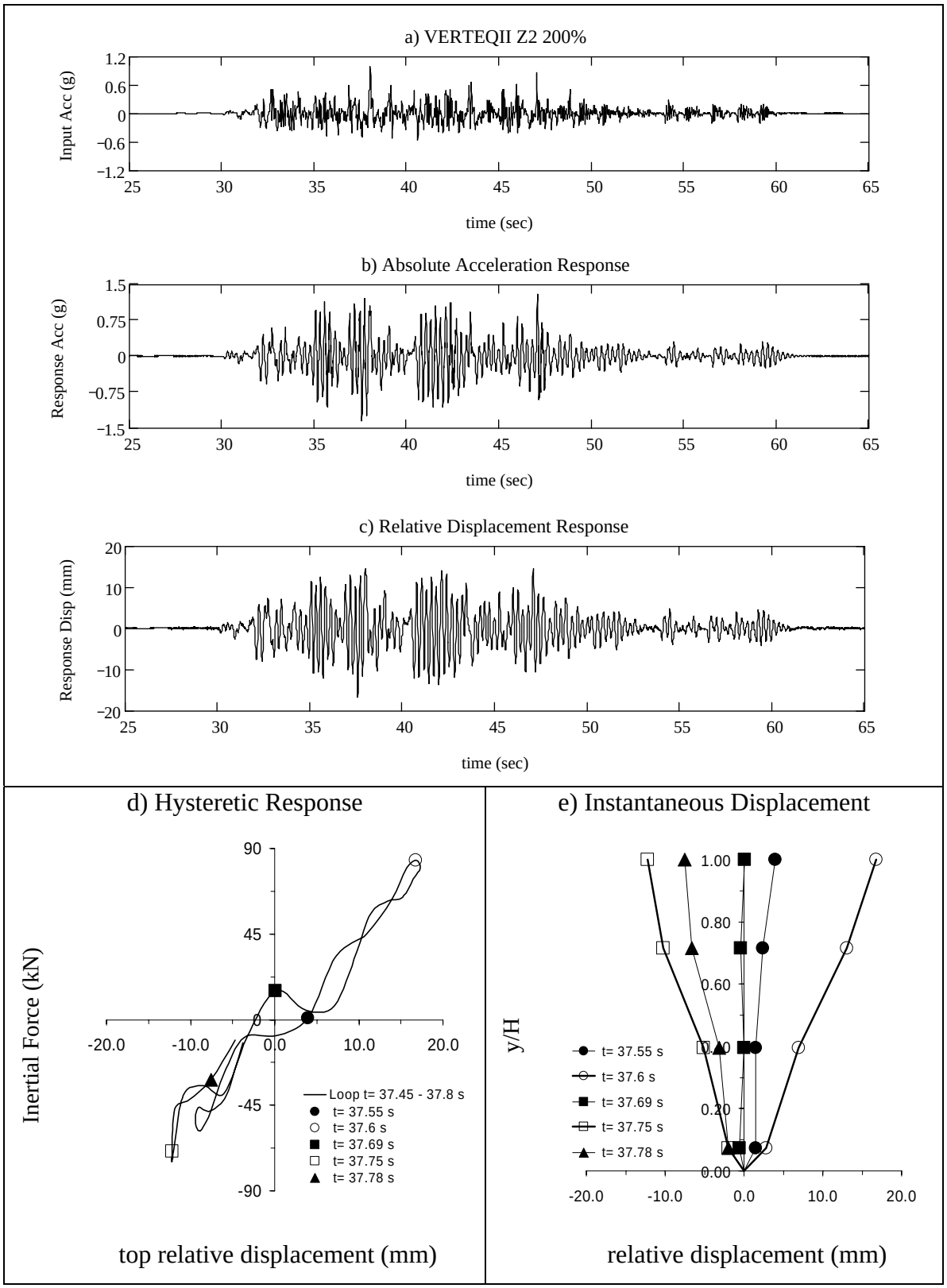

Figure C.5 Summary of Specimen 3 Response for Test#4

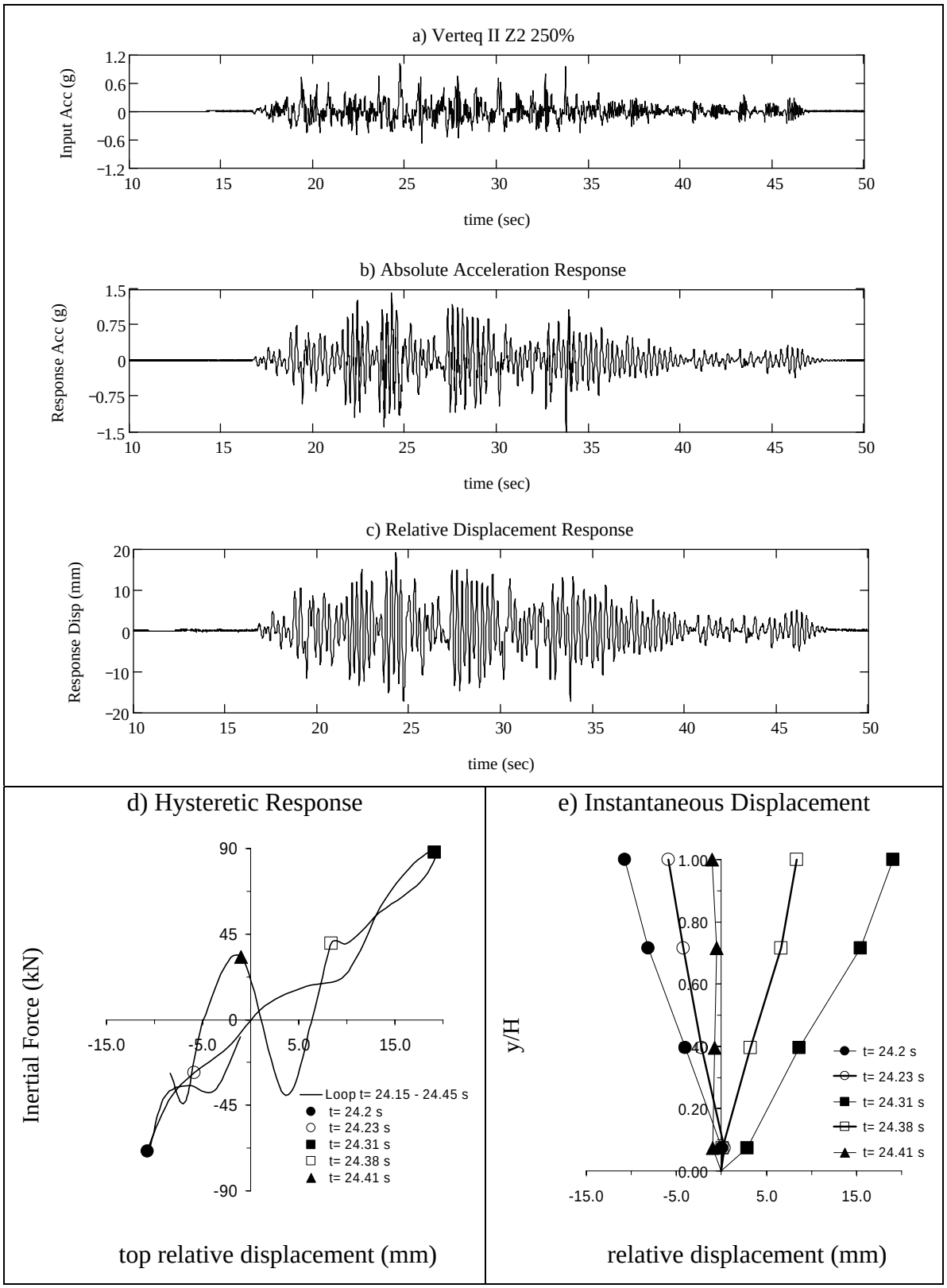

Figure C.6 Summary of Specimen 3 Response for Test#5

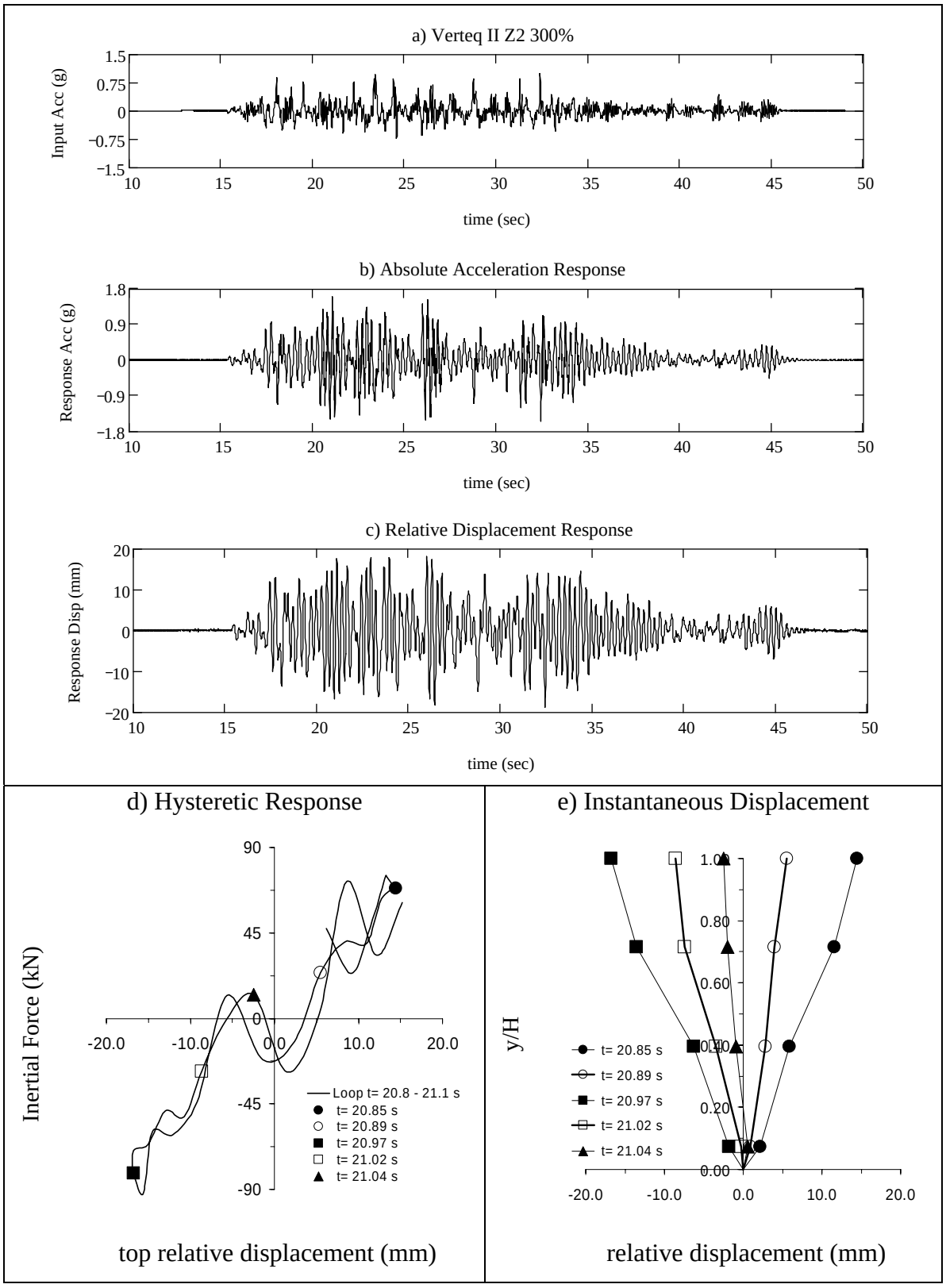

Figure C.7 Summary of Specimen 3 Response for Test#6

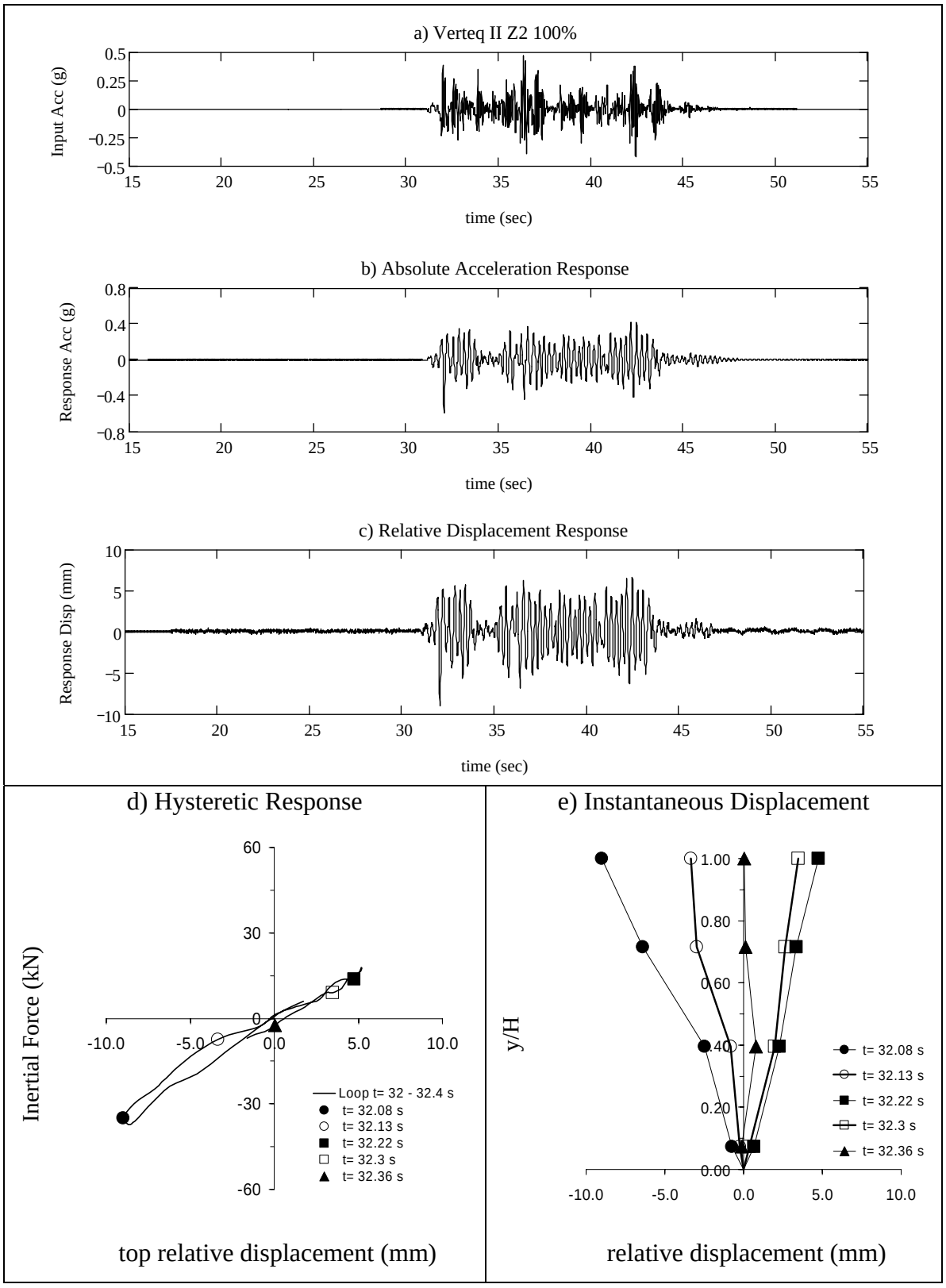

Figure C.8 Summary of Specimen 3 Response for Test#7

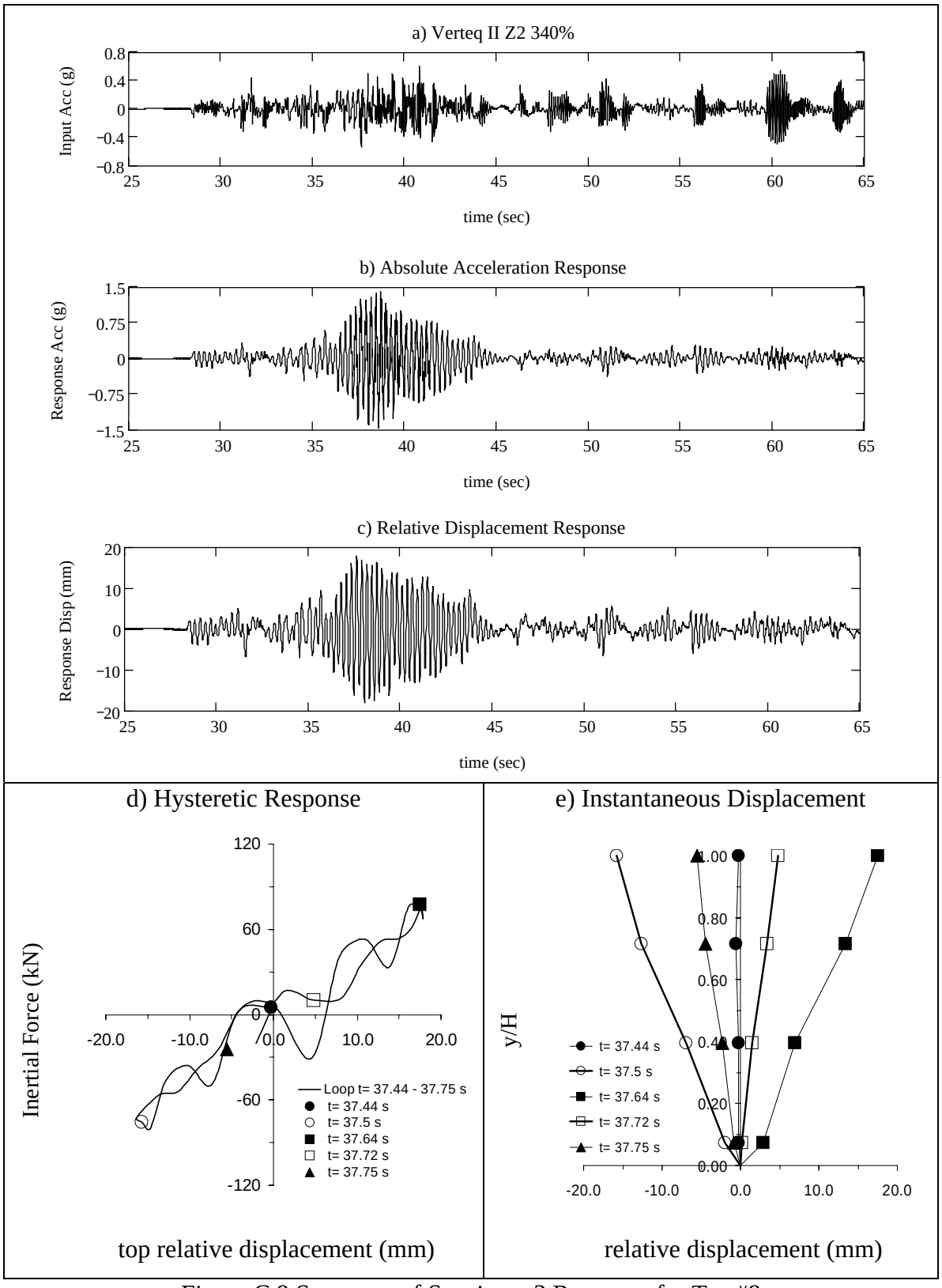

Figure C.9 Summary of Specimen 3 Response for Test#8